IN-SITU INVESTIGATION AND MITIGATION OF CARBON SUPPORT CORROSION OF CATHODE CATALYST IN PEM FUEL CELLS

by

WEI LI

A DISSERTATION

Submitted in partial fulfillment of the requirements
for the degree of Doctor of Philosophy
in the Department of Chemical and Biological Engineering
in the Graduate School of
The University of Alabama

TUSCALOOSA, ALABAMA

2010

ABSTRACT

Carbon support corrosion (CSC) is one of the key factors causing cathode electrocatalyst (Pt/C) degradation in proton exchange membrane fuel cells (PEMFC). It is electrochemical oxidation and thus needs to be investigated in-situ with potential imposed. CSC was characterized in-situ and correlated to the Pt redox reactions and Pt-catalyzed oxygen reduction reaction (ORR) by the differential electrochemical mass spectrometry (DEMS) spectra of cathode exhaust gases, CO_2, H_2 and O_2, from a PEMFC fed with humidified H_2 and He to the anode and cathode respectively. Furthermore, the catalytic effects on CSC from different oxidation states of Pt were indicated. To determine the oxygen sources and pathways of CSC, oxygen was isotopically labeled by replacing regular water with oxygen-18 (^{18}O) enriched water ($H_2{}^{18}O$, 98%) in DEMS, denoted as ^{18}O-DEMS. ^{18}O-DEMS spectra of the cathode exhaust gases O_2, $O^{18}O$, $^{18}O_2$, CO_2, $CO^{18}O$ and $C^{18}O_2$ during cyclic voltammetry and chronoamperometry were analyzed to verify that water is the main direct oxygen source for CSC. Moreover, water reacts with carbon to produce at least three types of carbon surface oxides, which are further electrochemically oxidized with water to produce CO_2 in different potential ranges. After accelerated testing of cathode catalyst degradation in PEMFC using potential cycling between 100–1400 mV at the rate of 400 mV/s, the changes of mass spectra of CO_2, H_2 and O_2 over time showed that the CSC decreases as Pt electrochemically active surface area (ECSA) decreases, i.e. catalyst activity decreases, but the membrane does not degrade significantly in gas permeability.

A hypothesis is proposed here that Au nanoparticles (NPs) added to a carbon-supported Pt (Pt/C) catalyst can mitigate the Pt catalytic effects on CSC by suppressing the Pt oxidation.

Several methods were tried to synthesize Pt/C (20 wt% Pt) and bimetallic AuPt/C (20 wt% Pt, 5 wt% Au) catalysts including deposition-precipitation, two phase liquid-liquid colloidal, polyol, microwave-assisted polyol, and surface redox methods. TEM pictures showed that the EG method (polyol method using ethylene glycol), microwave-assisted EG method, and colloidal method produced Pt/C catalysts with high dispersion and narrow particle size distribution of Pt NPs uniformly loaded on the carbon support. Au NPs with high dispersion and narrow particle size distribution can be made only by the colloidal method. AuPt/C catalysts were synthesized by two methods: physically by mixing Au NPs prepared by the colloidal method on Pt/C prepared by the EG method, and chemically by surface redox reactions of a Au precursor on Pt NPs prepared by the EG method and then loaded on the carbon support (denoted as AuPtC-EG-SR). The existence of Au on Pt/C was confirmed by EDX and by a larger ring current from ORR experiment using a rotating ring-disk electrode. Three membrane electrode assemblies (MEA) with commercial Etek Pt/C and those two types of AuPt/C catalysts as cathode catalyst respectively were fabricated for CSC comparison. Larger ECSA but less CO_2 intensity of the MEA with a AuPtC-EG-SR cathode than those of the MEA with Etek Pt/C gives preliminary confirmation of the hypothesis.

LIST OF ABBREVIATIONS AND SYMBOLS

B	Levich constant
BF	Bright field
c_0	Reactant concentration in the solution
CL	Catalyst layer
CSC	Carbon support corrosion
CV	Cyclic voltammogram
DHE	Dynamic hydrogen electrode
DP	Deposition-precipitation
DRIFTS	Diffuse reflectance infra-red Fourier transform spectroscopy
DT	Dodecanethiol
ECSA	Electrochemically active surface area
EDX	Energy-dispersive X-ray spectroscopy
EG	Ethylene glycol
GC	Glassy carbon
GDL	Gas diffuse layer
H_{OPD}	Overpotential deposition hydrogen
H_{UPD}	Hydrogen underpotential deposition
HAADF	High angle annular dark field
$H_2{}^{18}O$	^{18}O enriched water
HER	Hydrogen evolution reaction

HOR	Hydrogen oxidation reaction
HRTEM	High resolution transmission electron microscopy
i_d	Diffusion-limited current
i_k	Kinetically current
K-L	Koutecky–Levich
MEA	Membrane electrode assembly
MS	Mass spectrometry
MSE	Mercurous sulfate electrode
MW	Microwave assisted
NP	Nanoparticle
^{18}O	Oxygen-18
OAM	Oleylamine
OER	Oxygen evolution reaction
ORR	Oxygen reduction reaction
PAFC	Phosphoric acid fuel cell
PEM	Proton exchange membrane
PEMFC	Proton exchange membrane fuel cell
R(R)DE	Rotating (Ring) disk electrode method
SEM	Scanning electron microscopy
SHE	Standard hydrogen electrode
SR	Surface redox
STEM	Scanning transmission electron microscopy
TEM	Transmission electron microscopy

TGA	Temperature gravimetric analysis
TOABr	Tetraoctylammonium bromide
TPD	Temperature programmed desorption
TPO	Temperature programmed oxidation
UHP	Ultra high purity
UPD	Under potential deposition
XPS	X-ray photoelectron spectroscopy
ω	Rotating speed

ACKNOWLEDGEMENTS

First of all, I am heartily thankful to my advisor, Dr. Alan M. Lane, for his seeing my potential and bringing me into his group. His encouragement and support for my research topic and reading enable me to produce this wonderful topic and broaden my horizon; his patience and trust kept me focused and thinking deeply; his wisdom guidance helped me avoid misdirection and step faster. He deserves every research achievement I made in the past four years and after.

I would also like to thank all of my committee members, Dr. Tonya M. Klein, Dr. David E. Nikles, Dr. Shanlin Pan, Dr. Shane C. Street, and Dr. C. Heath Turner, for their invaluable input, inspiring questions, and support of both the dissertation and my academic progress.

I thank Johnny Goodwin at CAF for assistance in TEM experiments. Thanks extend to the lab mate Trevor Reed for all his help and cooperation in lab, and also to undergraduate students Ynhi Thai, Joy Driver, Paul Herring and Trent Elkins for their input on catalyst preparation and characterization.

I owe my deepest gratitude to my wife (Jia Chen), my parents, and parents-in-law for their support and love. I owe to my little boy, Kevin, for playing less time with him.

The list is endless and I offer my regards and blessings to all of those who supported me in any respect during the completion of the dissertation.

Lastly, I would like to thank funding from DOE, Alabama EPSCoR, Department of Chemical and Biological Engineering, and College of Engineering.

CONTENTS

LIST OF TABLES

LIST OF FIGURES

CHAPTER 1

INTRODUCTION

1.1 Proton Exchange Membrane Fuel Cells

The proton exchange membrane fuel cell (PEMFC) [1] is an environmental friendly electrochemical device, generating electricity through electrochemical reactions of hydrogen as the fuel gas and oxygen or air as the oxidant gas with the only product being water. It has many advantages, including no pollutants, high efficiency, low noise, and low temperature.

Figure 1-1 shows a schematic drawing of the structure and principle of a PEMFC. A typical single PEMFC mainly consists of a membrane electrode assembly (MEA) and flow field plates (two end plates, or bipolar plates in the middle for a stack). In practice, a single PEMFC is connected in series with others to form a stack at different power scales as power sources for transportation, stationary, and portable applications.

The MEA is the core component of PEMFC where the electrochemical reactions happen. It is composed of solid electrolyte proton exchange membrane (PEM) and two gas diffusion electrodes with catalyst layers (CL) made of Pt nanoparticles (NPs) dispersed on carbon black and gas diffusion layers (GDL) made of porous carbon paper or cloth. The flow field plates are so-called because they have gas delivery channels and function as gas distributors. They are made of conductive materials, such as graphite and metals.

Humidified H_2 and O_2 or air are fed to the anode and the cathode through the channels in

the flow field plates, respectively. The H_2 diffuses through the anode GDL and arrives at the anode CL, where it is oxidized to form protons and releases electrons. The protons transfer through the PEM and reach the cathode CL. At the same time, the electrons go though the external circuit, doing electrical work and arriving at the cathode CL. Similarly, the oxygen gas diffuses through the cathode GDL and reaches the cathode CL, where it is reduced with combination of the protons and electrons to produce water.

The key materials of PEMFC are the PEM and catalysts. PEMFC is so-called because PEM is employed as the solid electrolyte, which has the functions of proton conduction and separation of H_2 and O_2 or air. Although many types of PEM, including non-fluorinated, partially fluorinated, and perfluorinated, have been developed, Nafion [2], a perfluorinated-PEM product of DuPont starting in the 1960s, is still the most often employed in PEMFC. As for the catalysts, nanoparticle Pt on carbon black support (Pt/C) is still the most popular used catalyst in PEMFC stacks, although better performance catalysts, such as Pt alloyed with other metals, have been reported [3]. Much effort has been conducted to increase the utilization of Pt and improve the performance.

More detailed technical descriptions can be found in books [1, 4].

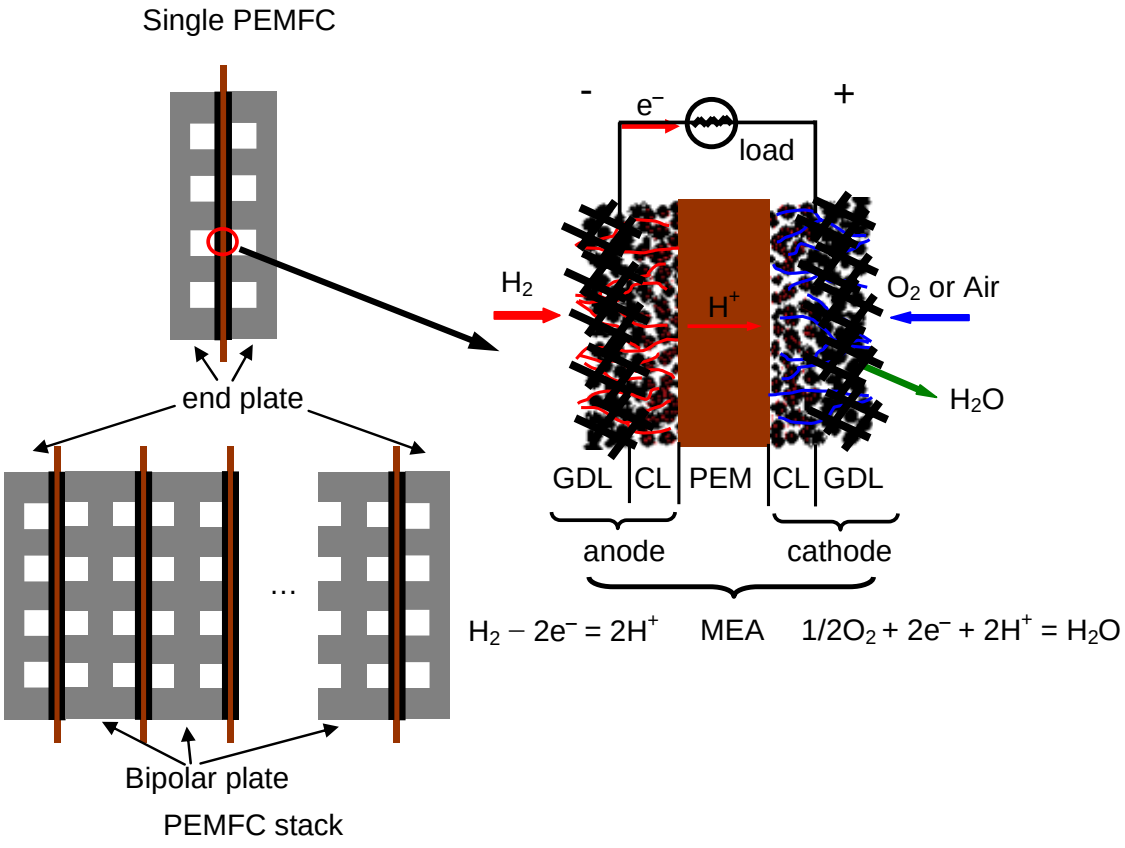

Figure 1-1 Schematic drawing of PEMFC structure and principle

1.2 Background

It was predicted that PEMFC driven vehicles would be commercialized by 2010. Unfortunately, they are still in demonstration because two major barriers of cost and lifetime for the commercialization are not yet overcome.

Before the early 2000s, most research emphasized improving the performance or decreasing the materials usage of a stack or a certain component at "beginning-of-life". Now, the emphasis has shifted to improve the durability, which is supported by the number of publications on PEMFC durability and its percentage of total PEMFC publications increased dramatically in 2000s, shown in Figure 1-2. Since the PEMFC currently is still not cost competitive for most applications, the durability research and development should improve lifetime without cost increase or performance loss [5]. For example, higher catalyst loading can improve catalyst durability due to extra catalyst, but it increases cost.

The factors reducing the lifetime of PEMFC include material degradation or durability, system reliability and operating conditions. Among them, materials degradation has received the most attention in durability research [6]. Understanding the material degradation mechanisms of different components of PEMFC is required to develop new materials with long lifetime but not prohibitively expensive. The commercialization of PEMFC depends on this breakthrough from material research.

Though much progress has been made in understanding the mechanisms, researchers have realized the importance of better understanding the roles of chemical, electrochemical, and operating conditions of PEMFC in the degradation processes [5], which requires the investigations be conducted in-situ. For instance, the electrode potential is the determinative factor for electrochemical oxidation of carbon support and platinum in PEMFC.

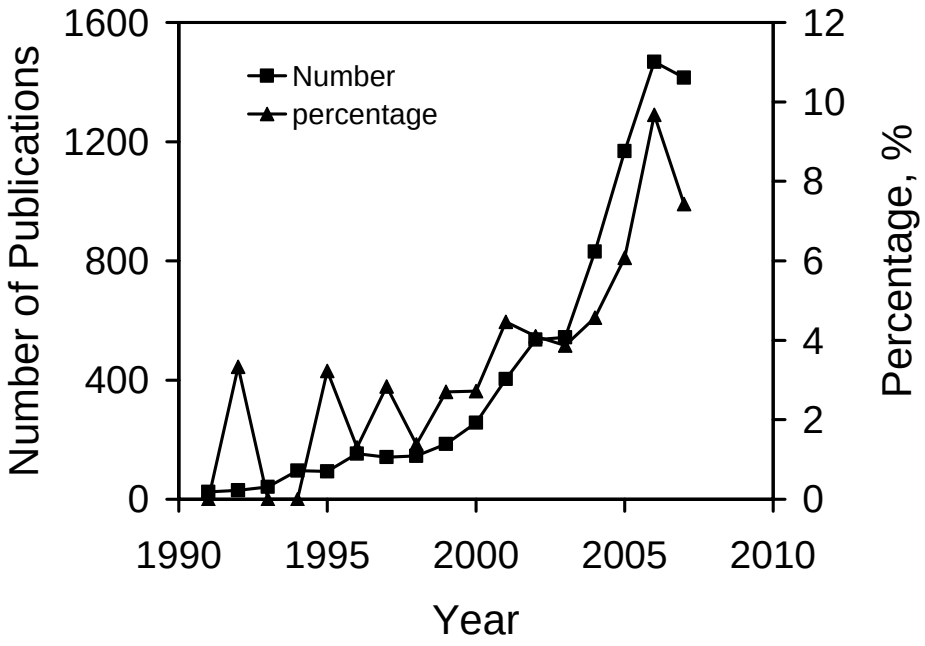

Figure 1-2 Number of publications of PEMFC and the percentage of PEMFC durability publications (The SciFinder Scholar was used to search the publications and analyze the results. Two commonly used names of proton exchange membrane fuel cell (PEMFC) and polymer electrolyte fuel cell (PEFC) were input for search. Results were combined to get the total publications. It was then refined with degradation and durability respectively, and both results were combined to get the publications on PEMFC durability.)

1.3 General Description of Cathode Catalyst Degradation

The electrocatalyst most employed in PEMFC stacks consists of platinum NPs on carbon black (Pt/C) at anode and cathode sides. Electrocatalyst degradation means loss of electrochemical active sites or electrochemically active surface area (ECSA). Similar to heterogeneous catalyst degradation factors [7], the factors contributing to the cathode electrocatalyst degradation can be classified as shown in Figure 1-3.

Fouling does not exist in PEMFC because no carbon is produced. But the cathode catalyst could undergo poisoning by impurities, such as SO_x and NO_x, in the oxidant gas (ambient air).

The cathode catalyst degradation processes related to sintering and catalyst loss in PEMFC are generally described as follows using Pt/C as an example. Pt becomes Pt ions by direct electrochemical oxidation, and/or by electrochemical oxidation to PtO_x which then experiences chemical reaction with acid to give Pt ions. Some Pt ions diffuse into the membrane and the electrochemically inaccessible parts of the MEA [8]. They do not return to the Pt particles and are dissolved away or lost.

At the same time, other Pt ions are reduced and precipitate on a Pt particle surface for recrystallization [8, 9]. Therefore, this process, named Ostwald-ripening, results in the growth of larger Pt particles at the expense of the smaller particles, which are easier to dissolve [10]. Also, the small Pt NPs move on the surface, aggregate together, and recrystallize leading to particle size growth. This process is driven by the tendency of NPs to reduce the surface energy (balance the force on the surface atoms) and is termed coalescence [10]. Carbon support corrosion (CSC) at the cathode accelerates this process by shortening the distance between Pt particles and also decreases the anchor sites for Pt so as to facilitate movement. Besides, oxidation of the carbon

support can also lead to changes in surface hydrophobicity that can cause gas transport to decrease. Change of pore morphology and pore surface characteristics has been investigated [11].

Sintering based on these two mechanisms causes a decrease in active sites [12-15] leading to performance degradation. Meanwhile, the recrystallization from Ostwald-ripening or coalescence also causes defects to decease so as to decrease the active sites.

Those processes can be classified into physical processes with Pt atoms or Pt small particles movement and aggregation, and chemical/electrochemical processes with Pt oxidized into Pt ions that dissolve and reduce back to Pt atoms, as well as the CSC.

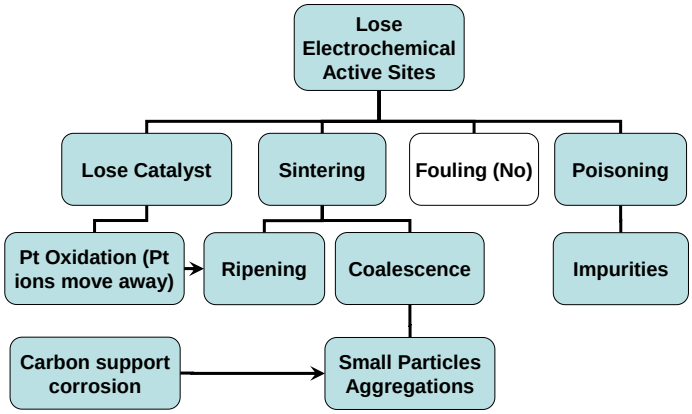

Figure 1-3 Cathode catalysts degradation factors

1.4 Carbon Support Corrosion

Vulcan XC72 is a type of furnace carbon black commonly used as electrode catalyst support in PEMFC. It is prepared by partially burning liquid or gaseous hydrocarbons in air, which create a high density of surface defects, where the surface species, mainly hydrogen and oxygen functional groups adsorb [16]. It is in the form of an amorphous cluster with aggregated

three-dimensional microcrystalline primary particles (20-50 nm in diameter) [16]. This sp^2-hybridized carbon is widely used as catalyst support due to its high electrical conductivity, good processability and availability in a wide variety of particle morphologies [17, 18]. Compared to other supports in heterogeneous catalysis, like alumina and silica for example, it also has relatively high chemical and thermal stability [18, 19].

Despite of those excellent properties, carbon black is known to undergo electrochemical oxidation, i.e. carbon support corrosion (CSC), to CO_2 and surface oxides at the cathode in a low temperature fuel cell, where it is subjected to low pH, high potential, high humidity, and high Pt loading.

CSC under phosphoric acid fuel cell (PAFC) conditions has been intensely studied in the literature [20-24]. This research includes the kinetics of carbon oxidation to surface oxides, adsorption of these oxides on the platinum surface, and ease of subsequent carbon oxidation to CO_2 in the PAFC [25]. CSC is also a serious problem at the cathode in PEMFC under the corrosive conditions of low pH, high water content, a high potential window 0.6 – 1.0 V [26] and up to 1.4 V under abnormal conditions [27-33], high oxygen concentration, and high Pt loading on the catalyst compared with PAFC. However, it has not been extensively studied in PEMFC until now. Though the conditions are different, the research methods and results from PAFC can be referenced to investigate CSC in PEMFC. In-situ investigations are definitely required to understand the CSC mechanisms in specific conditions.

CSC at the cathode in PEMFC can decrease performance due to loss of ECSA [34] and changes of pore morphology and surface characteristics in the catalyst layer [11]. It is an electrochemical oxidation which can be catalyzed by Pt or other metals loaded on the carbon support in a real PEMFC environment [25, 26] and under simulated PEMFC conditions [35].

There are two common proposed pathways for CSC [16]:

$$C + 2H_2O = CO_2 + 4H^+ + 4e^-,\ 25\ ºC,\ 0.207\ V\ vs.\ SHE$$

$$C + H_2O = CO + 2H^+ + 2e^-,\ 25\ ºC,\ 0.518\ V\ vs.\ SHE$$

CO is thermodynamically unstable with respect to CO_2, and

$$CO + H_2O = CO_2 + 2H^+ + 2e^- \quad -0.103V\ vs.\ SHE$$

Surface oxides might be formed as intermediates in both reactions. More detailed proposed mechanisms are that there are at least two anodic oxidation reactions for CSC. One is the CO produced from oxidation of accumulated surface oxide and the other is carbon oxidation to produce surface oxides, CO and CO_2 [16]. Thus the CSC producing CO_2 in an acid solution can be expressed in the two consecutive reaction steps as follows [16]:

$$C + [O^{2-}] = CO_{surf} + 2e^- \qquad [1\text{-}1]$$

$$CO_{surf} + [O^{2-}] = CO_2 + 2e^- \qquad [1\text{-}2]$$

here, the $[O^{2-}]$ represents reduced states of oxygen in the form of H_2O, OH^-, and/or passivated platinum (Pt-O or Pt-OH, which were speculated as the sources of catalytic effects) etc.

Both reaction rates depend on potential and temperature, and change with time. Several reaction schemes have been proposed to explain the formation of gaseous reaction products and surface oxides during electrochemical oxidation of carbon in aqueous electrolytes [16]. However, there is still no well accepted and proven mechanism.

Besides understanding the mechanism of CSC, it is also important to understand the sites where the corrosion happens and what type of surface oxides are produced. It is proposed that carbon oxidation starts at edges and corners of basal planes where there are high density of surface defects with unsaturated valences and free σ-electrons causing different activities [36]. However, the nature of sites at which these two reactions ([1-1], [1-2]) occur on carbon are not

well understood [16]. As for the types of surface oxides on the carbon support, we must distinguish those originally from the carbon and catalyst fabrication processes and those from the oxidation process. A wide variety of surface oxides such as phenols, carbonyls, carboxylic acids, ethers, quinones, and lactones have been identified on activated carbon by titration and infrared spectroscopy [37-45], thermal gravimetric analysis-mass spectrometry (TGA-MS) [11, 46-59], X-ray photoelectron spectroscopy (XPS) [11, 46-59], nitrogen adsorption, temperature programmed desorption (TPD), scanning electron microscopy (SEM), TGA-MS, XPS, and diffuse reflectance Infra-red Fourier transform spectroscopy (DRIFTS) [48, 60]. Those results can be used for reference to understand CSC of carbon black in PEMFC.

To sum up, in-situ investigations are required to better understand the mechanisms of CSC in PEMFC, including oxygen sources, pathways, intermediates, and preferred reaction sites as well as the kinetics.

1.5 Pt Redox Reaction and Its Catalytic Effects on CSC

Pt undergoes electrochemical oxidation and reduction during potential cycling at the cathode of PEMFC. Although the catalytic effects of Pt oxides have been confirmed by differential electrochemical mass spectrometry (DEMS) in our study [61], the mechanisms are still not clear. Understanding the mechanisms requires the identification of the chemical components, structure and formation or removal processes of the oxide film as a function of the potential, pH, liquid or solid acid, and time. Moreover, it is difficult to characterize these properties and processes at the nanoscale, i.e. Pt NPs or Pt NPs on a carbon black support, either ex-situ or in-situ. Most investigations were conducted on single crystal and polycrystalline bulk platinum in-situ [62, 63] and ex-situ [62]. These results can help to understand the mechanisms

of the Pt catalytic effects on CSC.

Pt oxidation includes a series of processes such as O and OH adsorption and place exchange between Pt and O at different potentials, while Pt reduction involves O and OH desorption and reverse place exchange between Pt and O [64]. The processes of OH and O species (from water) adsorption happens in the range of 0.5–0.8 V, and further Pt oxidation occurs in the higher potential range of 0.8–1.4 V with more complicated processes [65]: in the range of 0.8–1.15 V, O chemisorption and a monolayer oxide film is formed; in the range of 1.15–1.4 V, the place exchange of O and Pt occurs, followed with further formation of PtO to multilayer, and surface diffusion of PtO to energetically favorable sites. A more detailed model was proposed by Sun et al. [66] based on electrochemical impedance spectroscopy and XPS. They concluded that in the anodic direction, a multiple oxide film formed above 1.3 V consisting of an inner PtO layer and an outer layer of PtO_2. They also detected that there is a single oxide layer at lower potentials.

The detailed behaviors of O and OH adsorption as well as the place exchange of O and Pt are still under question. Numerous studies were conducted on single crystal surfaces in vacuum or in the gas phase [67]. Their results show that O and OH adsorption on Pt depends on a variety of factors including the crystal face, the coverage, the temperature and the presence of other adsorbed species. Unfortunately, the experimental findings are conflicted with the theoretical findings [68]. In an electrochemical cell with Pt electrochemical oxidation, the interface of metal/electrolyte contributes to different behaviors of O and OH adsorption [69] and difficulties of investigation using normal optical techniques [67].

Complicating matters, both gas phase oxidation and electrochemical oxidation of Pt coexist at the PEMFC cathode. Their differences, interrelated effects, and catalytic effects on

CSC have not been studied well in literature. Whether the presence of gas-phase oxygen accelerates the CSC in PEMFC is controversial. Paik showed that the presence of gas-phase oxygen accelerates the CSC using cyclic voltammetry [70]. Whereas, we showed that the oxygen gas does not contribute to CSC significantly using DEMS [61], which is consistent with the literature [26].

According to the description above, we proposed that those O or OH involved in the Pt oxidation and reduction could transfer to the surface of carbon black support to catalyze CSC to produce CO or CO_2 [20, 25, 26, 35]. It is believed that hydroxyl surface groups on Pt, which are destabilized at lower electrode potentials, not only react with protons to water but also combine with carbon surface groups to give carbon dioxide. However, there is still no direct evidence about the transfer/donation in-situ in PEMFC. On the other hand, there is no substantial experimental evidence that the platinum oxides present a passivated film for CSC in the applied potential range [20, 25, 26, 35].

1.6 Mitigation of CSC

Two possible strategies have been proposed in the literature [32] to mitigate the carbon corrosion: an alternative catalyst support with more corrosion resistance to eliminate, or at least reduce, performance decay; and an improved design to minimize the adverse conditions.

CSC is attributed to the nature of carbon black oxidation with water at high potential and low pH in PEMFC. It might be mitigated by replacing the carbon black with carbon nanotubes [71, 72], functionalized graphene sheets [73], conductive metal oxides [74], or by doping the carbon black with other elements [75]. In this study, it was intended to alleviate the CSC by modifying the Pt with Au NPs or clusters.

CSC becomes more severe in the cases of fuel starvation [29, 76], high potential over long period after stop [31], formation of air/fuel boundary at the anode [27], and the catalytic effect from Pt [25, 26, 35, 61]. These can be alleviated by optimizing the operation conditions.

1.7 Outline of the Dissertation

The knowledge and background of PEMFC were briefly introduced first in Chapter 1. The mechanisms and mitigation strategies of CSC were then generally reviewed. Specific topics are reviewed in each related chapter.

The employed preparation and characterization methods of bimetallic AuPt/C catalysts are summarized and reviewed in Chapter 2. It did not focus on their basic principles, but on their applications pertaining to this dissertation.

The catalytic effects of Pt and PtO_x on CSC were investigated and confirmed by DEMS, shown in Chapter 3. The CSC mechanism was further investigated by isotope labeling the oxygen to understand the oxygen sources and pathways in Chapter 4. The DEMS technique was then extended to characterize the cathode catalyst degradation in Chapter 5. Chapter 3 and 4 are reproduced from our publications in Electrochemistry Communications [77] and submitted to Journal of Electrochimica Acta, respectively.

Based on the results from Chapter 3, 4 and 5, a hypothesis to mitigate CSC by adding gold NPs or clusters on Pt/C is proposed. Bimetallic AuPt/C catalysts were thus prepared using different methods to test the hypothesis in Chapter 6.

In Chapter 7, the study was concluded and future work is suggested to answer some remaining questions, such as the CSC mechanism on a molecular level.

References:

1. Srinivasan, S., *Fuel Cells: From Fundamentals to Applications*. 1st ed. 2006: Springer. 692.

2. Mauritz, K.A. and R.B. Moore, *State of Understanding of Nafion.* Chem. Rev., 2004. **104**(10): p. 4535-4586.

3. Antolini, E., *Formation of carbon-supported PtM alloys for low temperature fuel cells: a review.* Mater. Chem. and Phys., 2003. **78**(3): p. 563-573.

4. Vielstich, W., A. Lamm, and H.A. Gasteiger, eds. *Handbook of Fuel Cells: Fundamentals, Technology, Applications*. 1st ed. 2003, Wiley. 3826.

5. Borup, R., J. Meyers, B. Pivovar, Y.S. Kim, R. Mukundan, N. Garland, D. Myers, M. Wilson, F. Garzon, D. Wood, P. Zelenay, K. More, K. Stroh, T. Zawodzinski, J. Boncella, J.E. McGrath, M. Inaba, K. Miyatake, M. Hori, K. Ota, Z. Ogumi, S. Miyata, A. Nishikata, Z. Siroma, Y. Uchimoto, K. Yasuda, K.i. Kimijima, and N. Iwashita, *Scientific Aspects of Polymer Electrolyte Fuel Cell Durability and Degradation.* Chem. Rev., 2007. **107**(10): p. 3904-3951.

6. Wilkinson, D.P. and J. St.-Pierre, *Durability,* in *Handbook of Fuel Cells: Fundamentals, Technology, and Applications*, W. Vielstich, A. Lamm, and H.A. Gasteiger, Editors. 2003, Wiley.

7. Butt, J.B. and E.E. Peterson, *Activation, deactivation and poisoning of catalysts*. From review by Richard D. Gonzalez, Univ. of Illinois, Chicago, in J. Am. Chem. Soc., Vol 111, No. 7(29 Mar 1989). 1988, United States: New York, NY (US); Academic. Pages: (505 p).

8. Ferreira, P.J., G.J. la O, Y. Shao-Horn, D. Morgan, R. Makharia, S. Kocha, and H.A. Gasteiger, *Instability of Pt/C Electrocatalysts in Proton Exchange Membrane Fuel Cells: A mechanistic investigation.* J. Electrochem. Soc., 2005. **152**(11): p. A2256-A2271.

9. Xie, J., D.L. Wood, Iii, K.L. More, P. Atanassov, and R.L. Borup, *Microstructural Changes of Membrane Electrode Assemblies during PEFC Durability Testing at High Humidity Conditions.* J. Electrochem. Soc., 2005. **152**(5): p. A1011-A1020.

10. Ascarelli, P., V. Contini, and R. Giorgi, *Formation process of nanocrystalline materials from x-ray diffraction profile analysis: Application to platinum catalysts.* J. Appl. Phys., 2002. **91**(7): p. 4556-4561.

11. Kangasniemi, K.H., D.A. Condit, and T.D. Jarvic, *Characterization of Vulcan Electrochemically Oxidized under Simulated PEM Fuel Cell Conditions.* J. Electrochem. Soc., 2004. **151**(4): p. E125--E132.

12. Kinoshita, K., J.T. Lundquist, and P. Stonehart, *Potential cycling effects on platinum electrocatalyst surfaces.* J. Electroanal. Chem., 1973. **48**(2): p. 157-166.

13. Komanicky, V., K.C. Chang, A. Menzel, N.M. Markovic, H. You, X. Wang, and D. Myers, *Stability and Dissolution of Platinum Surfaces in Perchloric Acid.* J. Electrochem. Soc., 2006. **153**(10): p. B446-B451.

14. Canullo, J.C., W.E. Triaca, and A.J. Arvia, *Electrochemical faceting of single crystal platinum electrodes.* J. Electroanal. Chem., 1986. **200**(1-2): p. 397-400.

15. Egli, W.A., A. Visintin, W.E. Triaca, and A.J. Arvia, *The development of facetting and roughening at platinum polyfacetted single-crystal electrodes in a chloroplatinic acid solution.* Appl. Surf. Sci., 1993. **68**(4): p. 583-593.

16. Kinoshita, K., *Carbon Electrochemical and Physicochemical Properties*. 1988, New York: Wiley.

17. Cameron, D.S., S.J. Cooper, I.L. Dodgson, B. Harrison, and J.W. Jenkins, *Carbons as supports for precious metal catalysts.* Catal. Today, 1990. **7**(2): p. 113-137.

18. Rodríguez-reinoso, F., *The role of carbon materials in heterogeneous catalysis.* Carbon, 1998. **36**(3): p. 159-175.

19. Auer, E., A. Freund, J. Pietsch, and T. Tacke, *Carbons as supports for industrial precious metal catalysts.* Appl. Catal. A: General, 1998. **173**(2): p. 259-271.

20. Passalacqua, E., P.L. Antonucci, M. Vivaldi, A. Patti, V. Antonucci, N. Giordano, and K. Kinoshita, *The influence of Pt on the electrooxidation behaviour of carbon in phosphoric acid.* Electrochim. Acta, 1992. **37**(15): p. 2725-2730.

21. Kinoshita, K. and J. Bett, *Electrochemical oxidation of carbon black in concentrated phosphoric acid at 135 ºC.* Carbon, 1973. **11**(3): p. 237-247.

22. Gruver, G.A., *The Corrosion of Carbon Black in Phosphoric Acid.* J. Electrochem. Soc., 1978. **125**(10): p. 1719-1720.

23. Kiho, M., K. Matsunaga, S. Morikawa, and O. Kato, *Influence of metal impurities on carbon corrosion in phosphoric acid fuel cells (PAFC).* Electrochem. 2001. **69**(8): p. 580-586.

24. Wei, Z., H. Guo, and Z. Tang, *Heat treatment of carbon-based powders carrying platinum alloy catalysts for oxygen reduction: influence on corrosion resistance and particle size.* J. Power Sources, 1996. **62**(2): p. 233-236.

25. Roen, L.M., C.H. Paik, and T.D. Jarvi, *Electrocatalytic Corrosion of Carbon Support in PEMFC Cathodes.* Electrochem. Solid-State Lett., 2004. **7**(1): p. A19-A22.

26. Maass, S., F. Finsterwalder, G. Frank, R. Hartmann, and C. Merten, *Carbon support oxidation in PEM fuel cell cathodes.* J. Power Sources, 2008. **176**(2): p. 444-451.

27. Tang, H., Z. Qi, M. Ramani, and J.F. Elter, *PEM fuel cell cathode carbon corrosion due to the formation of air/fuel boundary at the anode.* J. Power Sources, 2006. **158**(2): p. 1306-1312.

28. Mitsuda, K. and T. Murahashi, *Polarization Study of a Fuel Cell with Four Reference Electrodes.* J. Electrochem. Soc., 1990. **137**(10): p. 3079-3085.

29. Meyers, J.P. and R.M. Darling, *Model of Carbon Corrosion in PEM Fuel Cells.* J. Electrochem. Soc., 2006. **153**(8): p. A1432-A1442.

30. Yang, D., M.M. Steinbugler, R.D. Sawyer, L.L. Van Dine, and C.A. Reiser, *Procedure for starting up a fuel cell system having an anode exhaust recycle loop*, in US Patent 2003: United States.

31. Reiser, C.A., L. Bregoli, T.W. Patterson, J.S. Yi, J.D. Yang, M.L. Perry, and T.D. Jarvi, *A Reverse-Current Decay Mechanism for Fuel Cells.* Electrochem. Solid-State Lett., 2005. **8**(6): p. A273-A276.

32. Perry, M.L., T. Patterson, and C. Reiser, *Systems Strategies to Mitigate Carbon Corrosion in Fuel Cells.* ECS Trans., 2006. **3**(1): p. 783-795.

33. Yu, P.T., W. Gu, R. Makharia, F.T. Wagner, and H.A. Gasteiger, *The Impact of Carbon Stability on PEM Fuel Cell Startup and Shutdown Voltage Degradation.* ECS Trans., 2006. **3**(1): p. 797-809.

34. Antolini, E., *Formation, microstructural characteristics and stability of carbon supported platinum catalysts for low temperature fuel cells.* J. Mater. Sci., 2003. **38**(14): p. 2995-3005.

35. Willsau, J. and J. Heitbaum, *The influence of Pt-activation on the corrosion of carbon in gas diffusion electrodes--A dems study.* J. Electroanal. Chem., 1984. **161**(1): p. 93-101.

36. Stonehart, P., in *Progress in batteries and solar cells*, H. Shimotake, Editor. 1984, JEC Press, Inc., Cleveland, OH: United States. p. Pages: 260-263.

37. Yang, Y. and Z.G. Lin, *In situ FTIR characterization of the electrooxidation of glassy carbon electrodes.* J. Appl. Electrochem., 1995. **25**(3): p. 259-266.

38. Donnet, J.B., *The chemical reactivity of carbons.* Carbon, 1968. **6**(2): p. 161-176.

39. Zawadzki, J., *IR spectroscopy studies of oxygen surface compounds on carbon.* Carbon, 1978. **16**(6): p. 491-497.

40. O'Reilly, J.M. and R.A. Mosher, *Functional groups in carbon black by FTIR spectroscopy.* Carbon, 1983. **21**(1): p. 47-51.

41. Fanning, P.E. and M.A. Vannice, *A DRIFTS study of the formation of surface groups on carbon by oxidation.* Carbon, 1993. **31**(5): p. 721-730.

42. Ishizaki, C. and I. Mart, *Surface oxide structures on a commercial activated carbon.* Carbon, 1981. **19**(6): p. 409-412.

43. Contescu, A., M. Vass, C. Contescu, K. Putyera, and J.A. Schwarz, *Acid buffering capacity of basic carbons revealed by their continuous pK distribution.* Carbon, 1998. **36**(3): p. 247-258.

44. Yang, Y. and Z.-G. Lin, *In situ IR spectroscopic characterization of surface oxide species on glassy carbon electrodes.* J. Electroanal. Chem., 1994. **364**(1-2): p. 23-30.

45. Matsumura, Y., S. Hagiwara, and H. Takahashi, *Automatic potentiometric titration of surface acidity of carbon black.* Carbon, 1976. **14**(3): p. 163-167.

46. Yue, Z.R., W. Jiang, L. Wang, S.D. Gardner, and J.C.U. Pittman, *Surface characterization of electrochemically oxidized carbon fibers.* Carbon, 1999. **37**(11): p. 1785-1796.

47. Chun, B.-W., C. Randall Davis, Q. He, and R.R. Gustafson, *Development of surface acidity during electrochemical treatment of pan-carbon fibers.* Carbon, 1992. **30**(2): p. 177-187.

48. Aksoylu, A.E., M. Madalena, A. Freitas, M.F.R. Pereira, and J.L. Figueiredo, *The effects of different activated carbon supports and support modifications on the properties of Pt/AC catalysts.* Carbon, 2001. **39**(2): p. 175-185.

49. Proctor, A. and P.M.A. Sherwood, *X-ray photoelectron spectroscopic studies of carbon fibre surfaces--II: The effect of electrochemical treatment.* Carbon, 1983. **21**(1): p. 53-59.

50. Takahagi, T. and A. Ishitani, *XPS studies by use of the digital difference spectrum technique of functional groups on the surface of carbon fiber.* Carbon, 1984. **22**(1): p. 43-46.

51. Nakayama, Y., F. Soeda, and A. Ishitani, *XPS study of the carbon fiber matrix interface.* Carbon, 1990. **28**(1): p. 21-26.

52. Zielke, U., K.J. Hüttinger, and W.P. Hoffman, *Surface-oxidized carbon fibers: I. Surface structure and chemistry.* Carbon, 1996. **34**(8): p. 983-998.

53. Dekanski, A., J. Stevanovic, R. Stevanovic, B.Z. Nikolic, and V.M. Jovanovic, *Glassy*

carbon electrodes: I. Characterization and electrochemical activation. Carbon, 2001. **39**(8): p. 1195-1205.

54. Biniak, S., G. Szymanski, J. Siedlewski, and A. Swiatkowski, *The characterization of activated carbons with oxygen and nitrogen surface groups.* Carbon, 1997. **35**(12): p. 1799-1810.

55. Beck, N.V., S.E. Meech, P.R. Norman, and L.A. Pears, *Characterisation of surface oxides on carbon and their influence on dynamic adsorption.* Carbon, 2002. **40**(4): p. 531-540.

56. Marchon, B., J. Carrazza, H. Heinemann, and G.A. Somorjai, *TPD and XPS studies of O_2, CO_2, and H_2O adsorption on clean polycrystalline graphite.* Carbon, 1988. **26**(4): p. 507-514.

57. Takahagi, T. and A. Ishitani, *XPS study on the surface structure of carbon fibers using chemical modification and C1s line shape analysis.* Carbon, 1988. **26**(3): p. 389-395.

58. Proctor, A. and P. Sherwood, *X-ray photoelectron spectroscopic studies of carbon fibre surfaces. III - Industrially treated fibres and the effect of heat and exposure to oxygen.* Surf. Interface Anal., 1982. **4**(5): p. 212-219.

59. de la Puente, G., J.J. Pis, J.A. Menéndez, and P. Grange, *Thermal stability of oxygenated functions in activated carbons.* J. Anal. Appl. Pyrolysis, 1997. **43**(2): p. 125-138.

60. Figueiredo, J.L., M.F.R. Pereira, M.M.A. Freitas, and J.J.M. Órfão, *Modification of the surface chemistry of activated carbons.* Carbon, 1999. **37**(9): p. 1379-1389.

61. Serp, P. and J.L. Figueiredo, *Carbon materials for catalysis*. 2009, Hoboken, N.J.: John Wiley & Sons.

62. Jerkiewicz, G., G. Vatankhah, J. Lessard, M.P. Soriaga, and Y.-S. Park, *Surface-oxide growth at platinum electrodes in aqueous H2SO4: Reexamination of its mechanism through combined cyclic-voltammetry, electrochemical quartz-crystal nanobalance, and Auger electron spectroscopy measurements.* Electrochim. Acta, 2004. **49**(9-10): p. 1451-1459.

63. Nagy, Z. and H. You, *Applications of surface X-ray scattering to electrochemistry problems.* Electrochim. Acta, 2002. **47**(19): p. 3037-3055.

64. Conway, B.E., *Electrochemical Oxide Film Formation at Noble-Metals as a Surface-Chemical Process.* Prog. Surf. Sci., 1995. **49**(4): p. 331-452.

65. Uribe, F.A. and T.A. Zawodzinski, *A study of polymer electrolyte fuel cell performance at high voltages. Dependence on cathode catalyst layer composition and on voltage conditioning.* Electrochim. Acta, 2002. **47**(22-23): p. 3799-3806.

66. Sun, A., J. Franc, and D.D. Macdonald, *Growth and Properties of Oxide Films on Platinum.* J. Electrochem. Soc., 2006. **153**(7): p. B260-B277.

67. Teliska, M., W.E. O'Grady, and D.E. Ramaker, *Determination of O and OH Adsorption Sites and Coverage in Situ on Pt Electrodes from Pt L23 X-ray Absorption Spectroscopy.* J. Phys. Chem. B, 2005. **109**(16): p. 8076-8084.

68. Mukerjee, S. and S. Srinivasan, *Enhanced electrocatalysis of oxygen reduction on platinum alloys in proton exchange membrane fuel cells.* J. Electroanal. Chem., 1993. **357**(1-2): p. 201-224.

69. Tidswell, I.M., N.M. Marković, and P.N. Ross, *Potential dependent surface relaxation of the Pt(001)/electrolyte interface.* Phys. Rev. Lett., 1993. **71**(10): p. 1601.

70. Paik, C.H., G.S. Saloka, and G.W. Graham, *Influence of Cyclic Operation on PEM Fuel Cell Catalyst Stability.* Electrochem. Solid-State Lett., 2007. **10**(2): p. B39-B42.

71. Yan, Y., X. Wang, W. Li, Z. Chen, and M.M. Waje, *Characterization of Support Corrosion in PEM Fuel Cell: Improved Durability of Carbon Nanotube Based Electrode.* ECS Trans., 2006. **1**(8): p. 33-40.

72. Wang, X., W. Li, Z. Chen, M. Waje, and Y. Yan, *Durability investigation of carbon nanotube as catalyst support for proton exchange membrane fuel cell.* J. Power Sources, 2006. **158**(1): p. 154-159.

73. Shao, Y., J. Wang, R. Kou, M. Engelhard, J. Liu, Y. Wang, and Y. Lin, *The corrosion of PEM fuel cell catalyst supports and its implications for developing durable catalysts.* Electrochim. Acta, 2009. **54**(11): p. 3109-3114.

74. Kim, S. and S.-J. Park, *Effect of acid/base treatment to carbon blacks on preparation of carbon-supported platinum nanoclusters.* Electrochim. Acta, 2007. **52**(9): p. 3013-3021.

75. Acharya, C.K., W. Li, Z. Liu, G. Kwon, C. Heath Turner, A.M. Lane, D. Nikles, T. Klein, and M. Weaver, *Effect of boron doping in the carbon support on platinum nanoparticles and carbon corrosion.* J. Power Sources, 2009. **192**(2): p. 324-329.

76. Taniguchi, A., T. Akita, K. Yasuda, and Y. Miyazaki, *Analysis of electrocatalyst degradation in PEMFC caused by cell reversal during fuel starvation.* J. Power Sources, 2004. **130**(1-2): p. 42-49.

77. Li, W. and A.M. Lane, *Investigation of Pt catalytic effects on carbon support corrosion of the cathode catalyst in PEM fuel cells using DEMS spectra.* Electrochem. Comm., 2009. **11**(6): p. 1187-1190.

CHAPTER 2

EXPERIMENTAL BACKGROUND

The employed preparation and characterization methods of catalysts as well as the differential electrochemical mass spectrometry (DEMS) investigation of carbon support corrosion (CSC) are summarized and reviewed in this chapter. It does not focus on their basic principles, but on their applications pertaining to this dissertation. Specific experimental methods and conditions will be described in related chapters.

2.1 Preparation Methods of Bimetallic AuPt/C Catalysts

Au and Pt can exist in alloyed or bimetallic state in AuPt/C catalysts. The bulk Pt-Au phase diagram indicates that the solubility of each metal in the other is strictly limited [1]. However, a high extent of Pt-Au alloy was obtained at the nanoscale [2]. We proposed that the carbon support corrosion (CSC) might be mitigated by adding Au clusters or nanoparticles (NPs) on Pt/C. The Au thus needs to keep its own distinct metallic structure, i.e. Au and Pt are in bimetallic state. Therefore, this review focuses on the synthesis methods of bimetallic AuPt/C catalysts, listed in Figure 2-1.

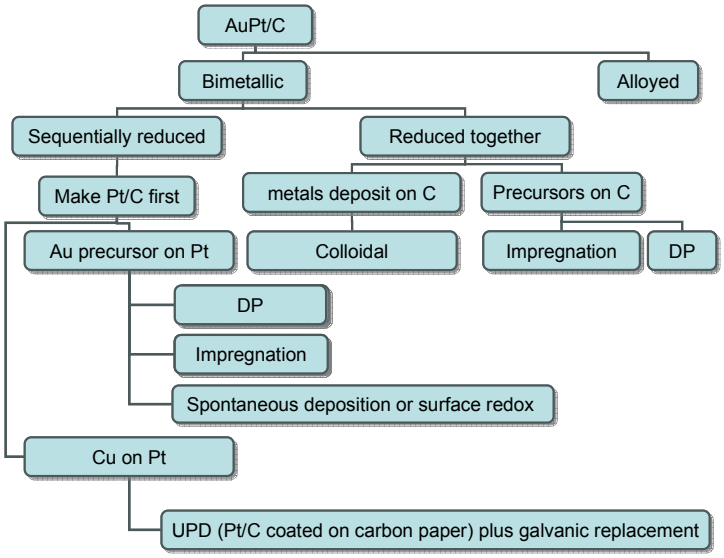

Figure 2-1. Preparation methods of bimetallic AuPt/C catalysts

Impregnation, including incipient wetness impregnation and wet impregnation, is probably the simplest method and usually utilized first to make catalysts for investigation. However, it is known that the prepared catalysts with carbon support have large mean size and wide distribution. It was not employed to synthesize the bimetallic AuPt/C catalysts in my study.

Under potential deposition (UPD) has been commonly utilized to prepare a uniform metal (sub) monolayer on a foreign metal substrate by deposition at potentials more positive than the Nernst equilibrium potential [3, 4]. However, it is not appropriate to prepare a large amount of catalyst because of the need for rigorous control of potential and the unavoidable iR drop across a large amount of nanoparticle metal substrate. Furthermore, the knowledge regarding the UPD process of Au on Pt surfaces is still rather limited [5].

It is very hard to make high dispersion Au NPs on carbon black because of the reducing nature of the carbon black and the weak interaction between the carbon black and the Au precursor [6]. The knowledge to make high dispersion Au and AuPt NPs on carbon black is still

very limited. We need to find the appropriate conditions for those methods used in this study: deposition-precipitation (DP), colloidal, ethylene glycol (EG), microwave assisted (MW)-EG, and surface redox (SR) methods.

2.1.1 Deposition-precipitation Method

The DP method is rather simple whereas it can give good dispersion under careful control. It achieves the deposition of active components from the solution onto a support by chemical reactions rather than by drying or adsorption. It is adopted most often in an excess of solution with respect to the pore volume of the support, which is in the form of powders. It is a relatively simple method with the advantages of good reproducibility, high metal dispersions and loadings, and uniform distribution of the active components over the support.

As for metal oxide supports, the strong interaction, formed between the metal hydroxide of the active component and the support, is essential for deposition on the support surface without nucleation in the bulk. However, for carbon supports, there is only weak interaction between the metal hydroxide and the carbon surface oxides, which causes non-uniform distribution [7] and quite low dispersion [8] of metal particles. Recently, success has been reported in preparing high dispersion and high loading of Pt/C catalysts with carefully controlled conditions [9, 10]. However, it is still a challenge to make Au/C with high dispersion and loading because Au is the most stable metal and its ions are very easily reduced, even by the carbon surface itself [6].

The properties of the support and precursor, the speed of deposition and reduction, the sequence of precipitation of precursors, pH control of the suspension, the method of mixing of reactants, and the temperature are key factors playing a vital role in the particle size and

distribution of metal NPs. Preparation conditions need to be determined to make AuPt/C catalysts with high dispersion, uniform distribution, and high loading.

2.1.2 Colloidal Method

The colloidal method is often used to make very high dispersion NPs. It is so-called because a well-dispersed colloidal metal solution is formed by adsorption of a capping agent or surfactant at the metal-solution interfaces, which limits the nucleation, growth and aggregation of metal NPs [11]. Colloidal solutions of metals have been recognized for a long time [12] and a large variety of preparative techniques is now available. The first attempt to prepare PEMFC electrocatalysts by colloidal method was made by Watanabe et al. [13] and then substantial progress was made by Böennemann et al. [14, 15].

The main advantage is that the colloidal method can make very highly dispersed and uniformly distributed supported metal catalysts, even a nearly monodisperse size distribution centered around 3 nm [16]. However, it has an intrinsic problem with the residue of the stabilizing organic materials on the surface of metal colloids, blocking the active sites for electrocatalysis. The surfactant must to be removed effectively with minimum sintering to get high performance PEMFC catalysts [11, 17-24]. In addition, the complexity of this method also hinders its widespread application.

In this study, a two-phase (water-toluene) liquid-liquid colloidal method was utilized to prepare Pt/C and AuPt/C with a capping agent removal step [25, 26]. Usage of simple precursors $HAuCl_4$ and/or H_2PtCl_6 makes it convenient to synthesize catalysts for investigation. However, a phase transfer reagent (tetraoctylammonium bromide, $[CH_3(CH_2)_7]_4NBr$) is needed to assist the $AuCl_4^-$(aq) or $PtCl_6^{2-}$(aq) transferring from aqueous phase to organic phase (toluene). Two-phase

redox reactions happen in the adjoining phases between sodium borohydride and metal ion complex with phase transfer agent. The produced metal particles are capped with dodecanethiol ($CH_3(CH_2)_{11}SH$) or oleylamine ($C_8H_{17}CH{=}CHC_8H_{16}NH_2$) to avoid the severe growth and aggregation. The overall reactions are summarized by Eq. [2-1] ~ [2-6] below [26].

$$AuCl_4^-(aq) + [CH_3(CH_2)_7]_4N^+(C_6H_5Me) \rightarrow N[CH_3(CH_2)_7]_4^+AuCl_4^-(C_6H_5Me) \quad [2\text{-}1]$$

$$mAuCl_4^-(C_6H_5Me) + nCH_3(CH_2)_{11}SH(C_6H_5Me) + 3me^- \rightarrow$$

$$4mCl^-(aq) + (Au_m)[CH_3(CH_2)_{11}SH]_n(C_6H_5Me) \quad [2\text{-}2]$$

$$mAuCl_4^-(C_6H_5Me) + nC_8H_{17}CH{=}CHC_8H_{16}NH_2(C_6H_5Me) + 3me^- \rightarrow$$

$$4mCl^-(aq) + (Au_m)(C_8H_{17}CH{=}CHC_8H_{16}NH_2)_n(C_6H_5Me) \quad [2\text{-}3]$$

$$PtCl_6^{2-}(aq) + [CH_3(CH_2)_7]_4N^+(C_6H_5Me) \rightarrow \{N[CH_3(CH_2)_7]_4^+\}_2PtCl_6^{2-}(C_6H_5Me) \quad [2\text{-}4]$$

$$mPtCl_6^{2-}(C_6H_5Me) + nCH_3(CH_2)_{11}SH(C_6H_5Me) + 4me^- \rightarrow$$

$$6mCl^{2-}(aq) + (Pt_m)[CH_3(CH_2)_{11}SH]_n(C_6H_5Me) \quad [2\text{-}5]$$

$$mPtCl_6^{2-}(C_6H_5Me) + nC_8H_{17}CH{=}CHC_8H_{16}NH_2(C_6H_5Me) + 3me^- \rightarrow$$

$$PtCl_6^{2-}(aq) + (Pt_m)(C_8H_{17}CH{=}CHC_8H_{16}NH_2)_n(C_6H_5Me) \quad [2\text{-}6]$$

where the e^- comes from BH_4^-.

There are three main methods to remove the surfactant shell, i.e. thermal decomposition [27], oxygen plasma [28] and UV/ozone washes [29]. The thermal decomposition is the most popular and effective method [30] and will be used in this study. Thermogravimetric analysis (TGA) is a common method to study the thermal decomposition of the surfactant shell. However, it cannot supply information about the thermal oxidation product. The temperature programmed oxidation (TPO) method was employed to investigate the mechanisms of thermal oxidation and removal of the surfactant shell.

2.1.3 Polyol Method – EG and MW-EG Method

The polyol method is an attractive alternative method because it is simple and convenient to make highly dispersed NPs without the need to remove organic chemicals. The polyol method was developed to prepare micron and submicron size particles of easily reducible metals such as copper, silver, cobalt, nickel, cadmium or lead [31]. Ethylene glycol (EG) is the commonly used polyol and works as solvent, stabilizer and reductant. The EG method (polyol method using EG) has been used to successfully synthesize highly dispersed and uniformly distributed Pt NPs with high loading on C supports for fuel cells [32-36]. The particle sizes of Pt can be adjusted using different ratio of EG/H_2O [33, 34]. However, no research in the literature reports that AuPt/C was made with mean particle size of AuPt NPs below 5 nm. The newest result was AuPt/C with an average particle size of ca. 5–6 nm made by the polyol method [37].

The microwave assisted EG (MW-EG) method was further developed by heating the reaction solution during the reduction reaction using microwave radiation, leading to the reduction time decrease from hours to 1 min [32] because of fast temperature rise rate and high localized temperatures at reaction sites [38]. More detailed mechanisms are not available in literature.

The overall reaction of EG method can be summarized as [39]:

$$2CH_2OHCH_2OH \xrightarrow{-2H_2O} 2CH_3CHO \xrightarrow{\text{Metalion}} CH_3COCOCH_3 + H_2O + \text{Metal} \qquad [2\text{-}7]$$

The metal NPs are formed by homogeneous nucleation and growth from the solution. A higher temperature helps to create more nuclei so as to get smaller particles; while an increase in the concentration of precursor causes the particle size to increase [39]. Higher dispersion can be achieved by replacing the homogenous nucleation with heterogeneous nucleation by adding external foreign nuclei or by producing the foreign nuclei in-situ [39]. When using the EG

method to make Pt/C, the surface groups on carbon black work as the seeds for heterogeneous nucleation. It was found that basic surface groups on carbon black result in high dispersion, while acidic groups give low dispersion [40].

2.1.4 Surface Redox Method

Surface redox method is so-called because the deposited Au complex on the Pt surface is reduced by redox reactions with the underlying Pt [41-43]. The driving force is from the difference in redox standard potential of both redox couples of metal/metal ion or complex. Unlike the UPD method, it does not involve an applied potential, and is thus immune to IR drop constraints, which makes it possible to prepare a large amount of catalyst. Though it is thermodynamically favorable, its weak nonspecific adsorption may be problematic in some cases. Appropriate conditions have to be determined by experiments.

Au deposition on Pt by surface redox reactions is thermodynamically favorable according to their redox standard potential as follows [44]:

$PtCl_4^{2-} + 2e^- = Pt + 4Cl^-$ $E°=0.73$ V

$PtCl_6^{2-} + 4e^- = Pt + 6Cl^-$ $E°=0.74$V

$AuCl_4^- + 3e^- = Au + 4Cl^-$ $E°=0.99$ V

The $AuCl_4^-$ can be reduced to metallic gold and Pt oxidized to either $PtCl_4^{2-}$ or $PtCl_6^{2-}$:

$3Pt+2AuCl_4^- +4Cl^- \rightarrow 3PtCl_4^{2-} +2Au$

$3Pt+4AuCl_4^- +2Cl^- \rightarrow 3PtCl_6^- +4Au$

The yield of $AuCl_4^-$ deposition on a Pt/SiO_2 is 100% when the atomic ratio of Au/Pt is less than 0.33 [43], and the $AuCl_4^-$ reduction rate is equal to 10^{17} atom of Au reduced per s and per m^2 of Pt [43].

Surface redox reactions require a very clean Pt NP surface. The EG method has the ability to make highly dispersed Pt NPs without the capping agent coating. A combination of EG method and surface redox method is proposed here to make AuPt/C. The Pt NPs or Pt/C was made by the EG method and then $AuCl_4^-$ was introduced, deposited, and spontaneously reduced on Pt NPs or Pt/C to get AuPt or AuPt/C. The former is then loaded on carbon black to get AuPt/C.

2.2 Characterization Methods

2.2.1 Transmission Electron Microscopy (TEM)

TEM is currently the only method to directly visualize the NPs and measure their particle size and distribution. Equipped with Energy-dispersive X-ray spectroscopy (EDX), it can also determine the surface composition of NPs in the scanning transmission electron microscopy (STEM) mode.

TEM uses an accelerated electron beam transmitting through the sample to form a two dimensional projection of the sample, which is further magnified by an electromagnetic lens system to generate an image [45]. A bright-field image is so-called because the transmitted beam and diffraction beams are both collected to form the image. It has rich information on topography. A dark field image is formed with certain diffraction beams without the transmitted beam. It gives crystallographic information. A high resolution TEM (HRTEM) image is a kind of bright-field image with very high resolution. With careful exclusion of the scattering beams from the substrate, such as the carbon film of the grid and the carbon support of Pt/C, the HRTEM can also give the crystallographic information from the lattice fringes.

Most modern TEM have a scanning mode, in which a nanosized electron bean is scanned

over the sample line by line. The emitted secondary electrons are collected to form an image. It could be clearer than a TEM image when the substrate of sample scatters the electrons severely. The electron beam scanning on the sample induces X-rays, and the characteristic X-rays are detected to form the EDX spectra for sample surface composition analysis.

As the penetration depth of electrons is usually low, thin TEM sample layers have to be prepared. In the particle size and components analysis, the catalyst dispersion has to be diluted very much and then spread onto a conducting grid and dried.

2.2.2 Cyclic Voltammetry

Cyclic Voltammetry is an electrochemical method utilizing control of potential. The working electrode is commonly imposed with a triangular potential-time waveform. The response current is recorded and displayed as cyclic voltammogram (CV). It is usually the first tool to study the mechanisms of electrochemical reactions. In the study of fuel cell electrocatalysts, it is mainly used to measure the electrochemically active surface area (ECSA).

A typical potential profile and CV of Pt/C (20% Pt, Etek) in 0.50 M H_2SO_4 are shown in Figure 2-2a and b respectively.

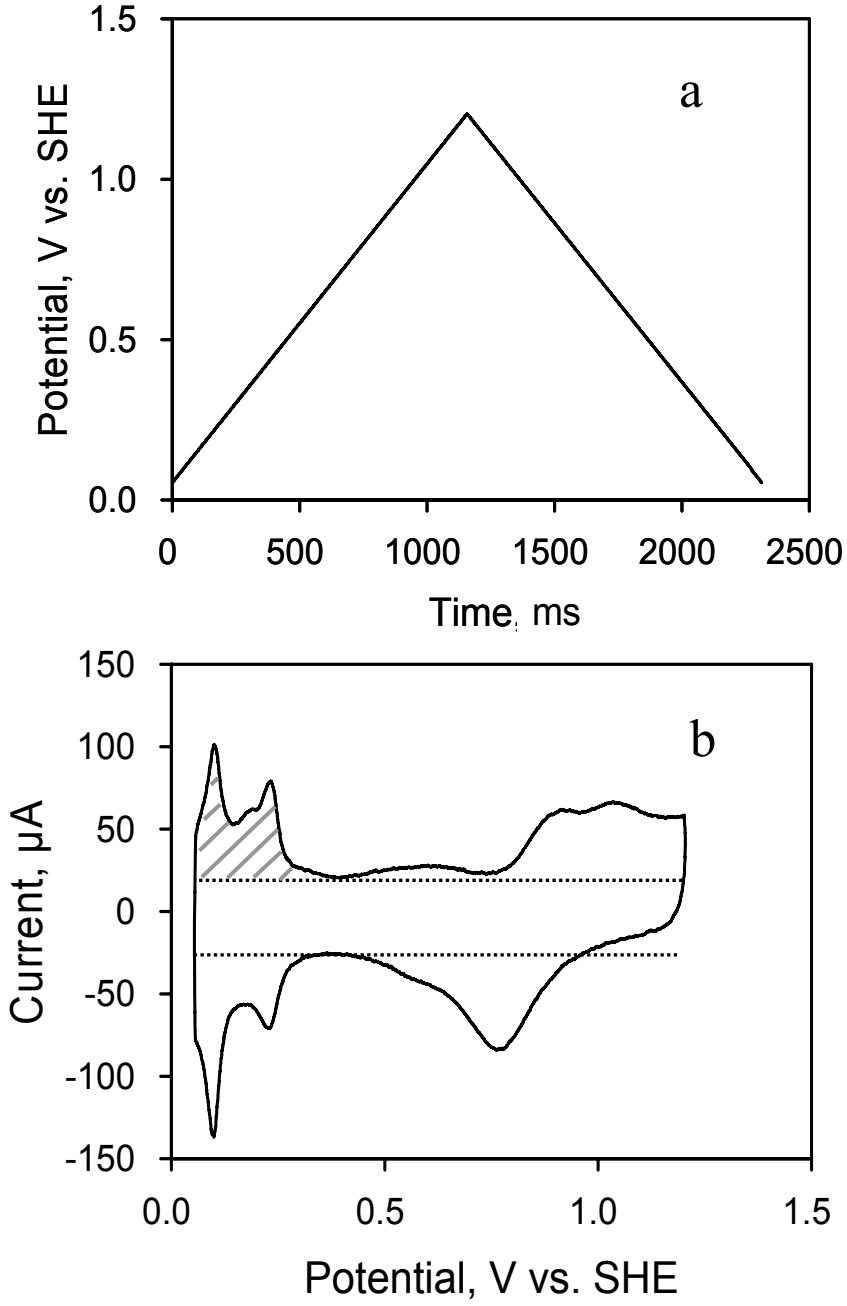

Figure 2-2. A triangular potential-time waveform (a) and CV (b) (from our lab)

Hydrogen underpotential deposition (H_{UPD}) occurs in the range of 0.05–0.35 V described as follows:

$$Pt + H^+ + e^- = Pt\text{-}H$$

where hydrogen is adsorbed on the Pt atom with ratio of 1:1. The total charge of monolayer H_{upd} on Pt NPs corresponds to the overall number of Pt surface atoms, which can be used to determine the ECSA of Pt/C [46]. The well-resolved H_{UPD} peaks mean that the Pt NPs have different index crystal faces on the surface. Equal distribution of the three low index planes ((111), (110) and (100)) was assumed to determine the ECSA [46].

In Figure 2-2b, the points at ca. 0.40 V and 0.35 V in the anodic and cathodic direction respectively are the places where no electrochemical reactions happen. They are so-called double layer region with current only from the charging of the electrochemical double layer. This current exists in the whole potential scanning range and is coupled with the current of electrochemical reactions. The upper dotted line represents the double layer charging current in the anodic direction; whereas the lower dotted line is the charging current in the cathodic direction.

When potential scanning above 0.4 V, carbon support oxidation starts and then follows with Pt oxidation with water.

The ECSA is quantified based on the total H_{UPD} desorption charge as shown in the equation below:

$$\mathrm{ECSA}\,[\mathrm{m^2 \cdot g^{-1}}] = \frac{(H_{UPD}\ \mathrm{charge}\,[\mu C]/210\,[\mu C \cdot \mathrm{cm}^2_{Pt}]) \times 10^{-4}}{\mathrm{catalyst\ mass}\,[g]} \qquad [2\text{-}8]$$

here the 210 $\mu C/cm_{Pt}^2$ [47] is the charge of monolayer hydrogen UPD on Pt with equal distribution of the three low index planes (111), (110) and (100). The total charge of H_{UPD} is represented by the shadow area in Figure 2-2b, which is equal to the total charge without the

double layer charge.

2.2.3 Rotating (Ring) Disk Electrode Method

Rotating (Ring) disk electrode method (R(R)DE) method is a type of hydrodynamic voltammetry with convective mass transport involved. The main advantages of R(R)DE [48] are that the steady flow pattern is built up rather quickly and the mass transfer to the electrode surface is faster than in the case of stationary electrodes where mass transfer is determined solely by diffusion. Consequently, the electron-transfer kinetics is less influenced by mass transfer in general than in the case of stationary electrodes, leading to a more precise measurement.

RDE measures a combination of kinetically determined resistances and diffusion resistances as shown by Koutecky-Levich equation below [48]:

$$\frac{1}{i} = \frac{1}{i_k} + \frac{1}{i_d} = \frac{1}{i_k} + \frac{1}{Bc_0\omega^{0.5}} \qquad [2\text{-}9]$$

where i_k and i_d are the kinetically and diffusion-limited current, respectively; the other parameters are the Levich constant B, the reactant concentration in the solution c_0, and the rotating speed of RDE ω.

The kinetic current is obtained by plotting 1/i against $1/\omega^{0.5}$, the so-called Koutecky–Levich (K-L) plot, and extending the rotating speed (ω) to infinity, where the diffusion resistance ($1/i_d$) has disappeared and $1/i = 1/i_k$.

As for a RRDE experiment, the species generated on the disk electrode can be transported to the ring electrode through radial convection. The species are thus detected with specific electrochemical reactions on the ring electrode at a potential controlled independently by a bi-potentiostat.

In this study, the ORR occurs on the Pt/C coated on the disk electrode of a R(R)DE. The

$2e^-$ ORR produces H_2O_2, which is transported to the ring electrode with a potential of 1.2 V vs. SHE. The H_2O_2 is quantified based on the ring current from its oxidation and the collection efficiency of R(R)DE.

Several things [48] need consideration in this experiment. In theory, the rotating rate of R(R)DE should in the range of about 100–10,000 rpm. In reality, the range is always narrower than this because of the limits of the electrode fabrication, the volume of electrochemical cell, and the alignment of the rotating axis, etc. At too low rotating rate, the hydrodynamic boundary layer becomes large, and when it approaches the disk radius, the calculation approximations for mass transport break down. At too high rotating rate, a steady flow pattern cannot be attained. The potential scan rate used in R(R)DE method is usually less than 20 mV/s. Too large scan rate causes the i-E curve to move away from an S-shape and produce a peak like a linear scan voltammetry [48].

When R(R)DE is used for powder electrocatalyst study, the catalyst (Pt/C and AuPt/C in this study) should be coated on the disk electrode of R(R)DE uniformly. Otherwise, the i-E curve deviates from an S-shape as shown in Figure 2-3 and the collection efficiency is different with the design number. Also the electrocatalyst coating should not cross the gap between the disk and ring, which connects the ring and disk electrodes, leading to a mixture of ring and disk current.

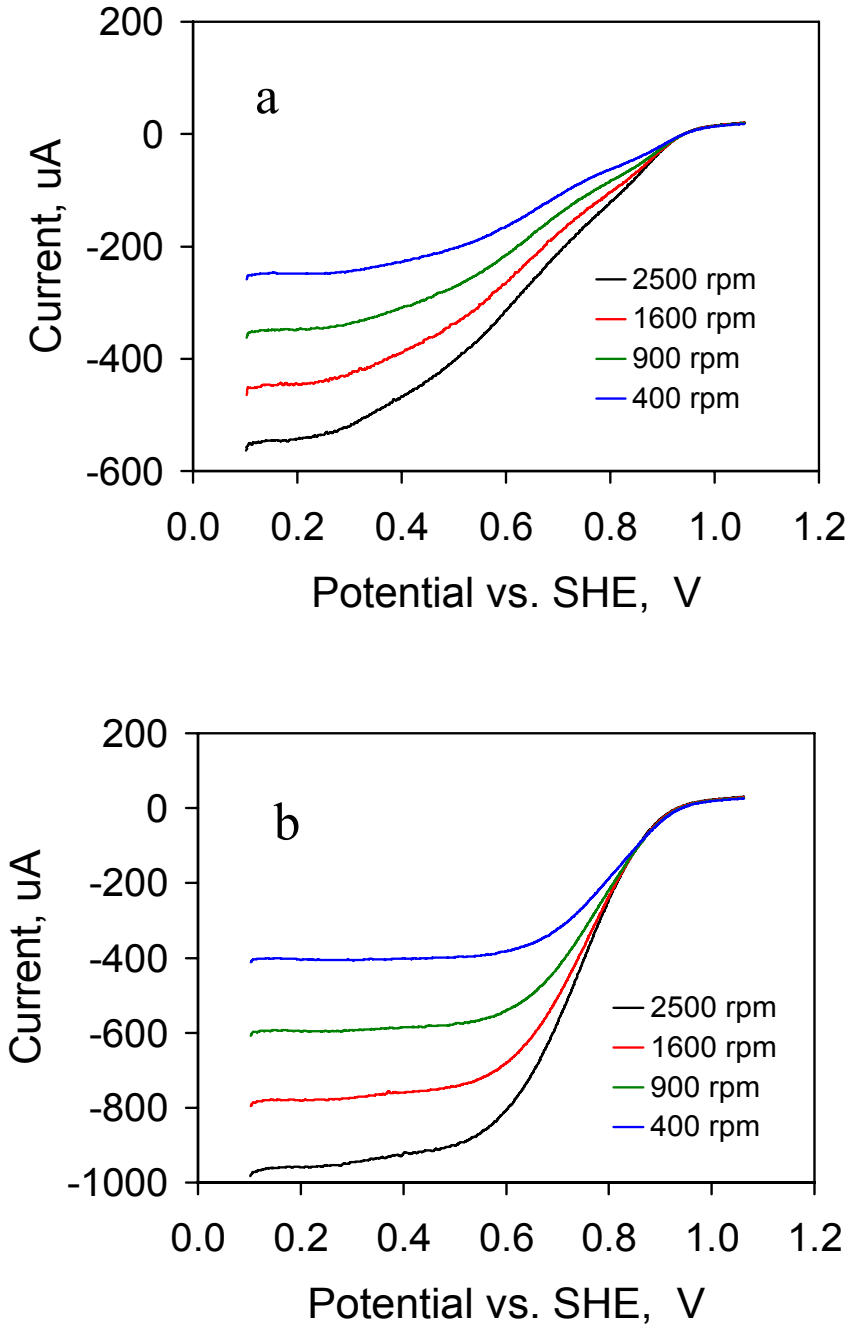

Figure 2-3. Disk current of RDE with catalyst uneven coating (a) and even coating (b) (from our lab)

2.2.4 Differential Electrochemical Mass Spectrometry

Cyclic voltammetry is always the first tool to investigate electrochemical reactions, and it is commonly used to investigate cathode degradation mechanisms. However, it has limitations. For instance, the anodic current signals from the two main reactions, carbon support corrosion (CSC) and platinum dissolution caused by platinum oxidation, overlap and are impossible to resolve. Coupling cyclic voltammetry with a mass spectrometer can overcome this limit by identifying the volatile products from CSC.

Differential electrochemical mass spectrometry (DEMS) [15, 49] uses an online mass spectrometer to sample gases from the working electrode in the electrochemical cell, with potential cycling imposed by an electrochemical potentiostat. DEMS has the capability to resolve the current of CSC producing CO_2 from that of Pt redox, which makes it a powerful tool to investigate in-situ the mechanisms and kinetics of CSC at the PEMFC cathode. It also makes it easier to model CSC using the DEMS spectrum, because it does not have the double layer current.

Willsau [50] made a systematic investigation of CSC in gas diffusion electrodes in liquid electrolyte under simulated conditions of PEMFC using DEMS. Reon [51] and Masss [52] confirmed the results using DEMS and online non-dispersive IR respectively in real PEMFC conditions with humidified helium at the cathode. Roen [51] did not offer an explanation for all observed phenomena while Maass [52] gave a systematic investigation and explanation. However, they did not correlate Pt redox reaction to carbon support corrosion and also did not indicate what oxidation state of Pt has catalytic effects on CSC.

We have succeeded in characterizing carbon support corrosion and Pt redox reactions at the same time by measuring the exhaust gases from the cathode of a 5 cm^2 single PEMFC, which

is significantly smaller than the cell used by Roen [51] and Maass [52]. The DEMS spectra of CO_2, H_2 and O_2 can characterize most reactions at cathode and indicate what oxidation state of Pt has catalytic effects on CSC. Isotope labeling using oxygen-18 enriched water helps to further explore the mechanisms by determining the oxygen sources and verifying the pathways. Besides, the small area MEA requirement makes it convenient to compare different catalysts in research labs.

References:

1. Bond, G.C., *The Electronic Structure of Platinum-Gold Alloy Particles.* Platinum Met. Rev., 2007. **51**(2): p. 63.

2. Teng, X., M. Feygenson, Q. Wang, J. He, W. Du, A.I. Frenkel, W. Han, and M. Aronson, *Electronic and Magnetic Properties of Ultrathin Au/Pt Nanowires.* Nano Lett., 2009. **9**(9): p. 3177-3184.

3. Kolb, D.M., M. Przasnyski, and H. Gerischer, *Underpotential deposition of metals and work function differences.* J. Electroanal. Chem., 1974. **54**(1): p. 25-38.

4. Budevski, E., G. Staikov, and W.J. Lorenz, *Electrochemical Phase Formation and Growth*. 1996, Weinheim-New York-Basel-Cambridge-Tokyo: VCH.

5. Bakos, I. and S. Szab, *Study of electrochemical gold adsorption on polycrystalline platinum substrates.* J. Electroanal. Chem., 1993. **344**(1-2): p. 303-311.

6. Prati, L. and M. Rossi, *Gold on Carbon as a New Catalyst for Selective Liquid Phase Oxidation of Diols.* J. Catal., 1998. **176**(2): p. 552-560.

7. Wigmans, T., J. van Doorn, and J.A. Moulijn, *Deactivation of nickel during gasification of activated carbon, studied by X-ray photoelectron spectroscopy.* Surf. Sci., 1983. **135**(1-3): p. 532-552.

8. Prinsloo, F.F., D. Hauman, and R. Slabbert. in Carbon'01, International Conference on Carbon. 2001. Lexington, KY.

9. Toebes, M.L., M.K. van der Lee, L.M. Tang, M.H. Huis in `t Veld, J.H. Bitter, A.J. van Dillen, and K.P. de Jong, *Preparation of Carbon Nanofiber Supported Platinum and Ruthenium Catalysts: Comparison of Ion Adsorption and Homogeneous Deposition Precipitation.* J. Phys. Chem. B, 2004. **108**(31): p. 11611-11619.

10. Jhung, S.H., J.-H. Lee, J.-M. Lee, J.H. Lee, D.-Y. Hong, M.W. Kim, and J.-S. Chang*, *Effect of Preparation Conditions on the Hydrogenation Activity and Metal Dispersion of Pt/C and Pd/C Catalysts.* Bull. Korean Chem. Soc., 2005. **26**(4): p. 563.

11. H. Bönnemann, R.B., P. Britz, U. Endruschat, R. Mörtel, U. A. Paulus, G. J. Feldmeyer, T. J. Schmidt, H. A. Gasteiger and R. J. Behm, *Nanoscopic Pt-bimetal colloids as precursors for PEM fuel cell catalysts.* J. New Mater. Electrochem. Syst., 2000. **3**: p. 199.

12. Mellor, J.W., *A Comprehensive Treatise on Inorganic and Theoretical Chemistry*. Vol. III. 1923, London: Longmans, Green & Co.

13. Watanabe, M., M. Uchida, and S. Motoo, *Preparation of highly dispersed Pt + Ru alloy clusters and the activity for the electrooxidation of methanol.* J. Electroanal. Chem., 1987.

229(1-2): p. 395-406.

14. Bönnemann, H., W. Brijoux, R. Brinkmann, R. Fretzen, T. Joussen, R. Köppler, B. Korall, P. Neiteler, and J. Richter, *Preparation, characterization, and application of fine metal particles and metal colloids using hydrotriorganoborates.* J. Mol. Catal., 1994. **86**(1-3): p. 129-177.

15. Baltruschat, H., *Differential electrochemical mass spectrometry.* J. Am. Soc. Mass Spectrom., 2004. **15**(12): p. 1693-1706.

16. Kenjiro Meguro, M.T., Kunio Esumi, *The Preparation of Organo Colloidal Precious Metal Particles.* Bull. Chem. Soc. Jpn., 1988. **61**: p. 341-345.

17. Freeman, R.G., K.C. Grabar, K.J. Allison, R.M. Bright, J.A. Davis, A.P. Guthrie, M.B. Hommer, M.A. Jackson, P.C. Smith, D.G. Walter, and M.J. Natan, *Self-Assembled Metal Colloid Monolayers: An Approach to SERS Substrates.* Science, 1995. **267**(5204): p. 1629-1632.

18. Grabar, K.C., K.J. Allison, B.E. Baker, R.M. Bright, K.R. Brown, R.G. Freeman, A.P. Fox, C.D. Keating, M.D. Musick, and M.J. Natan, *Two-Dimensional Arrays of Colloidal Gold Particles: A Flexible Approach to Macroscopic Metal Surfaces.* Langmuir, 1996. **12**(10): p. 2353-2361.

19. Grabar, K.C., R.G. Freeman, M.B. Hommer, and M.J. Natan, *Preparation and Characterization of Au Colloid Monolayers.* Anal. Chem., 2002. **67**(4): p. 735-743.

20. Grabar, K.C., P.C. Smith, M.D. Musick, J.A. Davis, D.G. Walter, M.A. Jackson, A.P. Guthrie, and M.J. Natan, *Kinetic Control of Interparticle Spacing in Au Colloid-Based Surfaces: Rational Nanometer-Scale Architecture.* J. Am. Chem. Soc., 1996. **118**(5): p. 1148-1153.

21. Dubau, L., F. Hahn, C. Coutanceau, J.M. Léger, and C. Lamy, *On the structure effects of bimetallic PtRu electrocatalysts towards methanol oxidation.* J. Electroanal. Chem., 2003. **554-555**: p. 407-415.

22. Dubau, L., C. Coutanceau, E. Garnier, J.M. Léger, and C. Lamy, *Electrooxidation of methanol at platinum–ruthenium catalysts prepared from colloidal precursors: Atomic composition and temperature effects.* J. Appl. Electrochem., 2003. **33**(5): p. 419-429.

23. Schmidt, T.J., M. Noeske, H.A. Gasteiger, R.J. Behm, P. Britz, and H. Bonnemann, *PtRu Alloy Colloids as Precursors for Fuel Cell Catalysts.* J. Electrochem. Soc., 1998. **145**(3): p. 925-931.

24. Brimaud, S., C. Coutanceau, E. Garnier, J.M. Léger, F. Gérard, S. Pronier, and M. Leoni, *Influence of surfactant removal by chemical or thermal methods on structure and electroactivity of Pt/C catalysts prepared by water-in-oil microemulsion.* J. Electroanal.

Chem., 2007. **602**(2): p. 226-236.

25. Luo, J., M.M. Maye, V. Petkov, N.N. Kariuki, L. Wang, P. Njoki, D. Mott, Y. Lin, and C.-J. Zhong, *Phase Properties of Carbon-Supported Gold&-Platinum Nanoparticles with Different Bimetallic Compositions.* Chem. Mater., 2005. **17**(12): p. 3086-3091.

26. Brust, M., M. Walker, D. Bethell, D.J. Schiffrin, and R. Whyman, *Synthesis of thiol-derivatised gold nanoparticles in a two-phase Liquid-liquid system.* J. Chem. Soc., Chem. Commun., 1994: p. 801-802.

27. Kim, T., M. Takahashi, M. Nagai, and K. Kobayashi, *Preparation and characterization of carbon supported Pt and PtRu alloy catalysts reduced by alcohol for polymer electrolyte fuel cell.* Electrochim. Acta, 2004. **50**(2-3): p. 817-821.

28. Gun, J., D. Rizkov, O. Lev, M. Abouzar, A. Poghossian, and M. Schöning, *Oxygen plasma-treated gold nanoparticle-based field-effect devices as transducer structures for bio-chemical sensing.* Microchim. Acta, 2009. **164**(3): p. 395-404.

29. Guo, D., S. Entani, S. Ikeda, and K. Saiki, *Effect of UV/ozone treatment of the dielectric layer on the device performance of pentacene thin film transistors.* Chem. Phys. Lett., 2006. **429**(1-3): p. 124-128.

30. Liu, Z., M. Shamsuzzoha, E.T. Ada, W.M. Reichert, and D.E. Nikles, *Synthesis and activation of Pt nanoparticles with controlled size for fuel cell electrocatalysts.* J. Power Sources, 2007. **164**(2): p. 472-480.

31. Figlarz, M., F. Fievet, and J.P. Lagier, *Process for the reduction of metallic compounds by polyols, and metallic powders obtained by this process*. 1988.

32. Chen, W.X., J.Y. Lee, and Z. Liu, *Microwave-assisted synthesis of carbon supported Pt nanoparticles for fuel cell applications.* Chem. Comm., 2002(21): p. 2588-2589.

33. Li, W., C. Liang, W. Zhou, J. Qiu, Z. Zhou, G. Sun, and Q. Xin, *Preparation and Characterization of Multiwalled Carbon Nanotube-Supported Platinum for Cathode Catalysts of Direct Methanol Fuel Cells.* J. Phys. Chem. B, 2003. **107**(26): p. 6292-6299.

34. Zhou, Z., S. Wang, W. Zhou, G. Wang, L. Jiang, W. Li, S. Song, J. Liu, G. Sun, and Q. Xin, *Novel synthesis of highly active Pt/C cathode electrocatalyst for direct methanol fuel cell.* Chem. Comm., 2003(3): p. 394-395.

35. Oh, H.S., J.G. Oh, Y.G. Hong, and H.S. Kim, *Investigation of carbon-supported Pt nanocatalyst preparation by the polyol process for fuel cell applications.* Electrochim. Acta, 2007. **52**(25): p. 7278-7285.

36. Oh, H.-S., J.-G. Oh, and H. Kim, *Modification of polyol process for synthesis of highly platinum loaded platinum-carbon catalysts for fuel cells.* J. Power Sources, 2008. **183**(2):

p. 600-603.

37. Senthil Kumar, S. and K.L.N. Phani, *Exploration of unalloyed bimetallic Au-Pt/C nanoparticles for oxygen reduction reaction.* J. Power Sources, 2009. **187**(1): p. 19-24.

38. Komarneni, S., D. Li, B. Newalkar, H. Katsuki, and A.S. Bhalla, *Microwave-polyol Process for Pt and Ag Nanoparticles.* Langmuir, 2002. **18**(15): p. 5959-5962.

39. Fievet, F., J.P. Lagier, B. Blin, B. Beaudoin, and M. Figlarz, *Homogeneous and heterogeneous nucleations in the polyol process for the preparation of micron and submicron size metal particles.* Solid State Ionics, 1989. **32-33**(Part 1): p. 198-205.

40. Kim, S. and S.-J. Park, *Effect of acid/base treatment to carbon blacks on preparation of carbon-supported platinum nanoclusters.* Electrochim. Acta, 2007. **52**(9): p. 3013-3021.

41. Del Angel, P., J.M. Dominguez, G. Del Angel, J.A. Montoya, E. Lamy-Pitara, S. Labruquere, and J. Barbier, *Aggregation State of Pt-Au/C Bimetallic Catalysts Prepared by Surface Redox Reactions.* Langmuir, 2000. **16**(18): p. 7210-7217.

42. Del Angel, P., J.M. Dominguez, G. Del Angel, J.A. Montoya, J. Capilla, E. Lamy-Pitara, and J. Barbier, *Selective Modification of Pt Active Sites on Pt–Au/C Catalysts Prepared by Surface Redox Reactions.* Top. Catal., 2002. **18**(3): p. 183-191.

43. Barbier, J., P. Marécot, G. Del Angel, P. Bosch, J.P. Boitiaux, B. Didillon, J.M. Dominguez, I. Schiftef, and G. Espmosa, *Preparation of platinum-gold bimetallic catalysts by redox reactions.* Appl. Catal. A: General, 1994. **116**(1-2): p. 179-186.

44. Charlot, G., J. Badoz-Lambing, and B. Trémillon, *Les réactions électrochimiques*. 1959, Mason et Cie, Paris.

45. Williams, D.B. and C.B. Carter, *Transmission Electron Microscopy: A Textbook for Materials Science*. 1st ed. 2004: Springer. 703.

46. Biegler, T., D.A.J. Rand, and R. Woods, *Limiting oxygen coverage on platinized platinum; Relevance to determination of real platinum area by hydrogen adsorption.* J. Electroanal. Chem., 1971. **29**(2): p. 269-277.

47. Bagotzky, V.S. and Y.B. Vassilyev, *Mechanism of electro-oxidation of methanol on the platinum electrode.* Electrochim. Acta, 1967. **12**(9): p. 1323-1343.

48. Bard, A.J. and L.R. Faulkner, *Electrochemical Methods: Fundamentals and Applications*. 2 ed. 2001, New York: Wiley.

49. Bruckenstein, S. and R.R. Gadde, *Use of a porous electrode for in situ mass spectrometric determination of volatile electrode reaction products.* J. Am. Chem. Soc., 1971. **93**(3): p. 793-794.

50. Willsau, J. and J. Heitbaum, *The influence of Pt-activation on the corrosion of carbon in gas diffusion electrodes--A dems study.* J. Electroanal. Chem., 1984. **161**(1): p. 93-101.

51. Roen, L.M., C.H. Paik, and T.D. Jarvi, *Electrocatalytic Corrosion of Carbon Support in PEMFC Cathodes.* Electrochem. Solid-State Lett., 2004. **7**(1): p. A19-A22.

52. Maass, S., F. Finsterwalder, G. Frank, R. Hartmann, and C. Merten, *Carbon support oxidation in PEM fuel cell cathodes.* J. Power Sources, 2008. **176**(2): p. 444-451.

CHAPTER 3

INVESTIGATION OF PLATINUM CATALYTIC EFFECTS ON CARBON SUPPORT CORROSION OF THE CATHODE CATALYST IN PEM FUEL CELLS USING DEMS SPECTRA

3.1. Introduction

Carbon support corrosion (CSC) [1] is a major factor causing cathode catalyst (platinum nanoparticles on carbon black, Pt/C) degradation in proton exchange membrane fuel cells (PEMFC) [2-5], and has been extensively studied recently [6-17]. However, there is still no well accepted mechanism. Generally, the electrochemical oxidation of carbon black in an acid solution proceeds by two consecutive reaction steps as follows [1]:

$$C + [O^{2-}] = CO_{surf} + 2e^{-} \quad [1\text{-}1]$$

$$CO_{surf} + [O^{2-}] = CO_2 + 2e^{-} \quad [1\text{-}2]$$

The $[O^{2-}]$ represents reduced states of oxygen in the form of H_2O, OH^{-}, and/or an oxide film on platinum (PtO or PtOH), which were claimed as the sources of oxygen.

It was postulated that nanoparticle Pt catalyzes the CSC by transferring the O and/or OH to the carbon [6-8, 18]. However, there are no substantiated experimental results determining what oxidation states of Pt have these catalytic effects and how they achieve them.

Differential electrochemical mass spectrometry (DEMS) [19, 20] employs an online mass spectrometer to sample gases from the working electrode in the electrochemical cell, with

potential cycling imposed by a potentiostat. It has been used to investigate CSC in gas diffusion electrodes in sulfuric acid under PEMFC simulated conditions [8] and in a real PEMFC [6]. However, they did not characterize Pt-catalyzed ORR and Pt electrochemical redox reactions, correlate them to CSC in DEMS spectra, nor identify what oxidation states of Pt have these catalytic effects on CSC.

This work characterizes the Pt-catalyzed ORR and Pt electrochemical redox reactions, as well as correlates them to CSC in DEMS spectra, based on the measurement of the exhaust gases, CO_2, H_2 and O_2, from the cathode of a 5 cm^2 single PEMFC. The oxidation states of Pt with different catalytic capacity for CSC are elucidated.

3.2. Experimental

Two 5 cm^2 square membrane electrode assemblies (MEA) with different cathodes were fabricated by hot-pressing an anode, a piece of Nafion 1135 membrane (DuPont) and a cathode together, and then assembled in a 5 cm^2 single cell hardware (Electrochem.) for testing. Carbon paper (TGP-H-060, Toray**)** was coated with 0.5 mg/cm^2 carbon black (Vulcan 72R, Cabot) on one side as a diffusion layer and then the entire sample was loaded with 20 wt% Teflon (Aldrich). Two identical anodes and one cathode (Pt/C cathode) were brushed with 0.5 mg_{Pt}/cm^2 catalyst (20 wt% Pt/C, E-Tek) on the diffusion layer. The other cathode (C cathode) was brushed with 2 mg/cm^2 carbon black only. Both catalyst and carbon black ink used for coating contained 20 wt% Nafion® polymer (Aldrich).

A fuel cell test station was made to control the temperatures, mass flow rates and humidities. H_2 (UHP, Airgas, 50 sccm) and He (UHP, Airgas, 30 sccm), both fully humidified at 30 °C, were fed to the anode and cathode, respectively. A quadrupole mass spectrometer (QIC-

20, Hiden Analytical) was coupled online to sample gases from the outlet of the cathode, with potential cycling imposed from 100 to 1400 mV at 10 mV/s scan rate using a bipotentiostat (AFCBP1, Pine instrument).

The anode of the MEA, referred to the dynamic hydrogen electrode (DHE), worked as counter and reference electrode. All potentials given in this paper refer to this DHE.

3.3. Results and Discussion

Carbon support corrosion main product CO_2 and platinum redox probe gases H_2 and O_2, exiting together from the cathode during potential cycling, were detected by a mass spectrometer. The cyclic voltammogram (CV) is shown in Figure 3-1a. The mass spectrometry (MS) spectra of CO_2 (m/z = 44) and H_2 (m/z = 2) in Figure 3-1b were turned into the DEMS spectra in Figure 3-1c by indentifying the potentials using the CO_2 MS signal at 1400 mV as a reference mark. This potential is where the CO_2 signal achieves the maximum with the largest overpotential for CSC in this CV range. Similarly, DEMS spectrum of O_2 was obtained and shown in Figure 3-1d. H_2 and O_2 DEMS spectra in Figure 3-1c and d were presented here for the first time and their plateau features were utilized to characterize Pt redox and Pt-catalyzed ORR in this work.

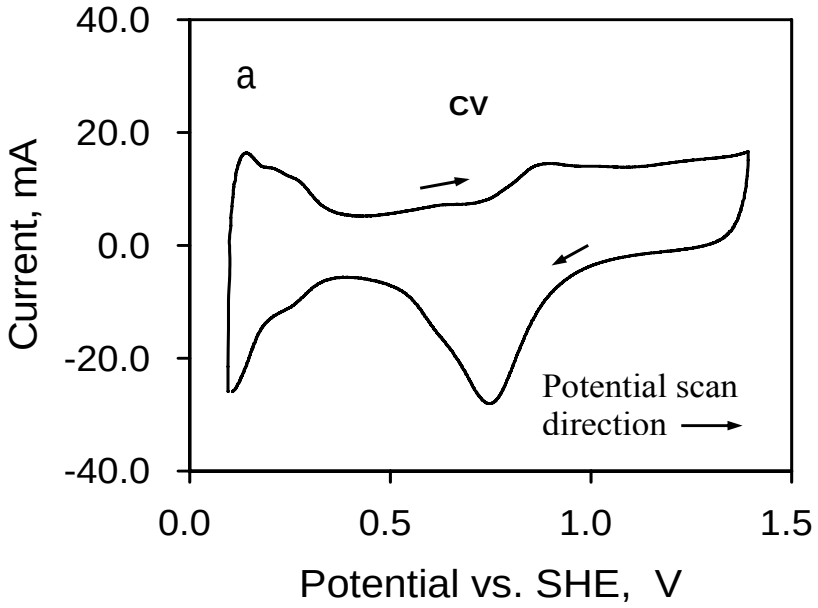
a
cv
Current, mA
40.0
20.0
0.0
-20.0
-40.0
0.0
0.5
1.0
1.5
Potential vs. SHE, V
Potential scan
direction

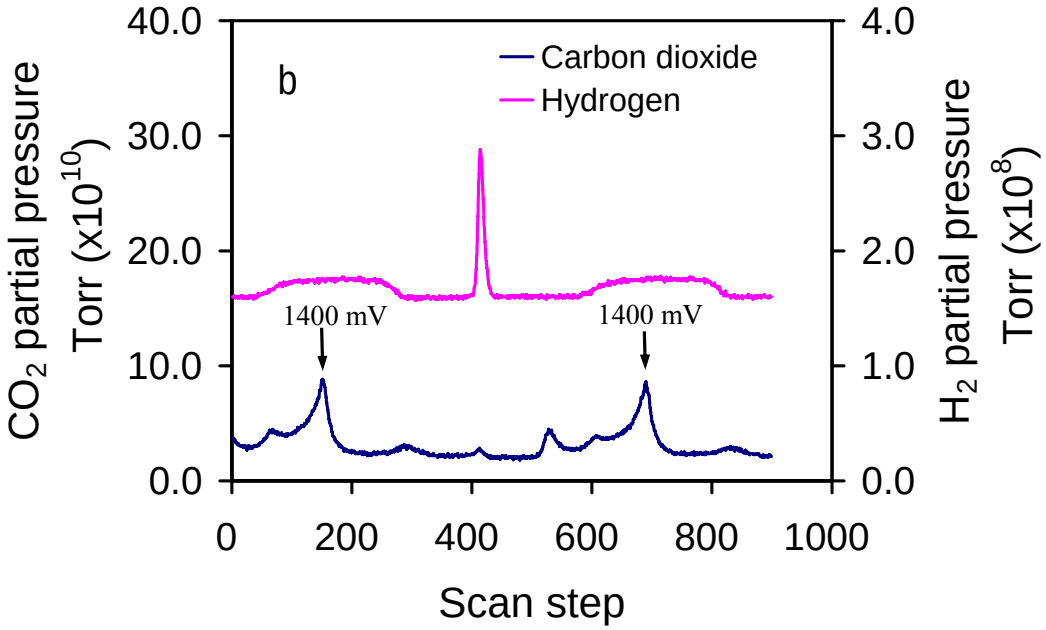
b
Carbon dioxide
Hydrogen
1400 mV
1400 mV
CO2 partial pressure
Torr (x10^10)
H2 partial pressure
Torr (x10^8)
40.0
30.0
20.0
10.0
0.0
4.0
3.0
2.0
1.0
0.0
0
200
400
600
800
1000
Scan step

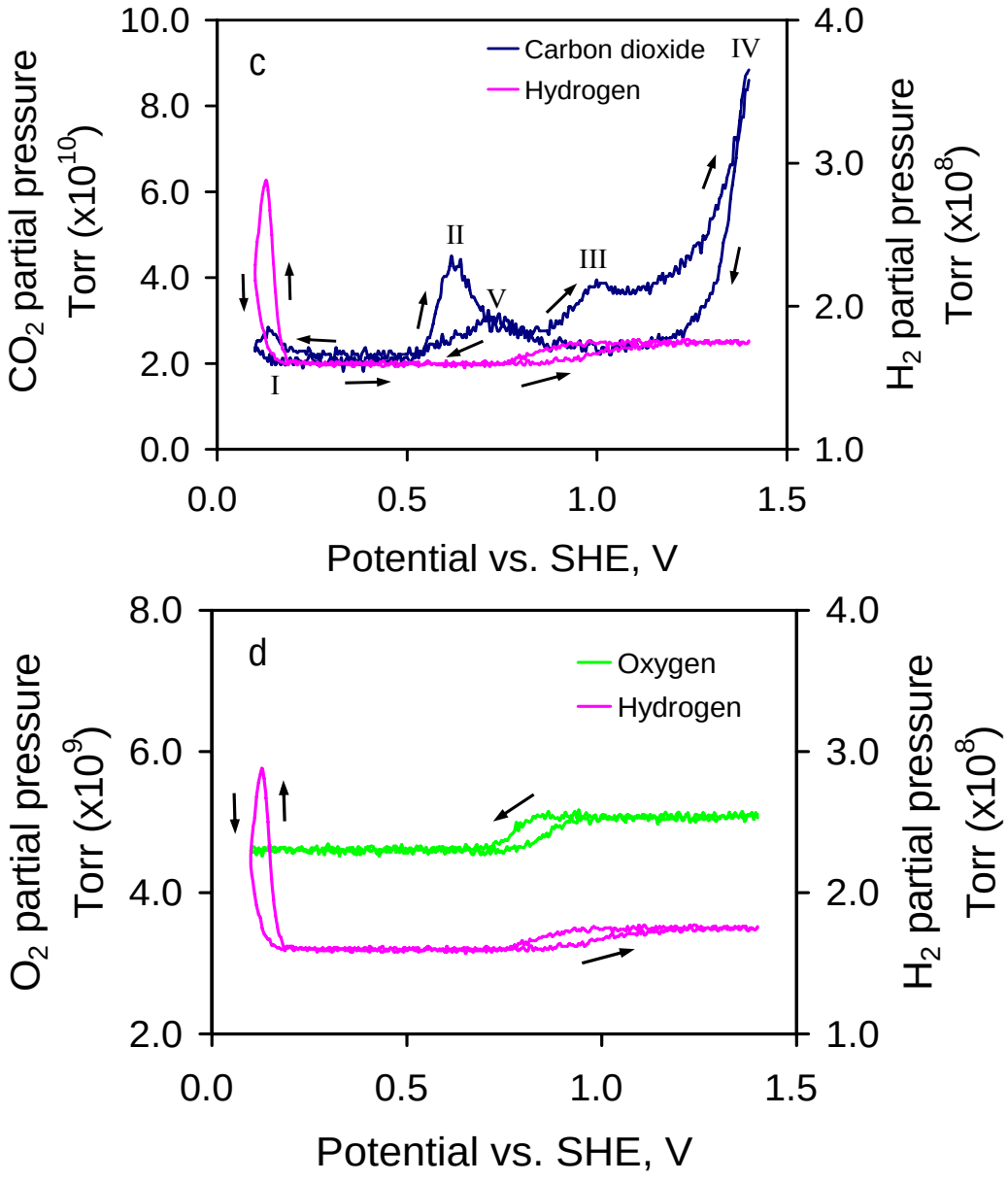

Figure 3-1. Pt/C cathode DEMS spectra 30 °C: (a) CV; (b) MS spectra of H_2 and CO_2 (scan step means the mass spectrometer data acquisition step. The numbers on axis are relative.); (c) DEMS spectra of H_2 and CO_2; (d) DEMS spectra of H_2 and O_2

CO_2 DEMS spectrum in Figure 3-1c has five peaks located at 100 mV (I), 600 mV (II), 1000 mV (III) and 1400 mV (IV) in anodic direction and at 750 mV (V) in cathodic direction respectively, which are consistent with those in the literature [6-8]. However, there are only two maximum CO_2 signals at 100 mV and 1400 mV for the carbon cathode in Figure 3-2. Three more peaks for the Pt/C cathode suggest it has additional reactions contributing to the carbon support corrosion. In addition, it has stronger CO_2 signals at 100 mV and 1400 mV than those of the C cathode. Both imply that Pt with certain oxidation states catalyzes the carbon support corrosion by different pathways.

A small part of overpotential deposition hydrogen (H_{OPD}) on metallic Pt is believed to extend to the underpotential deposition hydrogen (H_{UPD}) region [21]. The small hydrogen peak shown in 0.1–0.2 V in Figure 3-1b, c and d could be attributed to it. It is not strongly related to this paper and we will publish it elsewhere.

The H_2 at the anode permeates through the membrane to the cathode and undergoes the hydrogen oxidation reaction (HOR) on metallic Pt. With a very small permeation rate, the reversible HOR on Pt becomes mass transfer limited with even a small overpotential. It forms the H_2 DEMS spectrum baseline between 0.2–0.7 V in Figure 3-1c and d. Similarly, a small amount of O_2 leaks into the cathode from the environment. It also forms O_2 DEMS spectrum baseline because of mass transfer limitations with high ORR rate but at high overpotential starting from 0.1 V to 0.7 V in Figure 3-1d. Both H_2 and O_2 baselines reveal the Pt in metallic state between 0.1–0.7 V. Thus, peaks I and II of the CO_2 DEMS spectrum are attributed to the chemical oxidation of carbon by H_2O_2 from the $2e^-$ ORR [22] and the electrochemical oxidation of CO with water on Pt [23] respectively, and are catalyzed by metallic Pt. Furthermore, because there is no significant O_2 signal change at around 0.6 V, the O_2 does not directly contribute to the peak

II as a reactant.

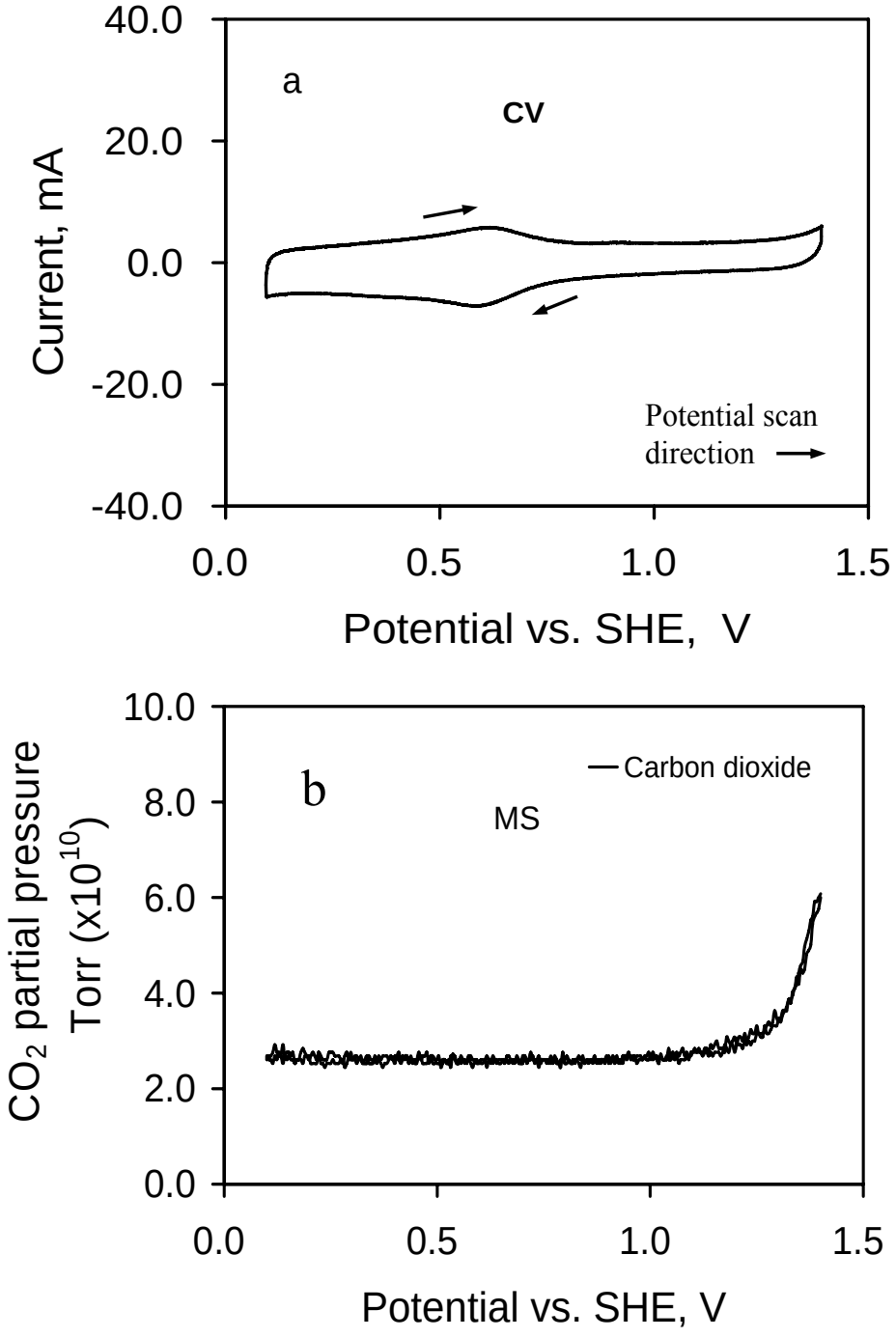

Figure 3-2. C cathode DEMS spectra at 30 °C: (a) CV; (b) DEMS spectra of CO_2

In Figure 3-1c, as the potential increases to ca. 0.9 V, the H_2 signal starts to increase, which means that the HOR consumes less H_2 with overpotential increase. This is opposite to that expected from electrochemical kinetics, and therefore the surface of Pt must undergo changes. It is due to Pt electrochemical oxidation with water to form an oxide film, which reduces the fraction of metallic Pt at surface so as to decrease the active sites for HOR resulting in the H_2 signal increase in Figure 3-1c and d.

The O_2 signal starts to increase after ca. 0.75 V in the anodic scan in Figure 3-1d as the overpotential of the ORR decreases. Thus the increase could be attributed to the ORR rate decreasing significantly because of overpotential decrease. Admittedly, it also could be that active sites on the Pt surface decrease due to Pt electrochemical oxidation after ca. 0.9 V resulting in less O_2 consumption.

The CV in Figure 3-1a shows the anodic current starting to increase at ca. 0.75 V and achieving a local maximum at ca. 0.9 V. It corresponds to the O_2 DEMS signal increase in the anodic direction in Figure 3-1d. The ORR current is quite small compared with the Pt oxidation current because of the very small O_2 partial pressure in this case. Notice that no significant current change was observed even between 0.4–0.5 V in the CV, where the ORR rate should be rather large. Thus the current increase starting at ca. 0.75 V in the CV should be attributed to Pt electrochemical oxidation.

However, as discussed above, the H_2 DEMS signals in Figure 3-1c and d do not start to increase until ca. 0.9 V. This implies that the Pt oxide formed starting at ca. 0.75 V does not influence the HOR or is not large enough to cause a significant rate decrease, but the Pt oxide formed after ca. 0.9 V does. It can be concluded now that there are at least two types of Pt oxides formed between 0.75–1.1 V. It has been demonstrated that there are Pt oxides of Pt_4OH, Pt_2OH

and PtOH formed in sequence between 0.75–1.1 V, in which PtOH formation starts at 0.9 V and a monolayer OH is formed at 1.1 V [24]. Therefore, Pt oxidation below a monolayer can be divided into two stages, stage I of Pt_4OH and Pt_2OH and stage II of PtOH. They were indicated by the O_2 and H_2 DEMS spectra plateaus respectively.

CO_2 DEMS signals in Figure 3-1c keep significantly increasing with potential increase between 0.75–0.9 V, compared with that in Figure 3-2. It implies that the CSC is catalyzed by Pt_4OH and Pt_2OH, which are characterized by increased O_2 DEMS signal. Peak III occurs coincidently with OH formation at ca. 0.9 V in Figure 3-1c, which is characterized by increased H_2 DEMS signal. It suggests that PtOH has a larger catalytic effect; the difference could come from its capacity to supply OH.

The H_2 DEMS spectrum reaches a local maximum at ca. 1.1 V, where a monolayer of OH is formed on Pt surface [24] and could completely cover the original active sites for HOR and ORR. To make matters worse, Pt with higher oxidation states and a multilayer oxide film are formed after 1.1 V [24]. The H_2 DEMS signals stay at the maximum until the potential is scanned back to around 1.0 V and then decrease till ca. 0.75 V. Similarly, the O_2 signals stay at the maximum until the potential is scanned back around 0.85 V and then decrease till ca. 0.65 V. Compared with the signal increase in the anodic direction, both signals start to decrease at a lower potential in the cathodic scan, which is caused by slow removal of the oxide film [22].

After Pt surfaces are covered with Pt oxides completely, the CO_2 DEMS signal in Figure 3-1c still exponentially increases faster than that in Figure 3-2 till the maximum at 1400 mV (peak IV). It means that catalytic effects contribute to this higher corrosion rate. PtO, higher oxidation state Pt oxides and a multilayer oxide film are possible catalysts for CSC in this range.

When He was fed to cathode, the partial pressure of the O_2 was ca. 5e-9 Torr at 1.0 V,

which was about 10 times of the CO_2 partial pressure in Figure 3-1c and d. At 1.4 V, the CO_2 partial pressure increased about 2 fold but the O_2 partial pressure was almost same. We can conclude that the O_2 is not the reactant of CSC to produce CO_2 in the range of 1.0–1.4 V.

The reverse anodic CO_2 peak V [6-8] in Figure 3-1c is located at ca. 750 mV in the cathodic scan and coincides with the reduction of the platinum oxides in the CV (Figure 3-1a), and characterized by decreased H_2 and O_2 DEMS signals. The OH released from the reduction of the Pt oxide film [25] could be the catalytic mechanism for CSC by Pt oxides at peak V.

3.4. Conclusions

We presented H_2, O_2 and CO_2 differential electrochemical mass spectrometry (DEMS) spectra of a small 5 cm^2 MEA to characterize and correlate the Pt redox reactions, Pt-catalyzed ORR, and carbon support corrosion (CSC) of a cathode catalyst in a PEMFC. The H_2 and O_2 DEMS spectra baselines between 0.1–0.75 V show Pt is in a metallic state with catalytic effects on CO_2 peaks I and II. The H_2 and O_2 DEMS spectra plateaus combined with CV illustrated that there are different types of sub-monolayer Pt oxides formed between 0.75–1.1 V with different catalytic capacities for CSC. Above 1.1 V, PtO, higher oxides and multilayers are formed that catalyze the CSC. Identification of catalytic capacity of Pt with different oxidation states at each CO_2 peak of CSC helps to further understand the CSC mechanisms.

References:

1. Kinoshita, K., *Carbon Electrochemical and Physicochemical Properties*. 1988, New York: Wiley.

2. Kinoshita, K., J.T. Lundquist, and P. Stonehart, *Potential cycling effects on platinum electrocatalyst surfaces.* J. Electroanal. Chem., 1973. **48**(2): p. 157-166.

3. Komanicky, V., K.C. Chang, A. Menzel, N.M. Markovic, H. You, X. Wang, and D. Myers, *Stability and Dissolution of Platinum Surfaces in Perchloric Acid.* J. Electrochem. Soc., 2006. **153**(10): p. B446-B451.

4. Canullo, J.C., W.E. Triaca, and A.J. Arvia, *Electrochemical faceting of single crystal platinum electrodes.* J. Electroanal. Chem., 1986. **200**(1-2): p. 397-400.

5. Egli, W.A., A. Visintin, W.E. Triaca, and A.J. Arvia, *The development of facetting and roughening at platinum polyfacetted single-crystal electrodes in a chloroplatinic acid solution.* Appl. Surf. Sci. 1993. **68**(4): p. 583-593.

6. Roen, L.M., C.H. Paik, and T.D. Jarvi, *Electrocatalytic Corrosion of Carbon Support in PEMFC Cathodes.* Electrochem. Solid-State Lett., 2004. **7**(1): p. A19-A22.

7. Maass, S., F. Finsterwalder, G. Frank, R. Hartmann, and C. Merten, *Carbon support oxidation in PEM fuel cell cathodes.* J. Power Sources, 2008. **176**(2): p. 444-451.

8. Willsau, J. and J. Heitbaum, *The influence of Pt-activation on the corrosion of carbon in gas diffusion electrodes--A dems study.* J. Electroanal. Chem., 1984. **161**(1): p. 93-101.

9. Antolini, E., *Formation, microstructural characteristics and stability of carbon supported platinum catalysts for low temperature fuel cells.* J. Mater. Sci., 2003. **38**(14): p. 2995-3005.

10. Kangasniemi, K.H., D.A. Condit, and T.D. Jarvic, *Characterization of Vulcan Electrochemically Oxidized under Simulated PEM Fuel Cell Conditions.* J. Electrochem. Soc., 2004. **151**(4): p. E125-E132.

11. Tang, H., Z. Qi, M. Ramani, and J.F. Elter, *PEM fuel cell cathode carbon corrosion due to the formation of air/fuel boundary at the anode.* J. Power Sources, 2006. **158**(2): p. 1306-1312.

12. Mitsuda, K. and T. Murahashi, *Polarization Study of a Fuel Cell with Four Reference Electrodes.* J. Electrochem. Soc., 1990. **137**(10): p. 3079-3085.

13. Meyers, J.P. and R.M. Darling, *Model of Carbon Corrosion in PEM Fuel Cells.* J. Electrochem. Soc., 2006. **153**(8): p. A1432-A1442.

14. Yang, D., M.M. Steinbugler, R.D. Sawyer, L.L. Van Dine, and C.A. Reiser, *Procedure for starting up a fuel cell system having an anode exhaust recycle loop*, in US Patent 2003: United States.

15. Reiser, C.A., L. Bregoli, T.W. Patterson, J.S. Yi, J.D. Yang, M.L. Perry, and T.D. Jarvi, *A Reverse-Current Decay Mechanism for Fuel Cells.* Electrochem. Solid-State Lett., 2005. **8**(6): p. A273-A276.

16. Perry, M.L., T. Patterson, and C. Reiser, *Systems Strategies to Mitigate Carbon Corrosion in Fuel Cells.* ECS Trans., 2006. **3**(1): p. 783-795.

17. Yu, P.T., W. Gu, R. Makharia, F.T. Wagner, and H.A. Gasteiger, *The Impact of Carbon Stability on PEM Fuel Cell Startup and Shutdown Voltage Degradation.* ECS Trans., 2006. **3**(1): p. 797-809.

18. Passalacqua, E., P.L. Antonucci, M. Vivaldi, A. Patti, V. Antonucci, N. Giordano, and K. Kinoshita, *The influence of Pt on the electrooxidation behaviour of carbon in phosphoric acid.* Electrochim. Acta, 1992. **37**(15): p. 2725-2730.

19. Bruckenstein, S. and R.R. Gadde, *Use of a porous electrode for in situ mass spectrometric determination of volatile electrode reaction products.* J. Am. Chem. Soc., 1971. **93**(3): p. 793-794.

20. Baltruschat, H., *Differential electrochemical mass spectrometry.* J. Am. Soc. Mass Spectrom., 2004. **15**(12): p. 1693-1706.

21. Woods, R., *Chemisorption at Electrodes, Hydrogen and Oxygen on Nobel Metals and Their Alloys*, in *Electroanalytical Chemistry: A Series of Advances*, A. Bard, Editor. 1976, Dekker.

22. Paulus, U.A., T.J. Schmidt, H.A. Gasteiger, and R.J. Behm, *Oxygen reduction on a high-surface area Pt/Vulcan carbon catalyst: a thin-film rotating ring-disk electrode study.* J. Electroanal. Chem., 2001. **495**(2): p. 134-145.

23. Gasteiger, H.A., N. Markovic, P.N. Ross, and E.J. Cairns, *Carbon monoxide electrooxidation on well-characterized platinum-ruthenium alloys.* J. Phys. Chem., 1994. **98**(2): p. 617-625.

24. Angerstein-Kozlowska, H., B.E. Conway, and W.B.A. Sharp, *The real condition of electrochemically oxidized platinum surfaces: Part I. Resolution of component processes.* J. Electroanal. Chem., 1973. **43**(1): p. 9-36.

25. Conway, B.E., *Electrochemical Oxide Film Formation at Noble-Metals as a Surface-Chemical Process.* Prog. Surf. Sci., 1995. **49**(4): p. 331-452.

CHAPTER 4

ANALYSIS OF OXYGEN SOURCES AND PATHWAYS OF CARBON SUPPORT CORROSION AT CATHODE IN PEMFC USING OXYGEN-18 DEMS

4.1. Introduction

Vulcan XC-72, a type of furnace carbon black commonly used as a support for fuel cell catalysts, undergoes electrochemical oxidation, i.e. carbon support corrosion (CSC), to produce CO_2 and surface oxides at the cathode in proton exchange membrane fuel cells (PEMFC) [1-4]. Here it is subjected to low pH, high water content, high oxygen concentration, high Pt loading on the catalyst compared with phosphoric acid fuel cells (PAFC), and high potential up to 1.4 V under abnormal conditions [5, 6].

CSC is a key contributor to cathode catalyst degradation in PEMFC [6-14]. It accelerates catalyst sintering by shortening the distance between Pt nanoparticles as the support corrodes away [6-12], and decreases anchor sites on the support for Pt nanoparticles so as to facilitate their movement [13]. It also causes changes of pore morphology and surface characteristics in the catalyst layer, away from the optimized conditions for mass transfer, resulting in performance decrease [14].

Although CSC under PAFC conditions has been intensely studied [15-21], it has not been so well studied in PEMFC. Two common proposed pathways for CSC in an acidic environment [22] are expressed in the two consecutive reaction steps as follows [23]:

$$C + [O^{2-}] = CO_{surf} + 2e^{-} \quad [1\text{-}1]$$

$$CO_{surf} + [O^{2-}] = CO_2 + 2e^{-} \quad [1\text{-}2]$$

here, the $[O^{2-}]$ represents reduced states of oxygen in the form of H_2O, OH^{-}, and/or passivated platinum (Pt-O or Pt-OH). The reactions are catalyzed by Pt loaded on the carbon support in a real PEMFC environment [24] and under simulated PEMFC conditions [25, 26]. However, there is still no well accepted and proven mechanism.

Determination of the oxygen sources and pathways is the key to understand and mitigate CSC. Oxygen gas, water used to humidify the gases, and carbon surface oxides originated during carbon black synthesis and catalyst preparation (denoted as original surface oxides) are three possible sources of O. Pt is thought to catalyze the carbon corrosion by transferring the O and/or OH to carbon for the corrosion reaction, which could come from the Pt electrochemical redox reactions with water [15, 22, 25-27] and/or the Pt catalyzed oxygen reduction reaction (ORR). However, there are no substantiated experimental results that determine the oxygen sources. In-situ investigations are required to understand the CSC mechanisms in specific conditions because it relates to electrode potential.

Cyclic voltammetry is commonly used to investigate the mechanisms of electrochemical reactions. However, the current signals from the two main reactions, CSC and platinum oxidation, at the cathode in PEMFC overlap and are impossible to be resolved by cyclic voltammetry. Differential electrochemical mass spectrometry (DEMS) [15, 28, 29] can resolve these by using an online mass spectrometer to sample the volatile products from the cathode of PEMFC, with potential cycling or holding imposed by a potentiostat. This makes it a powerful in-situ tool to investigate CSC mechanisms [22, 25, 27].

To further understand the mechanisms of CSC in PEMFC, ^{18}O enriched water ($H_2{}^{18}O$,

98%) was used for isotopic labeling in DEMS. DEMS spectra of m/z equal to 32, 34, 36, 44, 46 and 48, corresponding to cathode exhaust gases O_2, $O^{18}O$, $^{18}O_2$, CO_2, $CO^{18}O$ and $C^{18}O_2$, were obtained and analyzed to get the ^{18}O distribution in the products from cyclic voltammetry (potential cycled for 100–1400 mV at the rate of 10 mV s^{-1}) and chronoamperometry. Based on the analysis, we determined the oxygen source, identified the mechanistic pathways, and classified the surface oxides on carbon for the Pt-catalyzed CSC.

4.2. Experimental

A 5 cm^2 square membrane electrode assembly (MEA) using a Pt/C catalyst (20 wt% Pt, Etek) was fabricated and assembled in a single cell hardware (Electrochem) for the DEMS study, details in ref. [27]. A quadrupole mass spectrometer (QIC-20, Hiden Analytical) was used to sample gases from the outlet of the cathode, with potential imposed using a bipotentiostat (AFCBP1, Pine instrument). The potentials given in the paper refer to the MEA anode, a dynamic hydrogen electrode. All DEMS experiments were conducted at 30 ºC and atmospheric pressure.

In non-isotopic labeling DEMS experiments, H_2 (50 sccm, UHP, Airgas) and He (30 sccm, UHP, Airgas) or 5% O_2 balanced with He (30 sccm, UHP, Airgas) were humidified (RH 100% at 30 ºC) by two home-made Nafion tube humidifiers and then fed to anode and cathode, respectively.

The schematic drawing of the ^{18}O isotopic labeling DEMS (^{18}O-DEMS) setup is shown in Figure 4-1. H_2 and He bypassed the Nafion tube humidifiers and were humidified by injecting $H_2{}^{18}O$ (50 μL, 98%, Medical Isotopes) using a syringe (gastight®, Hamilton) directly to the gas transfer tubes and vaporized just before the inlets of PEMFC. To get uniform humidification

similar to the Nafion tube humidifier, the temperatures of gas transfer tubes and the interval of injections were determined based on the mass spectrometry signal of water.

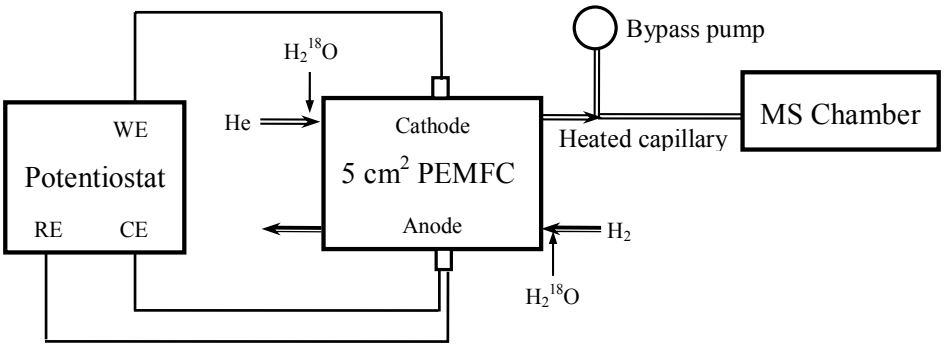

Figure 4-1. Schematic drawing of ^{18}O-DEMS setup

To replace H_2O with $H_2{}^{18}O$ in the MEA as completely as possible, the MEA was dried in-situ in a single PEMFC by feeding He (30 sccm, UHP, Airgas) to the anode and cathode respectively at 50 ºC for three days and then 70 ºC for 2 hours. The open circuit voltage of the dried MEA was about 20 mV measured by a voltammeter with H_2 (50 sccm, UHP, Airgas) in the anode and He (30 sccm, UHP, Airgas) in the cathode. Cyclic voltammetry conducted over a potential range of 100–1400 mV at 10 mV/s did not show the typical waves, but only noise. This means the MEA is dry for electrochemical reactions.

To determine the extent of oxygen isotope exchange between labeled water and CO_2 or O_2 in-situ in a PEMFC running with $H_2{}^{18}O$, 5 μL CO_2 (UHP, Airgas) and O_2 (Research, Airgas) were separately injected into the cathode at 600 mV and 1350 mV using a syringe (gastight®, Hamilton). Two CO_2 gases balanced with He (certified gas standards, 487.2 ppm ±2% and 2439 ppm ±2%, Airgas) were fed to the cathode respectively to quantify the oxygen isotope exchange

between water and CO_2. DEMS spectra of O_2, $O^{18}O$, $^{18}O_2$, CO_2, $CO^{18}O$ and $C^{18}O_2$ (m/z equal to 32, 34, 36, 44, 46 and 48 correspondingly), were obtained for analysis.

4.3. Results and Discussion

4.3.1. Oxygen Gas Effects on CSC

Oxygen gas is one of the three potential oxygen sources contributing to CSC of the PEMFC cathode. In this experiment, the MEA was dried and then humidified with $H_2{}^{18}O$. The O_2 effect on CSC was investigated by feeding humidified 5% O_2 or He into the cathode.

Figure 4-2a and c show the corresponding CVs with He and 5% O_2 respectively (notice the difference in scale). The large negative current in Figure 4-2c is produced from the ORR of 5% O_2 on Pt/C, which is also characterized by the O_2 signal decrease in Figure 4-2d. The weak O_2 signal shown in Figure 4-2b indicates that oxygen gas was leaking into the system from the environment when humidified He was fed to the cathode [27]. This amount of O_2 did not have a significant effect on the CV.

CO_2 intensities and profiles are similar in both cases shown in Figure 4-2b and d. The higher CO_2 baseline in the case of 5% O_2 in Figure 4-2d is caused by the higher total pressure in the mass spectrometer chamber of 7.7×10^{-7} Torr compared to 6.8×10^{-7} Torr in the case of He. Similarly, the higher CO_2 intensity between 0.8–1.2 V in Figure 4-2d could be a concentration effect in the mass spectrometer from large changes in O_2 or water produced [12]. The result implies that rates of O_2 chemical and electrochemical oxidation with carbon black at 30 ºC are very slow. This is consistent with the conclusion that the effect of oxygen partial pressure on cathode degradation is insignificant [30]. Thus the O_2 does not contribute to CSC significantly in this DEMS study. However, O_2 might affect CSC after a long period by ORR and/or gas-phase

oxidation with carbon black. There is still a lack of detailed information on these mechanisms and a need for more emphasis by researchers.

Therefore, it is reasonable to investigate the CSC mechanism as the PEMFC is fed with humidified He to the cathode. It also simplifies analysis of the ^{18}O isotope labeling technique by reducing the possible isotope exchange reactions. Certainly, there is a still small amount of oxygen leaking into the cell from the environment, but this will be ignored. The analysis will focus on the remaining potential sources of oxygen for CSC: water and surface oxides on carbon black.

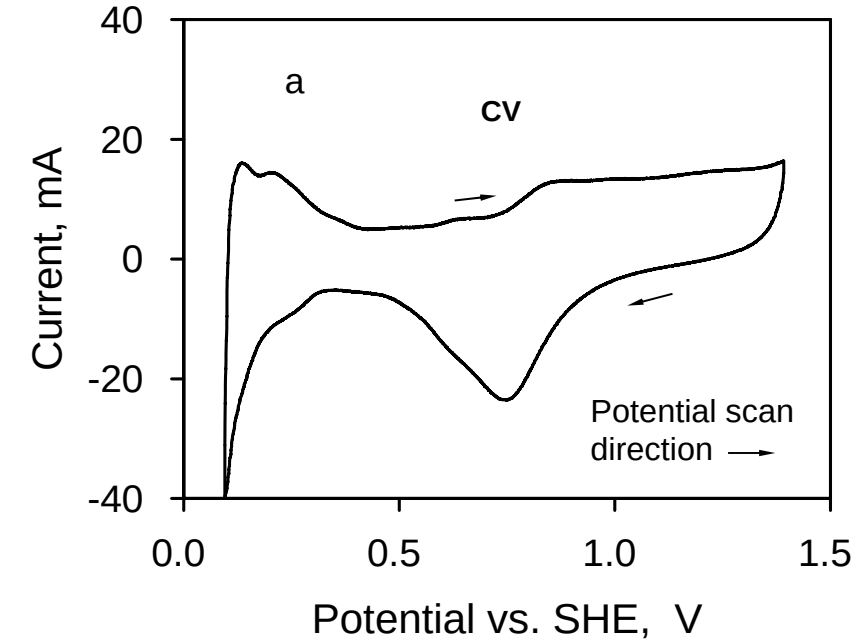
a
cv
Current, mA
40
20
0
-20
-40
0.0
0.5
1.0
1.5
Potential scan
direction
Potential vs. SHE, V

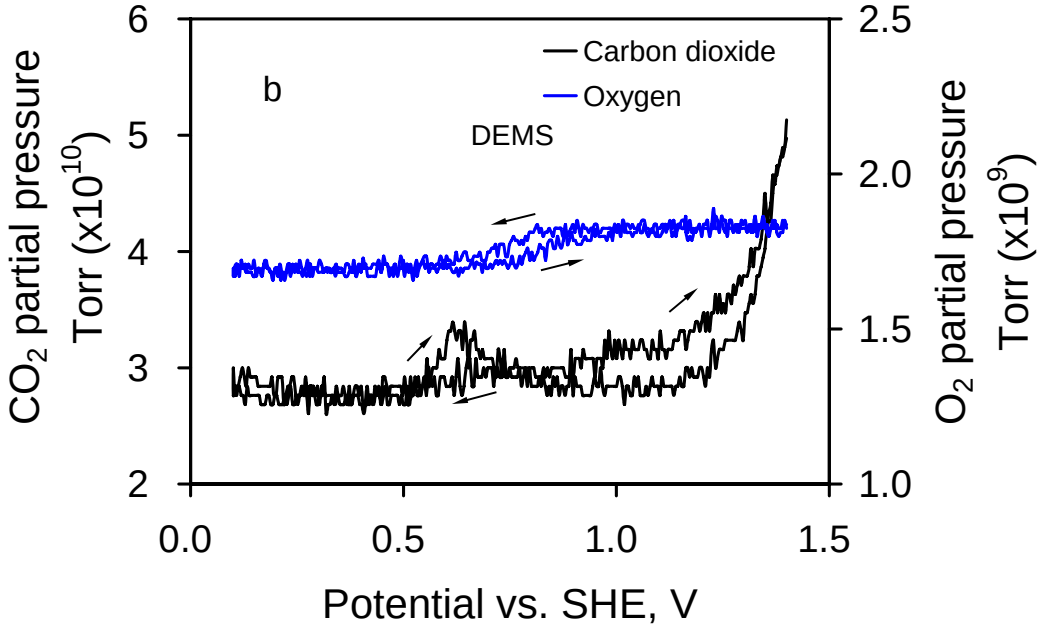
b
Carbon dioxide
Oxygen
DEMS
CO2 partial pressure
Torr (x10^10)
O2 partial pressure
Torr (x10^9)
6
5
4
3
2
2.5
2.0
1.5
1.0
0.0
0.5
1.0
1.5
Potential vs. SHE, V

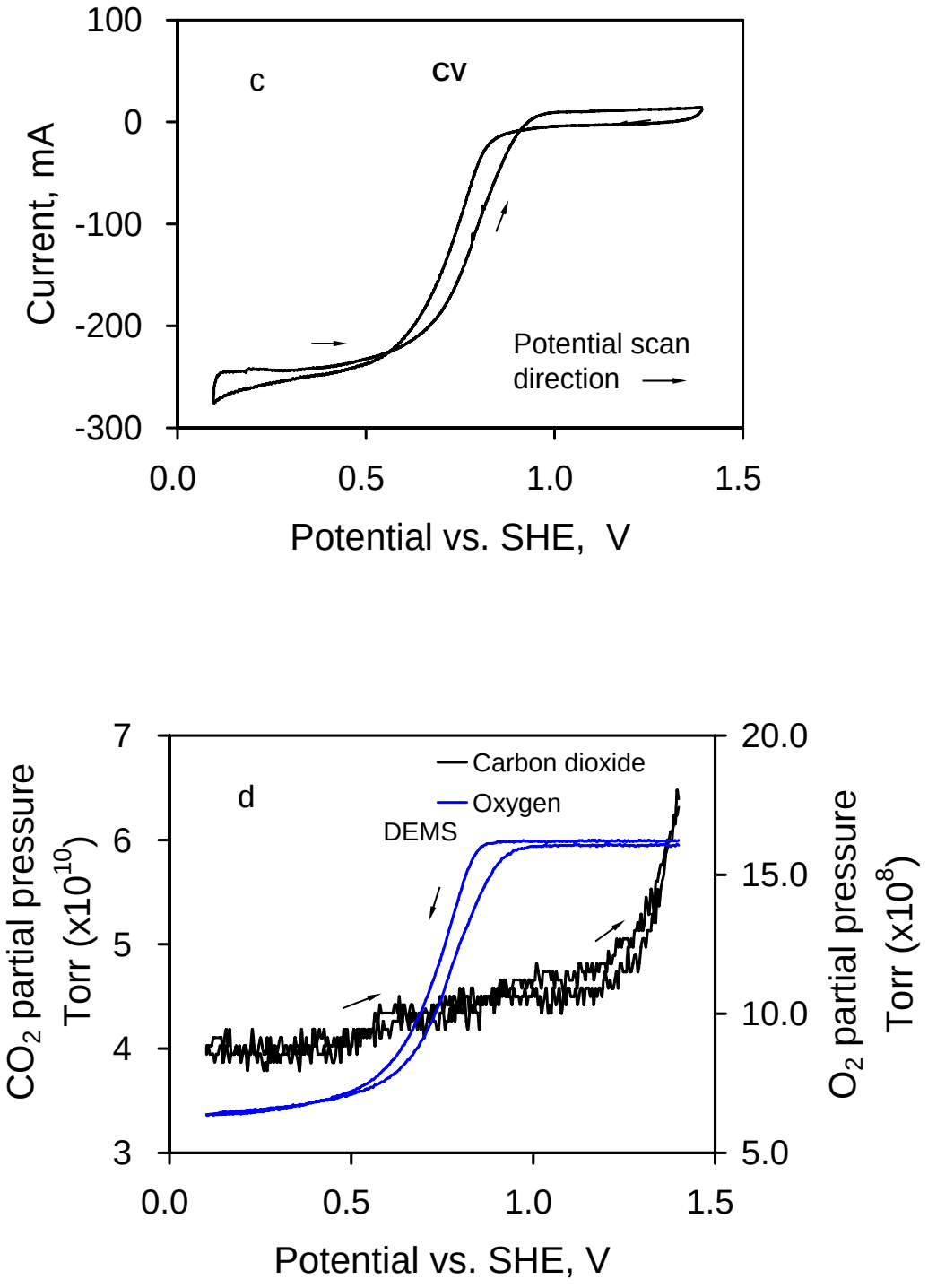

Figure 4-2. CV (a, c) and DEMS spectra of carbon dioxides (b, d) with He and 5% O_2 fed to cathode, respectively

4.3.2. Oxygen Isotope Exchange Determination

He humidified with $H_2{}^{18}O$ was fed through carbon black at 30 ºC. No significant signal change was detected by the mass spectrometer means no significant ^{18}O isotope exchange between the surface oxides on carbon black and $H_2{}^{18}O$. Thus two possible ^{18}O isotope exchange reactions at the cathode of PEMFC occur between $H_2{}^{18}O$ and CO_2 as well as $H_2{}^{18}O$ and O_2. The extent of their exchange reactions must be determined for interpretation of the ^{18}O-DEMS spectra of carbon dioxide. The MEA was dried and then saturated with $H_2{}^{18}O$. 5μL of O_2 and CO_2 was separately injected into the humidified He stream fed to the cathode while holding the cathode potential at 600 and 1350 mV, respectively.

Figure 4-3a shows no significant changes of O_2, $^{18}O_2$ and $O^{18}O$ when injecting 5 μL of O_2 at 600 mV, whereas Figure 4-3b shows an O_2 peak with $^{18}O_2$ and $O^{18}O$ signals unchanged at 1350 mV. The O_2 peak does not appear at 600 mV because it was completely consumed by the ORR at this high overpotential, which was confirmed by the corresponding ORR current peak in the chronoamperogram in Figure 4-3c. The O_2 peak shown at 1350 mV stands for the amount of O_2 injected because this potential is between the standard electrode potentials of ORR and oxygen evolution reaction (OER). Certainly, there was no corresponding ORR and OER current obtained in the chronoamperogram (not shown). Neither case showed a change in the $O^{18}O$ and $^{18}O_2$ signals indicating insignificant ^{18}O isotope exchange reaction between $H_2{}^{18}O$ and O_2, when the O_2 was at very low partial pressure because it was leaking into the fuel cell from environment.

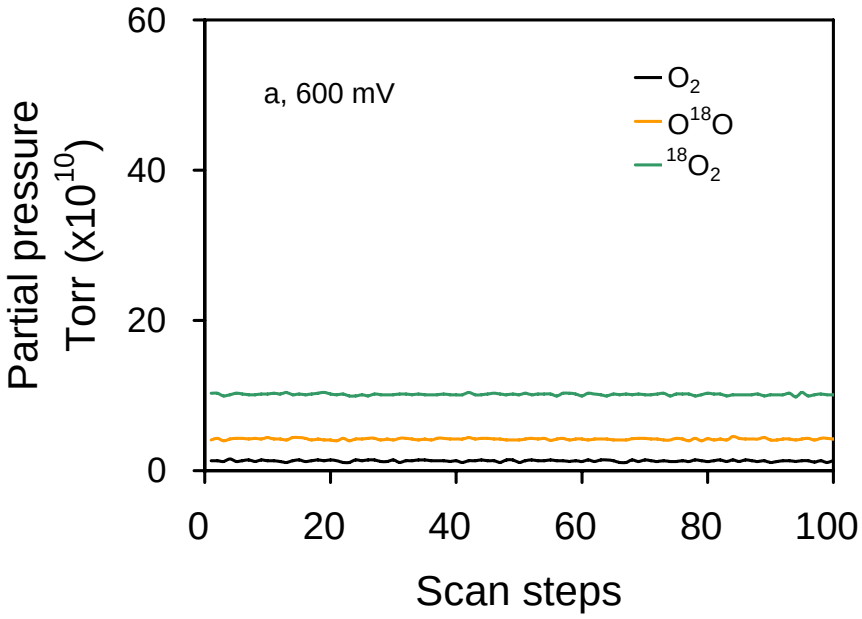
a, 600 mV
O_2
$O^{18}O$
$^{18}O_2$
Partial pressure
Torr (x10^{10})
60
40
20
0
0
20
40
60
80
100
Scan steps

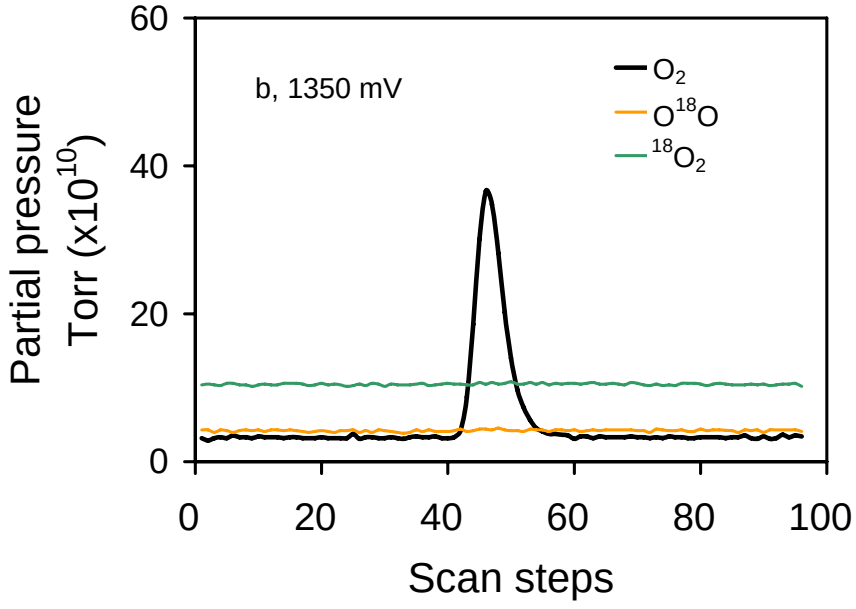
b, 1350 mV
O_2
$O^{18}O$
$^{18}O_2$
Partial pressure
Torr (x10^{10})
60
40
20
0
0
20
40
60
80
100
Scan steps

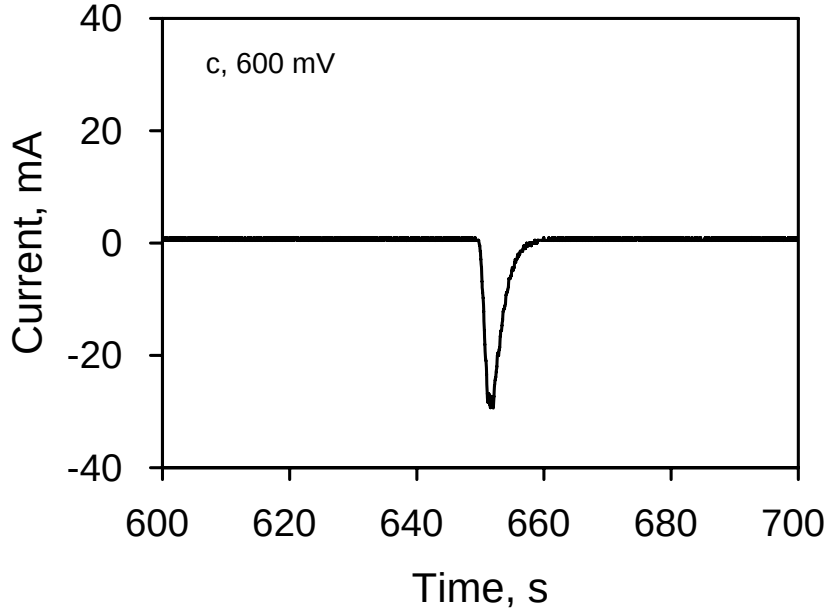

Figure 4-3. ^{18}O-mass spectra of oxygen gases at 600 mV (a), 1350 mV (b) and chronoamperogram at 600 mV (c) for in-situ measurement of oxygen isotope exchange between O_2 and $H_2{}^{18}O$ at cathode in PEMFC by injecting 5 μL O_2 (scan step in all figures means the mass spectrometer data acquisition step. The numbers on axis are relative.)

On the contrary, when 5 μL of CO_2 was injected at 600 and 1350 mV respectively, significant ^{18}O isotope exchange between CO_2 and H_2O was observed as shown in Figure 4-4a and b. No notable differences of CO_2, $CO^{18}O$ and $C^{18}O_2$ signals at the two potentials imply that Pt does not significantly influence the ^{18}O isotope exchange reaction under these conditions. This could be attributed to the weak interaction between CO_2 and Pt or PtO_x. The ^{18}O isotope exchange reactions were quantified by feeding the cathode with 487 ppm and 2439 ppm certified CO_2 gases balanced with He. The calibration curves in Figure 4-5 show the distribution of isotope exchange products after different concentrations of CO_2 were fed. The procedure is

explained below to use these calibration curves to exclude the isotope exchange effects on the CO_2, $CO^{18}O$ and $C^{18}O_2$ signals in the ^{18}O-DEMS spectra for the CSC mechanistic investigation.

The oxygen isotope exchange between gaseous CO_2 and water can be described as [31]: $CO_2(g) + H_2{}^{18}O(l) \xleftrightarrow{k_{tot}} C^{18}OO(g) + H_2O(l)$. An assumption was introduced in this study that the exchange between $C^{18}O_2$ and H_2O has the same rate and equilibrium as those between CO_2 and $H_2{}^{18}O$. It is reasonable because the isotope effect of ^{18}O for reaction can be neglected. In addition, since the ^{18}O enriched water used has only 2% H_2O, the exchange between $C^{18}O_2$ and H_2O can be ignored, which reasonably simplifies the analysis of ^{18}O-DEMS spectra of carbon dioxides.

Assume the exchange reactions have two steps: $CO_2 \xleftrightarrow{1,H_2{}^{18}O} CO^{18}O \xleftrightarrow{2,H_2{}^{18}O} C^{18}O_2$. The slopes of the calibration curves show the distribution ratio of CO_2, $CO^{18}O$ and $C^{18}O_2$ after exchange is 192:43:14. If there is no step 2, the $C^{18}O_2$ should contribute back to CO_2 and $CO^{18}O$ as the ratio of 192:43. Then the distribution of CO_2/$CO^{18}O$ after exchange is [192 + 14 × 192/(192 + 43)]:[43 + 14 × 43/(192 + 43)] = 203.4:45.6. Thus the CO_2 signal intensity was adjusted back to original intensity before isotope exchange by applying the factor of (203.4 + 45.6)/203.4. This increased amount of CO_2 was then subtracted from the $CO^{18}O$.

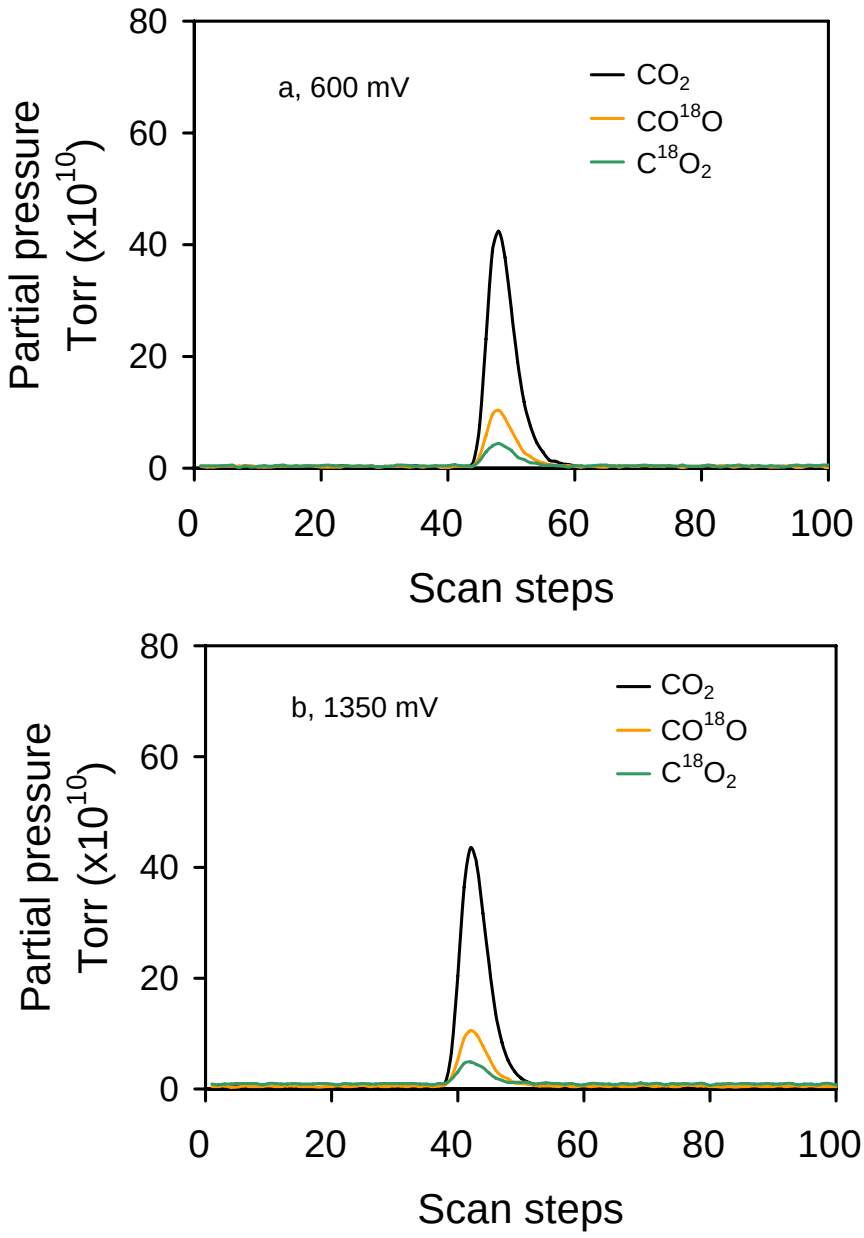

Figure 4-4. ^{18}O-mass spectra of carbon dioxides at 600 mV (a) and 1350 mV (b) for in-situ measurement of oxygen isotope exchange between CO_2 and $H_2{}^{18}O$ at cathode in PEMFC by injecting 5 μL CO_2

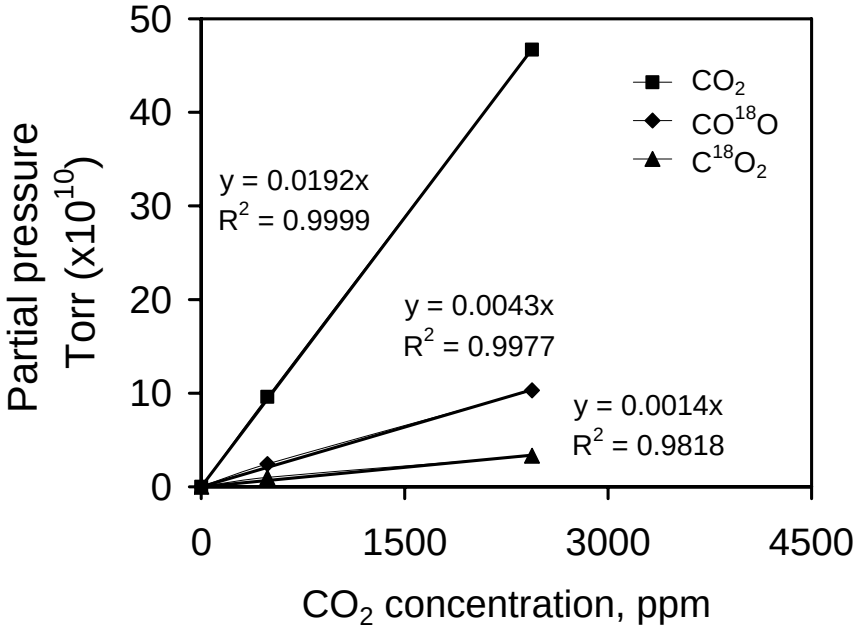

Figure 4-5. In-situ calibration of oxygen isotope exchange between CO_2 and $H_2{}^{18}O$ in PEMFC by feeding 487 ppm and 2439 ppm CO_2 respectively

4.3.3. Oxygen Sources and Pathways of CSC

^{18}O-DEMS experiments with $H_2{}^{18}O$ (98%) humidified H_2 and He fed into the anode and cathode respectively were employed to investigate the oxygen sources and pathways. Analysis of the ^{18}O-DEMS spectra requires eliminating the effect of ^{18}O isotope exchange first. According to our results from section 3.2, only oxygen isotope exchange reactions of CO_2 and $CO^{18}O$ with $H_2{}^{18}O$ need to be considered and adjusted. Actually, only exchange between $CO^{18}O$ and $H_2{}^{18}O$ was adjusted because the unlabelled CO_2 signal was not significant.

Based on the assumption earlier, the exchange extent between $CO^{18}O$ and $H_2{}^{18}O$ to produce $C^{18}O_2$ is the same as that between CO_2 and $H_2{}^{18}O$ to produce $CO^{18}O$ without step 2, shown in section 3.2. So the $CO^{18}O$ signal intensity was adjusted back to its original intensity

before isotope exchange using the same factor (249.0/203.4) of CO_2 in section 3.2. This increased amount of $CO^{18}O$ was then subtracted from the $C^{18}O_2$.

Figure 4-6a and b show the CV and ^{18}O-DEMS spectra of carbon dioxides, respectively. CO_2 is generated from the reactions of H_2O with carbon black or original surface oxides because they are the only remaining sources for O. Since the H_2O is only about 2% in the system, the reactions of carbon black with H_2O and the oxygen isotope exchange reactions of $C^{18}O_2$ and $CO^{18}O$ with H_2O to produce CO_2 can be neglected, which is demonstrated by the virtually unchanged CO_2 signal in Figure 4-6b. The investigation will focus on the analysis of the DEMS spectra of $C^{18}O_2$ and $CO^{18}O$.

Figure 4-6b shows four $C^{18}O_2$ peaks located at 100 mV (I), 600 mV (II), and 1400 mV (IV) in the anodic direction and at 750 mV (V) in the cathodic direction respectively, consistent with those of CO_2 DEMS spectra using regular water [22, 25, 27]. Peak III at 1000 mV in the CO_2 DEMS spectra [22, 25-27] should also exist in the $C^{18}O_2$ DEMS spectra in Figure 4-6b but is covered by peak IV. Given that $H_2{}^{18}O$ is the only source of ^{18}O, it can be deduced that $C^{18}O_2$ is produced from the reactions of C with $H_2{}^{18}O$. It needs to be confirmed if they produce surface oxides on carbon black as intermediate products.

Figure 4-6b also shows a very weak $CO^{18}O$ peak located at 600 mV (Figure 4-7 will show this peak more clearly) and a significant peak located at 1400 mV in the anodic direction. Because O_2 does not impact the CSC significantly in this potential scanning mode (Section 3.1), the O of $CO^{18}O$ should come from the original surface oxides on carbon black, which means that the surface oxides also react with water to produce CO_2.

Peak II is located around 600 mV in the anodic cycle in Figure 4-6b and coincides with the potential for electrochemical oxidation of CO on platinum [32]. CO stripping experiments

[33] suggested that peak II is due to oxidation of Pt-CO_{ad} or CO-like species on carbon in the vicinity of platinum. Peak II of $C^{18}O_2$ in the ^{18}O-DEMS spectra means that carbon was oxidized significantly with $H_2{}^{18}O$ to produce $C^{18}O_2$ at ca. 600 mV, whereas the very weak peak II of $CO^{18}O$ indicates that the reaction of the original surface oxides generating CO-like species below the onset potential of peak II is extremely slow. The main oxygen source of peak II was thus from the water.

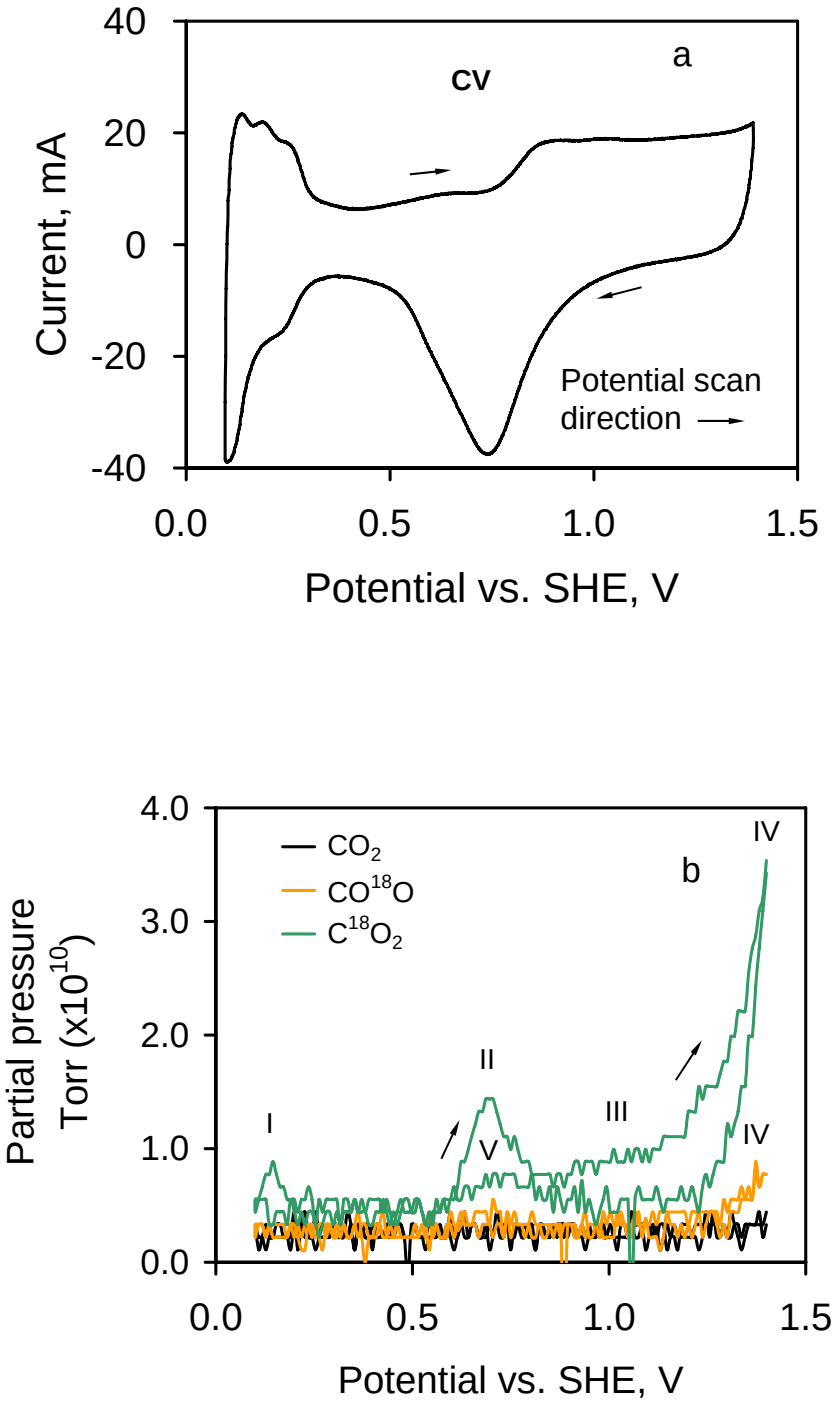

Figure 4-6. CV (a) and ^{18}O-DEMS spectra of carbon dioxides (b)

When the potential was then held at 450 mV, there were no $CO^{18}O$ and $C^{18}O_2$ MS peaks. After holding for 15 min and then resuming the scans, the peaks II of $CO^{18}O$ and $C^{18}O_2$ at 600 mV increase but only in the first potential cycle in Figure 4-7. No other peaks had significant change. This confirms that some surface oxides contributing to peak II formed and accumulated below the peak II onset potential (ca. 500 mV) and were consumed by one potential cycle. The increase in peak II of $C^{18}O_2$ means water reacted with carbon black to produce surface oxides, which further reacted with water to produce carbon dioxide. The increase in peak II of $CO^{18}O$ indicates that some types of original surface oxides transformed to the surface oxides contributing to peak II below the onset potential of peak II. The reaction rate should be quite low because there was no significant Faraday current wave observed when holding the potential at 450 mV. Carbon surface oxides contributing to peak II are denoted as C_s-O_{II}.

Peak III was located at ca. 1000 mV, where Pt oxidation started with OH groups covering the Pt surface forming an oxide film [22]. The carbon oxidized by accepting a hydroxyl group from this process to form this peak [22, 25-27]. In this ^{18}O-DEMS experiment, peak III of $C^{18}O_2$ verified the oxidation of Pt with $H_2{}^{18}O$ at ca. 1000 mV, which might form oxide film of Pt-$^{18}OH_{ad}$ or Pt-$^{18}O_x$. This supplies [^{18}OH] to the carbon surface oxides, produced from the reaction of water with carbon below 1000 mV, to produce $C^{18}O_2$. It might also supply [^{18}OH] to the original surface oxides on carbon to generate $CO^{18}O$. This type of surface oxide was denoted as C_s-O_{III}.

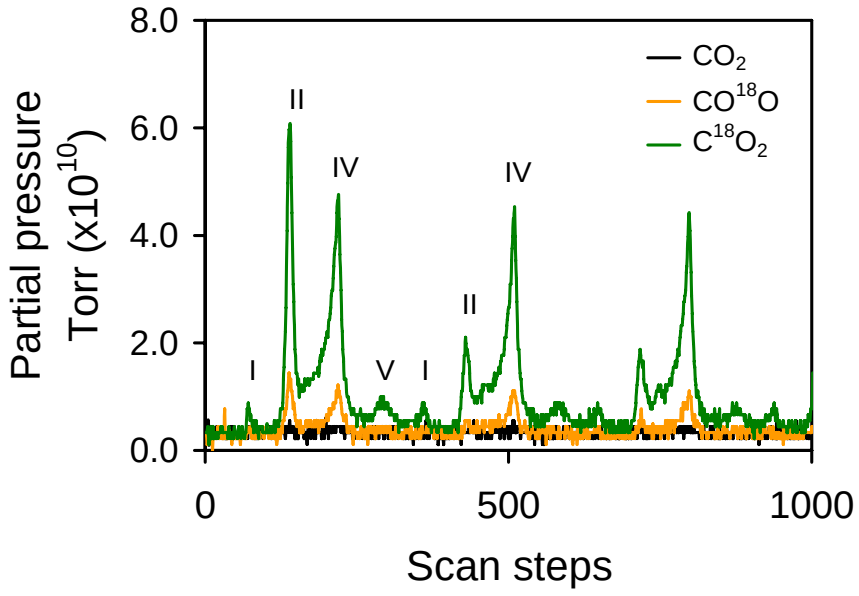

Figure 4-7. ^{18}O-mass spectra of carbon dioxides after holding potential at 450 mV for 15 min

The highest maximum IV in Figure 4-6b starts below 600 mV and exponentially increases from 1000 mV to the anodic potential limit of 1400 mV. It overlaps peak III and extends to the end of peak II, which means that peak IV could be ascribed to two types of surface oxides: C_s-O_{III} and C_s-O_{IV} (produced at potential higher than 1000 mV). Similar to peak II, a large peak IV of $C^{18}O_2$ means that $H_2{}^{18}O$ reacted significantly with carbon to produce $C^{18}O_2$; while moderate peak IV of $CO^{18}O$ indicates that original carbon surface oxides generated C_s-O_{III} and C_s-O_{IV} above the ending potential of peak II, which were further oxidized with $H_2{}^{18}O$ to produce $CO^{18}O$.

When the potential was held at 1400 mV for 15 min, both peaks of $C^{18}O_2$ and $CO^{18}O$ at 100 mV increase dramatically in Figure 4-8. The increase in peak IV of $C^{18}O_2$ confirms that carbon surface oxides were produced from water with carbon and accumulated at the potential of

1400 mV. The increase in peak IV of $CO^{18}O$ verified that original carbon surface oxides generated C_s-O_{III} and C_s-O_{IV} at 1400 mV. These surface oxides contribute to the peaks I of $C^{18}O_2$ and $CO^{18}O$ by oxidation with hydrogen peroxide [22, 25-27], indicated by the increase of peaks I in the next cycle.

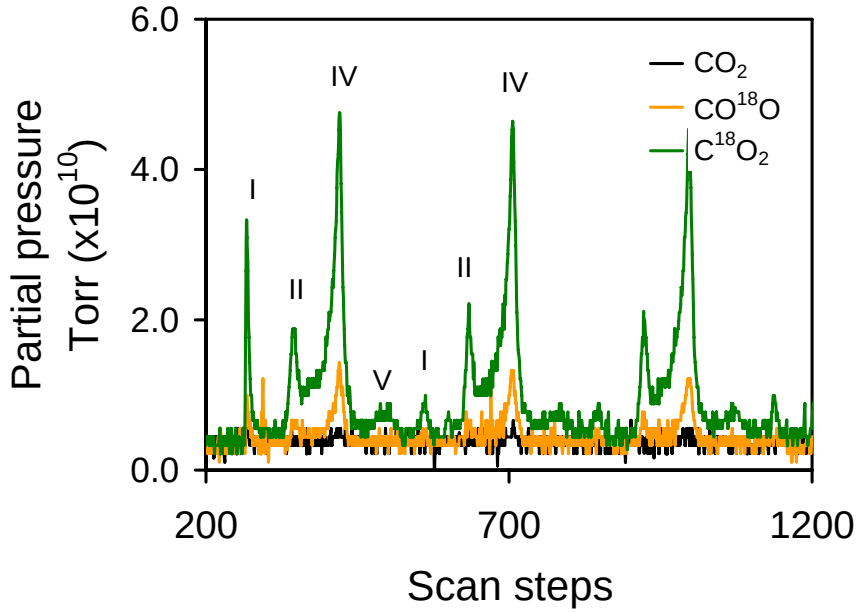

Figure 4-8. ^{18}O-mass spectra of carbon dioxides after holding potential at 1400 mV for 15 min

The different pathways of $C^{18}O_2$ and $CO^{18}O$ production were further investigated by the chronoamperograms at 1400 mV shown in Figure 4-9a. The early parts, approximating 2 s, were plotted as natural logarithm partial pressure (ln(PP)) vs. natural logarithm time (ln(t)) in Figure 4-9b. It shows that the $C^{18}O_2$ signal has a slope of 0.50 and $CO^{18}O$ has a slope of 0.42 by least squares fitting. They were obtained at the same conditions and time, which results in the same systematic errors. According to the current-time response theory [34], the difference of slopes implies that they are produced from two different reactions, i.e. carbon with $H_2{}^{18}O$ and surface

oxides with $H_2{}^{18}O$. That $C^{18}O_2$ decreases faster than $CO^{18}O$ might be ascribed to the requirement of water reacting with carbon to produce surface oxides before they are further oxidized to produce carbon dioxide.

Peak V is located at ca. 750 mV in the cathodic scan and coincides with the reduction of platinum oxides [22, 25-27], which implies it relates to the removal of the oxide film on Pt. CO_2 is the highest oxidation state for carbon and thus this peak is the reversible anodic peak representing the carbon oxidation reaction. It was proposed [26] that surface oxides produced during peak IV are also combined with the hydroxyl surface groups from the oxide films on Pt during reduction to produce CO_2 for peak V. This implies that the $^{18}O/^{18}OH$ released from the oxide films on Pt are strong oxidants, like $H_2{}^{18}O_2$ at peak I. The reaction here probably is not an electrochemical reaction, but a chemical reaction after an electrochemical reaction. Figure 4-6, 8 and 9 show only a significant peak V of $C^{18}O_2$, which means only surface oxides produced from the reaction of $H_2{}^{18}O$ with carbon can accept $^{18}O/^{18}OH$. It might be due to the surface oxides produced from water with carbon catalyzed by Pt and thus located in the vicinity of Pt.

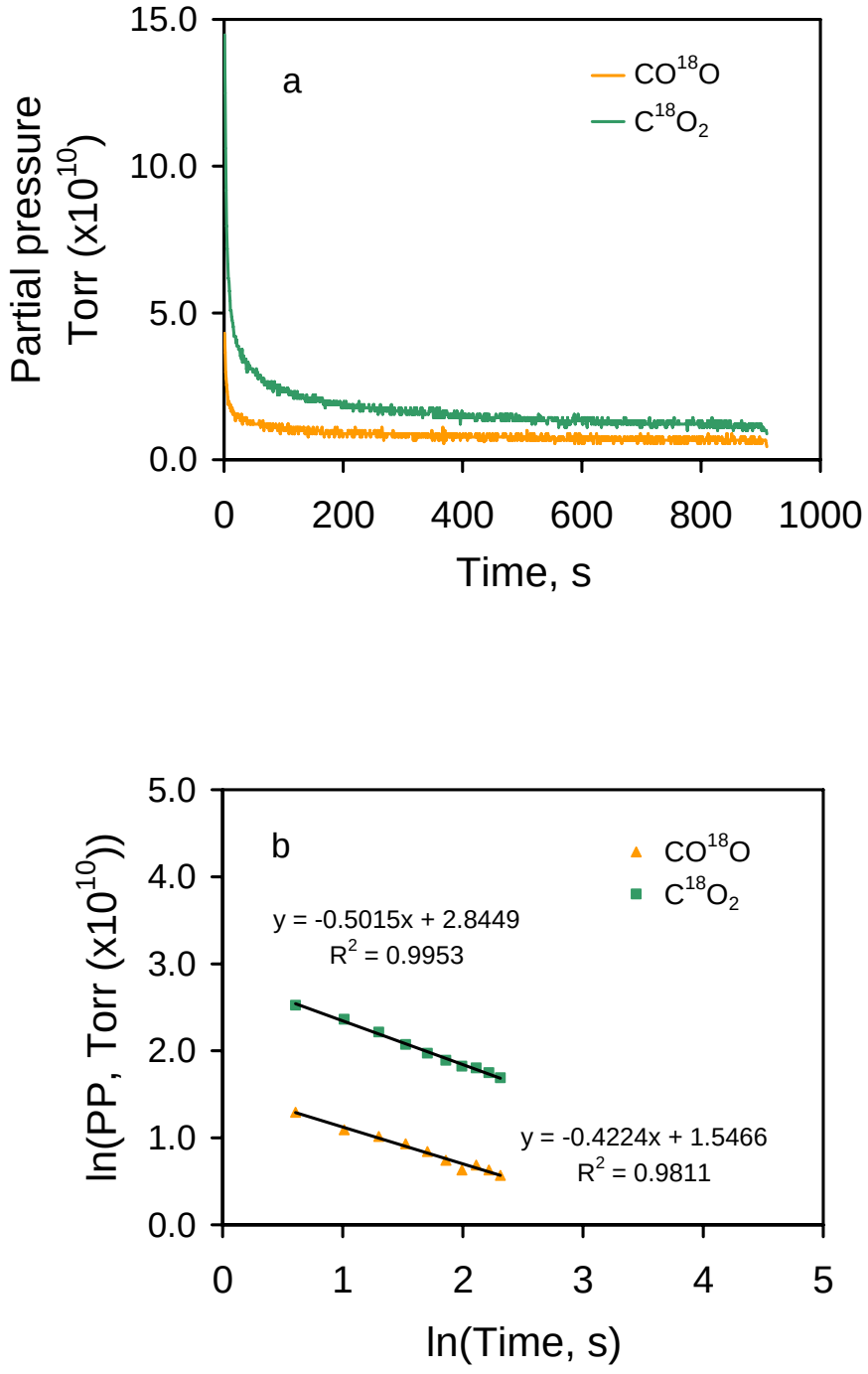

Figure 4-9. Chronoamperograms (a) and plots of ln(PP) against ln(t) (b) of $CO^{18}O$ and $C^{18}O_2$ at the potential of 1400 mV

4.4. Conclusions

Analysis of DEMS spectra of CO_2 and O_2 with humidified He and 5% O_2, fed into the cathode respectively, illustrated that oxygen gas does not affect the carbon support corrosion (CSC) significantly during potential cycling from 100–1400 mV at 10 mV/s. ^{18}O-DEMS spectra of carbon dioxides from the cathode with $H_2{}^{18}O$ humidified H_2 and He, fed to the anode and the cathode respectively, confirmed that water and original surface oxides on carbon are sources of CSC; but water is the main source. The total reactions of CSC producing CO_2 follow the pathways below:

$$C + H_2O \xrightarrow{Pt,PtO_x} CO_{surf} + 2e^-$$

$$CO_{surf} + H_2O \xrightarrow{Pt,PtO_x} CO_2 + 2e^-$$

In addition, it is proposed that there are at least three types of surface oxides, C_s-O_{II}, C_s-O_{III} and C_s-O_{IV}, contributing to CSC in the potential range of 100–500 mV, 700–1400 mV, and 1000–1400 mV, respectively. They are generated from the electrochemical oxidation of carbon with water and the preparation of the carbon black and catalysts. More complete characterization of C_s-O_{II}, C_s-O_{III}, and C_s-O_{IV} surface oxides will need further investigation using in-situ spectroscopy, such as diffuse reflectance infrared Fourier transform spectroscopy.

References:

1. Matsumoto, M., T. Manako, and H. Imai, *Degradation of carbon supports in PEFC cathode investigated by electrochemical STM: effects of platinum and oxygen on enhanced carbon corrosion.* ECS Trans., 2008. **16**(2): p. 751-760.

2. Franco, A.A., M. Gerard, M. Guinard, B. Barthe, and O. Lemaire, *Carbon catalyst-support corrosion in polymer electrolyte fuel cells: mechanistic insights.* ECS Trans., 2008. **13**(15): p. 35-55.

3. Siroma, Z., M. Tanaka, K. Yasuda, K. Tanimoto, M. Inaba, and A. Tasaka, *Electrochemical corrosion of carbon materials in an aqueous acid solution.* Electrochem., 2007. **75**(2): p. 258-260.

4. Chizawa, H., Y. Ogami, H. Naka, A. Matsunaga, N. Aoki, T. Aoki, and K. Tanaka, *Impacts of carbon corrosion on cell performance decay.* ECS Trans., 2007. **11**(1, Part 2, Proton Exchange Membrane Fuel Cells 7, Part 2): p. 981-992.

5. Patterson, T.W. and R.M. Darling, *Damage to the Cathode Catalyst of a PEM Fuel Cell Caused by Localized Fuel Starvation.* Electrochem. Solid-State Lett., 2006. **9**(4): p. A183-A185.

6. Reiser, C.A., L. Bregoli, T.W. Patterson, J.S. Yi, J.D. Yang, M.L. Perry, and T.D. Jarvi, *A Reverse-Current Decay Mechanism for Fuel Cells.* Electrochem. Solid-State Lett., 2005. **8**(6): p. A273-A276.

7. Tang, H., Z. Qi, M. Ramani, and J.F. Elter, *PEM fuel cell cathode carbon corrosion due to the formation of air/fuel boundary at the anode.* J. Power Sources, 2006. **158**(2): p. 1306-1312.

8. Mitsuda, K. and T. Murahashi, *Polarization Study of a Fuel Cell with Four Reference Electrodes.* J. Electrochem. Soc., 1990. **137**(10): p. 3079-3085.

9. Meyers, J.P. and R.M. Darling, *Model of Carbon Corrosion in PEM Fuel Cells.* J. Electrochem. Soc., 2006. **153**(8): p. A1432-A1442.

10. Yang, D., M.M. Steinbugler, R.D. Sawyer, L.L. Van Dine, and C.A. Reiser, *Procedure for starting up a fuel cell system having an anode exhaust recycle loop*, in US Patent 2003: United States.

11. Perry, M.L., T. Patterson, and C. Reiser, *Systems Strategies to Mitigate Carbon Corrosion in Fuel Cells.* ECS Trans., 2006. **3**(1): p. 783-795.

12. Yu, P.T., W. Gu, R. Makharia, F.T. Wagner, and H.A. Gasteiger, *The Impact of Carbon Stability on PEM Fuel Cell Startup and Shutdown Voltage Degradation.* ECS Trans., 2006. **3**(1): p. 797-809.

13. Ascarelli, P., V. Contini, and R. Giorgi, *Formation process of nanocrystalline materials from x-ray diffraction profile analysis: Application to platinum catalysts.* J. Appl. Phys., 2002. **91**(7): p. 4556-4561.

14. Antolini, E., *Formation, microstructural characteristics and stability of carbon supported platinum catalysts for low temperature fuel cells.* J. Mater. Sci., 2003. **38**(14): p. 2995-3005.

15. Passalacqua, E., P.L. Antonucci, M. Vivaldi, A. Patti, V. Antonucci, N. Giordano, and K. Kinoshita, *The influence of Pt on the electrooxidation behaviour of carbon in phosphoric acid.* Electrochim. Acta, 1992. **37**(15): p. 2725-2730.

16. Kinoshita, K. and J. Bett, *Electrochemical oxidation of carbon black in concentrated phosphoric acid at 135 ºC.* Carbon, 1973. **11**(3): p. 237-247.

17. Gruver, G.A., *The Corrosion of Carbon Black in Phosphoric Acid.* J. Electrochem. Soc., 1978. **125**(10): p. 1719-1720.

18. Kiho, M., K. Matsunaga, S. Morikawa, and O. Kato, *Influence of metal impurities on carbon corrosion in phosphoric acid fuel cells (PAFC).* Electrochem., 2001. **69**(8): p. 580-586.

19. Wei, Z., H. Guo, and Z. Tang, *Heat treatment of carbon-based powders carrying platinum alloy catalysts for oxygen reduction: influence on corrosion resistance and particle size.* J. Power Sources, 1996. **62**(2): p. 233-236.

20. Rodríguez-reinoso, F., *The role of carbon materials in heterogeneous catalysis.* Carbon, 1998. **36**(3): p. 159-175.

21. Cameron, D.S., S.J. Cooper, I.L. Dodgson, B. Harrison, and J.W. Jenkins, *Carbons as supports for precious metal catalysts.* Catal. Today, 1990. **7**(2): p. 113-137.

22. Willsau, J. and J. Heitbaum, *The influence of Pt-activation on the corrosion of carbon in gas diffusion electrodes--A dems study.* J. Electroanal. Chem., 1984. **161**(1): p. 93-101.

23. Kinoshita, K., *Carbon Electrochemical and Physicochemical Properties*. 1988, New York: Wiley.

24. Kangasniemi, K.H., D.A. Condit, and T.D. Jarvic, *Characterization of Vulcan Electrochemically Oxidized under Simulated PEM Fuel Cell Conditions.* J. Electrochem. Soc., 2004. **151**(4): p. E125--E132.

25. Roen, L.M., C.H. Paik, and T.D. Jarvi, *Electrocatalytic Corrosion of Carbon Support in PEMFC Cathodes.* Electrochem. Solid-State Lett., 2004. **7**(1): p. A19-A22.

26. Maass, S., F. Finsterwalder, G. Frank, R. Hartmann, and C. Merten, *Carbon support oxidation in PEM fuel cell cathodes.* J. Power Sources, 2008. **176**(2): p. 444-451.

27. Li, W. and A.M. Lane, *Investigation of Pt catalytic effects on carbon support corrosion of the cathode catalyst in PEM fuel cells using DEMS spectra.* Electrochem. Comm., 2009. **11**(6): p. 1187-1190.

28. Bruckenstein, S. and R.R. Gadde, *Use of a porous electrode for in situ mass spectrometric determination of volatile electrode reaction products.* J. Am. Chem. Soc., 1971. **93**(3): p. 793-794.

29. Baltruschat, H., *Differential electrochemical mass spectrometry.* J. Am. Soc. Mass Spectrom., 2004. **15**(12): p. 1693-1706.

30. Bi, W., Q. Sun, Y. Deng, and T.F. Fuller, *The effect of humidity and oxygen partial pressure on degradation of Pt/C catalyst in PEM fuel cell.* Electrochim. Acta, 2009. **54**(6): p. 1826-1833.

31. Horita, J. and C. Kendall, *Stable Isotope Analysis of Water and Aqueous Solutions by Conventional Dual-Inlet Mass Spectrometry,* in *Handbook of Stable Isotope Analytical Techniques*, A.d.G. Pier, Editor. 2004, Elsevier: Amsterdam. p. 1-37.

32. Paulus, U.A., T.J. Schmidt, H.A. Gasteiger, and R.J. Behm, *Oxygen reduction on a high-surface area Pt/Vulcan carbon catalyst: a thin-film rotating ring-disk electrode study.* J. Electroanal. Chem., 2001. **495**(2): p. 134-145.

33. Gasteiger, H.A., N. Markovic, P.N. Ross, and E.J. Cairns, *Carbon monoxide electrooxidation on well-characterized platinum-ruthenium alloys.* J. Phys. Chem., 1994. **98**(2): p. 617-625.

34. Bard, A.J. and L.R. Faulkner, *Electrochemical Methods: Fundamentals and Applications*. 2 ed. 2001, New York: Wiley.

CHAPTER 5

IN-SITU CHARACTERIZATION OF CATHODE CATALSYT DEGRADATION BY DEMS

The mechanism of carbon support corrosion was investigated in Chapter 3 and 4 mainly using DEMS and ^{18}O-DEMS spectra of CO_2. More detailed information about H_2 and O_2 MS signals during DEMS experiments are disclosed in this chapter. Furthermore, different with Chapter 3 and 4, this chapter reports the variations of MS signals of H_2, O_2 and CO_2 over time under accelerated degradation conditions. The cathode catalyst degradation was then understood based on these variations.

5.1 Introduction

Electrocatalyst degradation means the loss of the electrochemically active surface area (ECSA) over time. Pt dissolution and carbon support corrosion (CSC) are two keys factors contributing to the cathode catalyst (Pt/C) degradation in proton exchange membrane fuel cells (PEMFC) [1]. Pt dissolution causes Pt/C catalyst degradation by oxidizing the Pt to Pt ions and moving away [2, 3]. CSC, catalyzed by the Pt and its oxides [4-7], brings about the oxidation and shrinkage of the support of Pt/C in PEMFC leading to the Pt nanoparticles (NPs) loaded on it aggregating and moving away due to fewer anchor sites [8-11].

The Pt/C catalyst at the cathode is coated with a very thin Nafion film, which was used to build up a three dimensional catalyst layer to increase the Pt utilization [12]. Water vapor or

condensed water diffuses through the pores of carbon paper or cloth, reaches the particles surfaces, and then dissolves in Nafion. Different from PAFC, where the catalyst is in direct contact with liquid water in the phosphorous acid, the Pt and carbon black undergo electrochemical oxidation with the water dissolved in the Nafion wrapping the catalyst. Thus the Pt oxidation and CSC kinetics depend on the activity of water in this thin Nafion film, determined by the vapor partial pressure and temperature [13] as well as described by modeling [14, 15].

PEFMC lifetime requirements vary from 5,000 h for car applications and 40,000 h for stationary power sources applications [16]. It is impractical to test the PEMFC durability under normal operating conditions because of the cost and long time [17]. Accelerated degradation testing methods are commonly employed to study the durability of the PEMFC. For the electrocatalysts durability, two common methods of accelerated degradation testing, driven by the PAFC research during 70-80's, are potential cycling [18-21] and potential stepping [21-24].

To save cost and time, degradation can be alternatively investigated by modeling with mechanistic, semi-empirical, and phenomenological performance models incorporated with degradation models. It requires a trade-off between accuracy and computation time. Multi-dimensional microscopic modeling based on the classic conservation laws can achieve good accuracy and maximum predictive power. However, it leads to great complexity and makes it impractical to accurately predict the durability of PEMFC with solvability and afford computation time. A degradation model plugged into semi-empirical or phenomenological performance models is a feasible way to model the durability or accelerated durability process [25].

However, more efforts need to be put on the experiments to get accurate and reliable

parameters for the models. Cyclic voltammetry is commonly used to accelerate degradation of the electrocatalyst in PEMFC. Models [26, 27] were proposed recently to fit the CVs at different ages of MEA to describe cathode catalyst degradation. The models only considered the Pt redox reaction and neglected CSC, which makes them not fit the data well at the high potential range. It can be improved by incorporation with a CSC model. However, the CSC in the literature [1, 9, 28] did not consider the current wave above 1.0 V and without comparison with the experimental data. Better modeling requires experiments with capability to resolve the CSC current from Pt redox current, and characterize them during accelerated degradation testing.

Differential electrochemical mass spectrometry (DEMS) can resolve the CSC current from Pt redox reactions current by using an online mass spectrometer to sample the products from the cathode of PEMFC, with potential imposed by a potentiostat. DEMS spectra of cathode exhaust gases, CO_2, H_2 and O_2, coupled with cyclic voltammograms were analyzed to characterize the hydrogen evolution reaction (HER), hydrogen oxidation reaction (HOR), oxygen reduction reaction (ORR), Pt electrochemical redox reactions, as well as correlates them to CSC in a real 5 cm^2 single PEMFC. The DEMS spectra changing with time were also examined to characterize CSC and Pt redox reactions to better understand their effects on cathode catalyst degradation.

5.2 Experimental

Three 5 cm^2 square MEAs with different cathodes were fabricated for testing. A sheet of carbon paper (6 × 8 cm, TGP-H-060, Toray®) was coated with 0.5 mg/cm^2 carbon black (Vulcan XC-72R, Cabot) on one side as a diffusion layer and then loaded with 20 wt% Teflon (Aldrich). Five square pieces of 5 cm^2 were cut from the sheet for the electrodes with diffusion layers.

Another sheet of carbon paper (5 × 6 cm, TGP-H-060, Toray®) was only loaded with 20 wt% Teflon for an electrode without a diffusion layer. Three identical anodes and one cathode (denoted as PtC-cathode) were then made by brushing 0.5 mg_{Pt}/cm^2 catalyst (20 wt% Pt/C, E-tek) on the diffusion layer of four pieces of 5 cm^2 treated carbon paper, respectively. The other two cathodes were prepared by brushing with 2 mg/cm^2 carbon black on the diffusion layer (denoted as C-cathode) of a piece of 5 cm^2 treated carbon paper and 0.5 mg/cm^2 Pt black (Alfa Aesar) on a piece of 5 cm^2 treated carbon paper without the diffusion layer (denoted as Pt-cathode), respectively. Each MEA was fabricated by hot-pressing an anode, a piece of Nafion 1135 membrane and a cathode together like a sandwich using a hot press (Model C, Carver) at the condition of 160 ºC, 300 pounds, and 150 s. The MEAs with C-cathode, Pt-cathode, and PtC-cathode were denoted as C-MEA, Pt-MEA, and PtC-MEA, respectively. They were then assembled in a 5 cm^2 single cell hardware (Electrochem, Inc.) for testing.

The DEMS experiments were described in detail in Chapter 3 and 4. In this chapter, all DEMS experiments were conducted with humidified H_2 and humidified He fed to the anode and cathode respectively. Cyclic voltammetry or chronoamperometry were two strategies involved to control the cathode potential. The exhaust gases from the cathode were detected by a quadrupole mass spectrometer (QIC-20, Hiden Analytical) and MS signals with m/z = 2, 32, and 44 were recorded for analysis. O_2 and CO_2 are only sources contributing to MS signals with m/z = 32 and 44, respectively. However, the MS signal with m/z = 2 was generated from the H_2 and the fragment of water. To discriminate between them and determine the formation of the MS signal (m/z = 2) changes as potential cycling, H_2 and He were replaced by deuterium gas (D_2, 50 sccm, Research grade, Airgas) and Ar (30 sccm, UHP, Airgas), respectively. This type of DEMS experiment is denoted as D-DEMS.

Two different concentration standard CO_2 gases balanced with He (certified gas standards, 487.2 ppm ±2% and 2439 ppm ±2%, Airgas) were fed to the cathode to create a calibration curve for CO_2 concentration. 6 μL H_2 and CO_2 were injected to the cathode to quantify the peaks of H_2 and CO_2, respectively.

5.3 Results and Discussion

5.3.1 Identify the Sources and Changes of the MS Signals with m/z = 44 and 2

DEMS experiments show there are MS signals with m/z = 44 and 2. Because CO_2 is the only source of the MS signal with m/z = 44, its changes thus come from carbon corrosion. This carbon could be the carbon support of the catalyst or the carbon paper and need to be determined. The MS signal with m/z = 2 is generated from H_2 and a fragment of water. It needs to be known which actually contributes the signal changes. Furthermore, Pt and C are two components existing at the typical cathode with Pt/C catalyst. The relationship of both components and MS signal changes (m/z = 44 and 2) also need to be understood. DEMS results of three MEA (C-MEA, Pt-MEA and PtC-MEA) were thus compared to determine the sources of the CO_2 MS signal, and the relationship among the changes of CO_2 and m/z =2 MS signals, Pt and carbon support. Moreover, D-DEMS experiment was conducted to indentify water or H_2 contributing to the changes of MS signal with m/z = 2.

Figure 5-1a shows the CO_2 MS signals against the mass spectrometer data acquisition step when the cathode potential was cycled in the range of 100–1400 mV at 10 mV/s. It shows significant CO_2 MS signal peaks of the C- and PtC-MEA, while a very weak peak of the Pt-MEA. This means that the CO_2 signal comes from the oxidation of the carbon black. The very weak CO_2 MS signal peaks of Pt cathode might come from the oxidation of the carbon paper which

supports the Pt black. Figure 5-1a also shows three more peaks in the middle of the CO_2 MS spectra of PtC-MEA than that of C-MEA, which suggests there are three more different reactions contributing to the CSC at the cathode of PtC-MEA. In addition, the PtC-MEA has a stronger CO_2 signal at 1400 mV than that of C-MEA. Both indicate that Pt catalyzes the CSC by various pathways and intermediates [4-7]. The pathways and the oxygen sources of CO_2 were investigated by the ^{18}O-DEMS in chapter 4.

Figure 5-1b shows the changes of MS signal with m/z = 2 of the Pt-MEA and PtC-MEA, whereas no change is seen for the C-MEA. The similarity of these MS (m/z = 2) peaks and plateaus of Pt-MEA and PtC-MEA implies that these signal changes are related to the Pt with the same mechanisms.

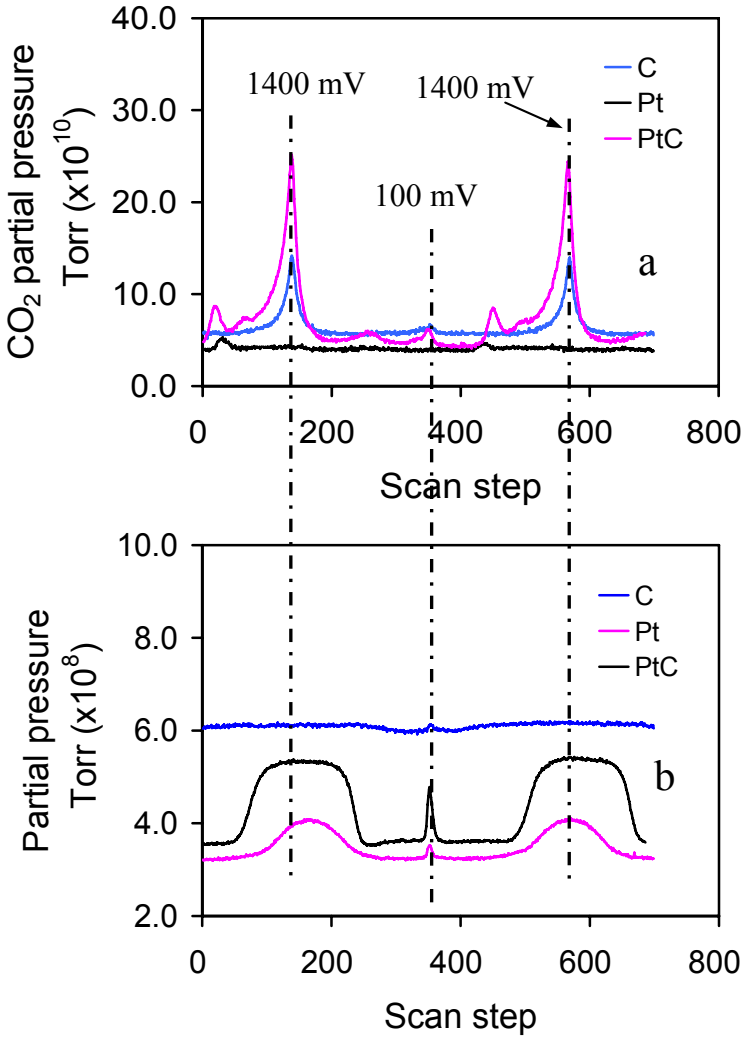

Figure 5-1 MS spectra of CO_2 (a) and m/z = 2 (b) of C-, Pt- and PtC-MEA at 30 ºC (scan step in all figures means the mass spectrometer data acquisition step. The numbers on axis are relative.)

However, an MS signal with m/z = 2 can be generated from the H_2 and a fragment of water. Thus, a D-DEMS experiment, H_2 replaced with D_2, was conducted to discriminate between them. The result shows there are peaks and plateaus of MS spectra with m/z = 3 and 4,

corresponding to DH and D_2 respectively in Figure 5-2. No significant change of MS signal with m/z = 2 was observed. The DH is ascribed to the isotope exchange of D_2 with water vapor on Pt and the active sites could be deactivated by the liquid water [29]. These results confirm that the changes of MS signal with m/z = 2 in Figure 5-1b are not attributed to water but H_2.

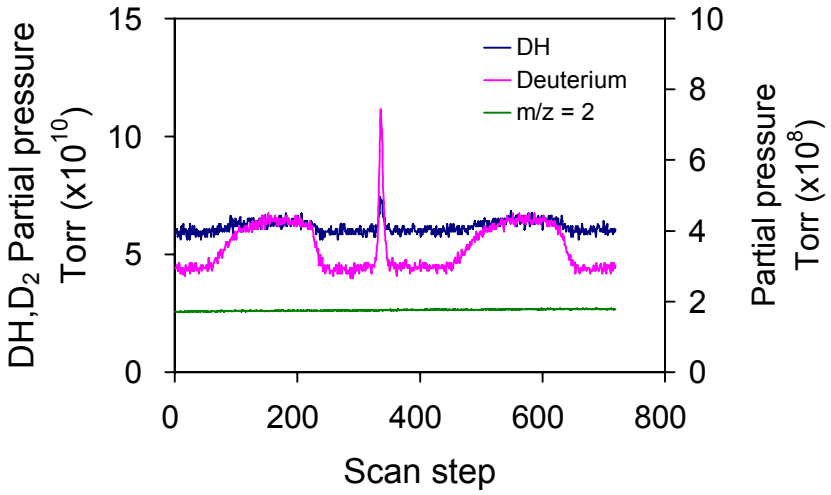

Figure 5-2 MS spectra of PtC-MEA with D_2 fed to the anode and Ar to the cathode at 30 ºC

5.3.2 Formation of H_2 Peak and Plateau

Peak and plateau are two types of H_2 MS signal change in DEMS experiments of PtC-MEA, shown in Figure 5-3. Their formation could be attributed to hydrogen oxidation reaction (HOR), hydrogen evolution reaction (HER) and/or hydrogen adsorption/desorption on Pt.

Because there is neither significant temperature increase (constant at 30 ºC) nor Pt surface structure changes means that the adsorption/desorption mechanisms can be excluded. Therefore, the H_2 peak and plateau should be attributed to hydrogen electrochemical reactions, i.e. HOR and HER.

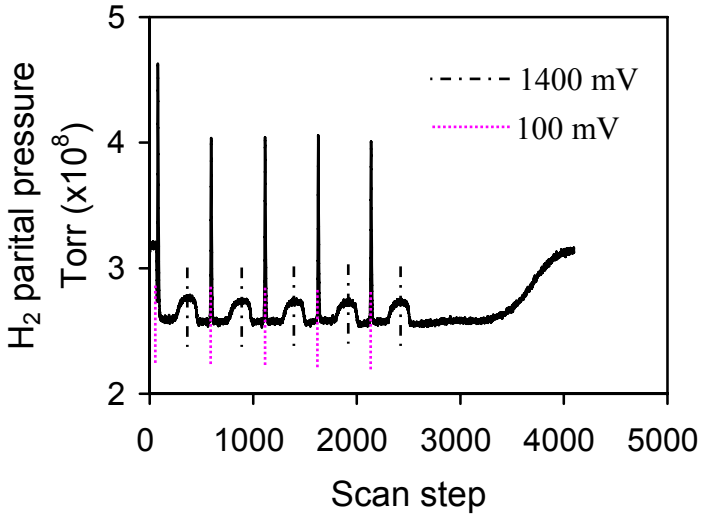

Figure 5-3 H_2 MS peaks and plateaus of PtC-MEA in a five-cycle period at 40 ºC

There are two types of H: underpotential deposition H (H_{UPD}, 0–400 mV), and overpotential deposition H (H_{OPD}, most below 0 mV). As known, only H_{OPD} contributes to hydrogen evolution as follows [30].

HER:

$$Pt + H^+ + e^- = Pt\text{-}H_{OPD} \text{ (Volmer)}$$

followed by either

$$Pt\text{-}H_{OPD} + Pt\text{-}H_{OPD} = 2Pt + H_2 \text{ (Tafel)}$$

or $$Pt\text{-}H_{OPD} + H^+ + e^- = Pt + H_2 \text{ (Heyrovsky)}$$

Though the range of 0–400 mV is the H_{UPD} region, there is small amount of H_{OPD} extending to this region [31].

The H_2 peak in DEMS was quantified with injection of 6 μL H_2 into the cathode, and compared with the amounts of H represented by the H waves of the CV to identify the formation

of the H_2 peak.

It was found that the amount r H_2 peak is quite small compared to the total amount of H from the H waves of the CV, with the double layer charge subtracted. This implies that the H_2 peak comes from the H_{OPD} extending to the H UPD region. In other words, the H waves in CV consist of main part of H_{UPD} and small part of H_{OPD}.

It was measured that the cathode potential is around 110–130 mV when the PEMFC is at open circuit. The cathode is also a hydrogen electrode in these DEMS experiments, but with lower concentration of H_2, permeating through the membrane from the anode. The H overpotential and underpotential depositions occur at this potential range. When the cyclic voltammetry experiment starts, the potential changes from 110–130 mV to 100 mV rapidly, leading to the H_{UPD} and H_{OPD} reduction but only H_{UPD} contributing to HER to produce the H_2 peak.

When the potential starts scanning from 100 mV in the anodic direction, the H_2 undergoes electrochemical oxidation causing the H_2 signal decrease. The HOR increases fast with potential but is limited by H_2 diffusion through the membrane, leading to a lower baseline (lower base of the plateau). The potential keeps increasing until the Pt surface is covered by an oxide film. This decreases the catalytic effects of Pt on HOR, leading to less H_2 consumption and thus H_2 signal increase. It is then limited by the kinetics of HOR and form the upper base of the plateau.

In a D-DEMS experiment, there are no significant changes of m/z = 2 signal in Figure 5-2, which is only from the fragment of water. This suggests that water is not the source of H for HOR and HER when H_2 exists at the cathode. It could be that it is much easier for the H from H_2 than from water to adsorb on Pt surface as H_{UPD} and H_{OPD}.

5.3.3 Determine the Limit Step of H_2 Peak and Plateau Formation

In the previous section, it has been shown that H_2 peak and plateaus are attributed to HER and HOR, respectively. This H_2 is permeated from anode thorough the membrane. Whether the formation of H_2 peak and plateaus is limited by kinetic or permeation through the membrane was determined by the experiments of temperature and potential scanning rate dependences.

Figure 5-4 shows that the H_2 peaks increase with temperature but the plateaus do not. The permeation of H_2 from the anode through the membrane to the cathode increases with temperature, leading to more H_{OPD} on the Pt at the cathode. Besides, the HER related to the peaks also becomes faster. Both of them contribute to larger H_2 peaks at a higher temperature. However, high temperature increases the rate of HOR, which causes more H_2 consumption at the cathode. It could compensate for the increase of H_2 permeating through the membrane from the anode. Overall, the heights of the H_2 plateau at different temperatures do not change significantly. Figure 5-4 also shows the H_2 baseline increase with temperature. This is attributed to both increase of the permeated H_2 and the water from the humidifiers.

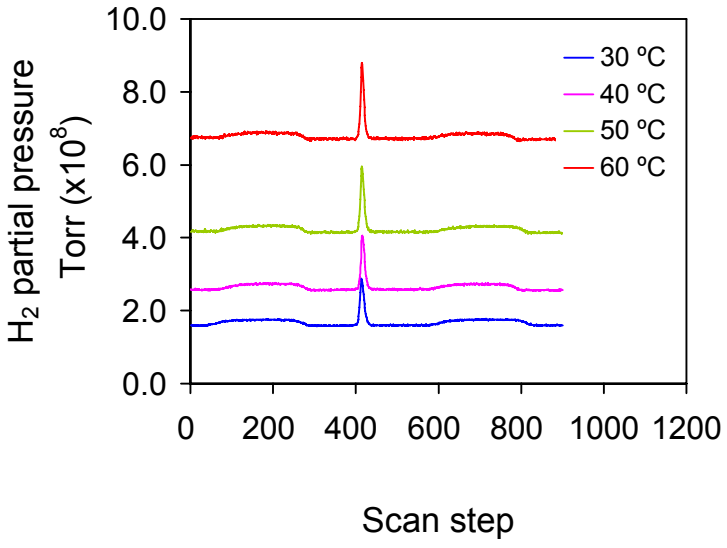

Figure 5-4 H_2 MS peaks and plateaus of PtC-MEA at 30, 40, 50 and 60 ºC

Figure 5-5 shows that the H_2 peaks decrease with the potential scan rate. According to cyclic voltammetry theory, faster potential scan rate should produce larger current, i.e. larger H_2 peak in this experiment, when the reaction is kinetic limited. The opposite result means it is diffusion limited. Faster potential scan rate means less time of one potential cycle, which brings about less H_2 transferring through the membrane for the peaks. Thus, the peak decrease with scan rate increase doubly confirms that the HER are controlled by the H_2 diffusion rate through the membrane. However, Figure 5-6 shows the plateaus change significantly with potential scanning rate also. Changing potential scan rate does not change the H_2 diffusion through the membrane and the concentration at the cathode. As discussed above, the lower bases of the plateaus are caused by the HOR with the diffusion limit of H_2 in the membrane. Thus the lower bases stay constant at different potential scan rates. The H_2 has to diffuse through the Nafion layer on the catalyst to be oxidized. Similarly, the constant height of plateaus means the HOR is controlled by the diffusion of H_2. It also might be the HOR is zero at the upper bases of the plateaus.

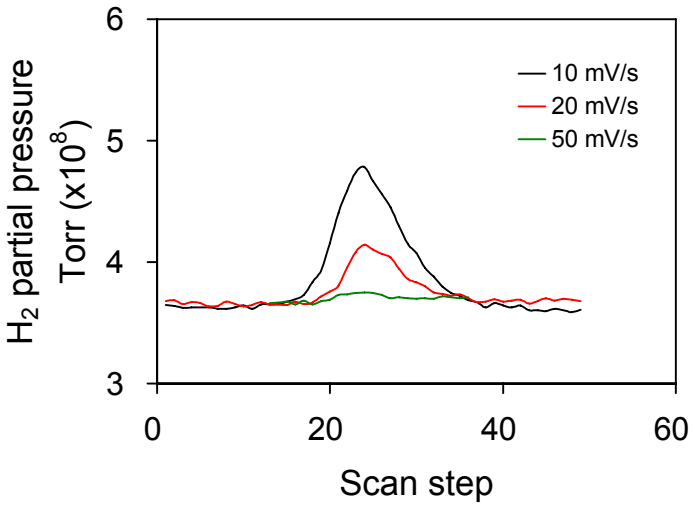

Figure 5-5 H_2 MS peaks of PtC-MEA at 10, 20 and 50 mV/s at 40 ºC

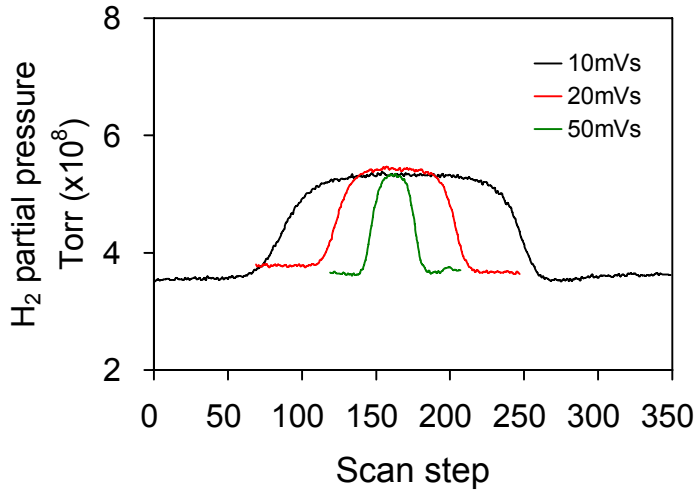

Figure 5-6 H_2 MS plateau of PtC-MEA at 10, 20 and 50 mV/s at 40 ºC

5.3.4 Reactions Occurred When PEMFC is at Open Circuit

During DEMS experiments, the PEMFC is very often at open circuit. MS signals of H_2 and CO_2 in the first several potentials cycles of DEMS experiments can tell if there are reactions occurred when the PEMFC is at open circuit. To understand it can exclude the effects from these reactions for DEMS investigation of CSC and characterization of cathode catalyst degradation.

Figure 5-7a shows the CO_2 MS signals in the first three cycles of DEMS experiments decrease significantly. Before the potential cycling, the PEMFC is at open circuit with measured cathode potential in the range of 110–130 mV. At this low potential, $2e^-$ ORR occurs to produce H_2O_2, which oxidizes the carbon to produce surface oxides and accumulated. These accumulated surface oxides were then oxidized to produce CO_2 when the potential starts cycling. The other factor is that the Pt was reduced much more completely leading to less oxide film on the Pt, which increases its catalytic effect on the CSC to produce more CO_2. These two factors effects were eliminated in about three cycles. All the DEMS study, if no mention, used the forth and fifth cycles of CV and DEMS spectra.

However, Figure 5-7b shows only the first peak of the H_2 MS signal is significantly larger than the later peaks. Similarly, Figure 5-7c shows only the first CV has slightly higher H reduction and Pt oxidation waves than those in the later CVs. As discussion above, the H_2 peaks are generated from the HER. Larger H_2 peak means more H_{OPD} is adsorbed on Pt and released by HER. At open circuit with the cathode potential of 110–130 mV, the Pt is continuously reduced while H_{OPD} is also continuously produced and adsorbed on the Pt surface. The first cycle thus has longer adsorption time and more Pt metallic sites for H_{OPD} adsorption, leading to more H_{OPD} thus to larger H_2 MS peak. It was also shown with larger H reduction waves in the first CV. The larger Pt oxidation current could be attributed to the CSC current increase at the first cycle. The

following cycles did not show significant difference implies the HER is fast and complete.

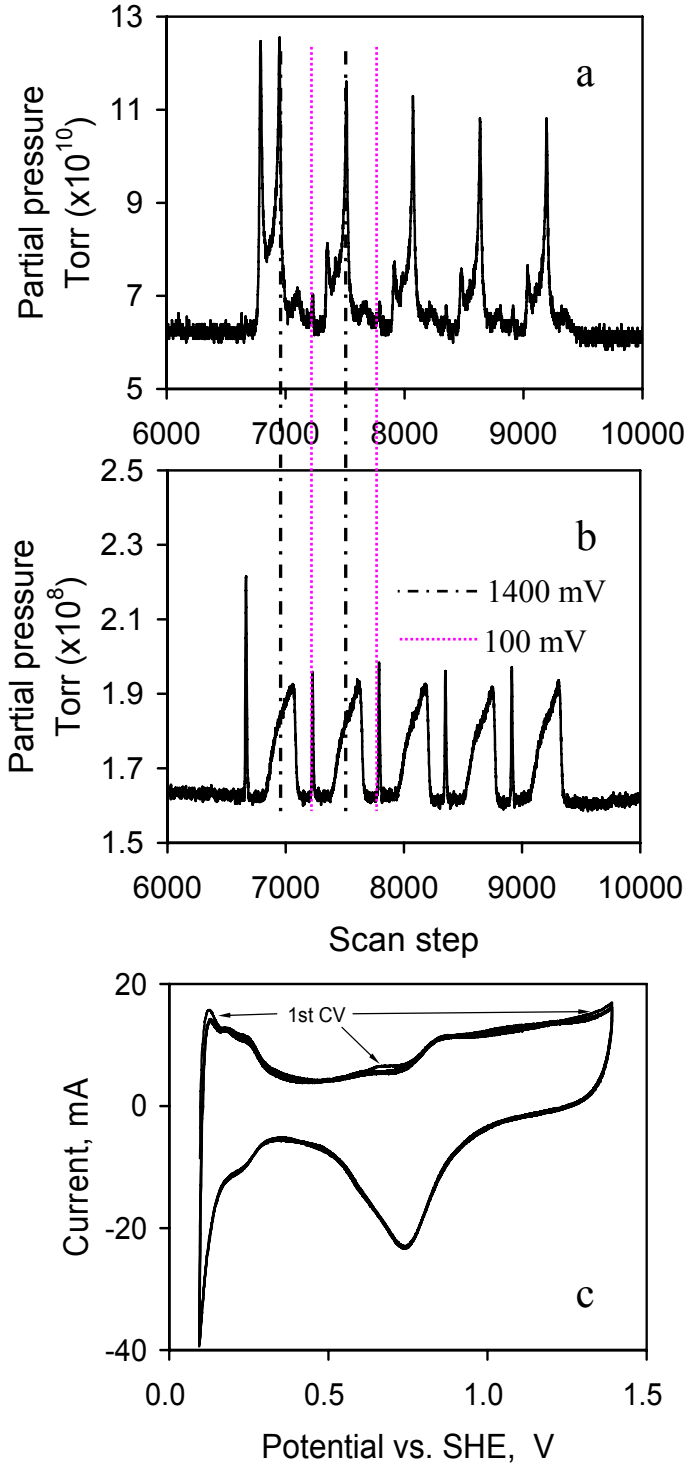

Figure 5-7 MS spectra of CO_2 (a) and H_2 (b), and CVs (c) of the PtC-MEA in a five-cycle period at 40 ºC

5.3.5 Quantify and Resolve the CSC Current and Pt Redox Current

The CV of Pt/C in sulfuric acid or a real PEMFC consists of Pt redox current and CSC oxidation current, which overlap. To model the CV, it is required to resolve and quantify the CSC current and Pt redox current. DEMS has the capability to resolve the CSC current and Pt redox current by detecting the CO_2 produced from CSC. The amount of CO_2 produced in one potential cycle of DEMS can be determined by injection of 6 μL CO_2 to the cathode.

Figure 5-8 shows the CO_2 MS peaks of three injections of 6 μL CO_2 with quite good reproducibility. When the cathode has the catalyst (20% Pt/C) loading of 0.5 mg_{Pt}/cm^2, the carbon black support can be consumed up in less than 2000 potential cycles in the range of 100–1400 mV at the rate of 10 mV/s, which is a good match with the literature [5].

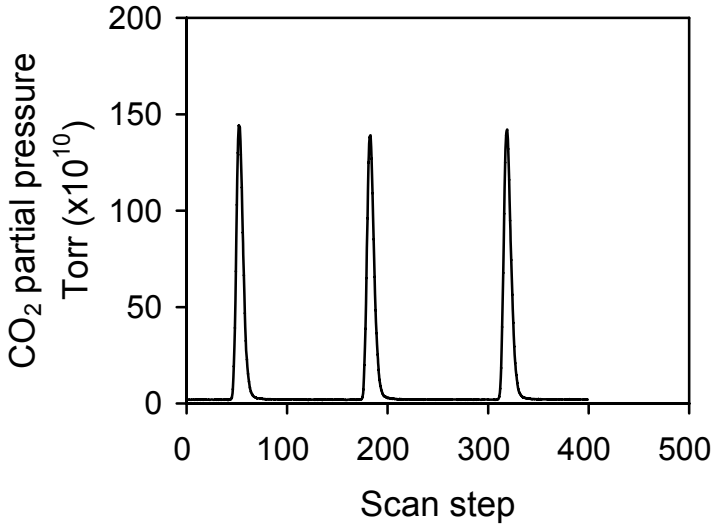

Figure 5-8 Calibration of CO_2 peaks (6uL) in PEMFC with Pt/C-MEA at 30 ºC

CSC current could be significant compared with the Pt redox reactions current contributing to the CV. The concentration of CO_2 produced from CSC was determined using the

calibration curve in Figure 5-9, constructed by feeding two different concentration CO_2 gases to the cathode at the open circuit. According to the Faraday law, the CSC current was then calculated from the concentration of CO_2. The Pt redox reactions and CSC were thus resolved shown in Figure 5-10 with the total CV and the CV from the CSC producing CO_2.

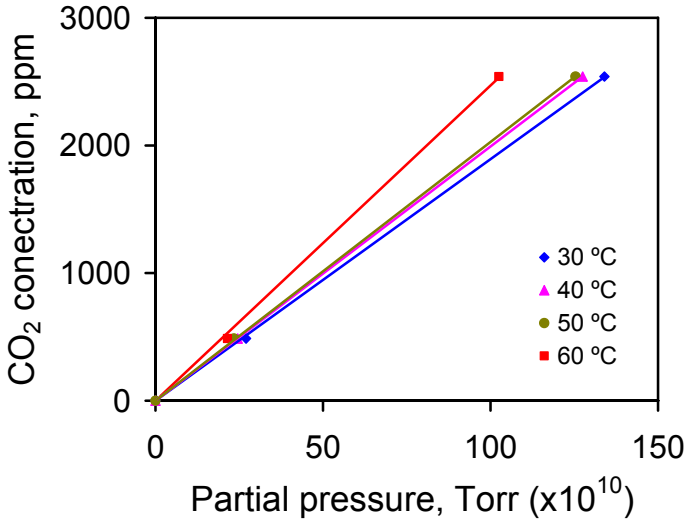

Figure 5-9 Calibration of CO_2 intensity in PEMFC with PtC-MEA at 30, 40, 50 and 60 ºC

In Figure 5-10, the current from CSC increases dramatically after 1.2 V, which makes it non-negligible to model the total CV. This is the reason that the model of Pt dissolution at the cathode without consideration of CSC did not fit the CV well especially at high potential [27]. It also suggests that if the potential is lower than 1.2 V, it is not necessary to consider the CSC in the modeling.

Carbon oxidation could produce surface oxides as nonvolatile products as well as CO and CO_2 as volatile products. In the cathode of PEMFC, the CO could be ignored because Pt catalyzes the CO electrochemical oxidation to CO_2 extensively. Chapter 4 showed that the

surface oxides from CSC have one pathway to be further oxidized to CO_2 and the other pathway to accumulate on the carbon surface. The ratio of current from both pathways is not yet determined in the literature. The total current of CSC should larger than the current of CSC producing CO_2.

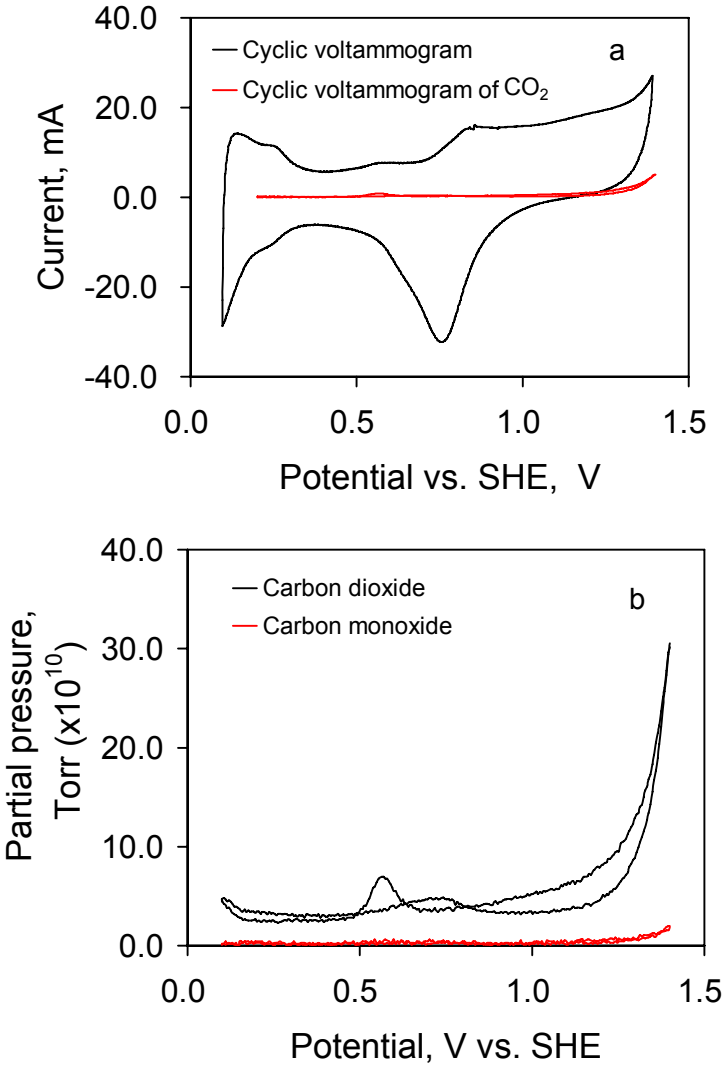

Figure 5-10 DEMS spectra of CO_2 (a) and CVs (b) of the PtC-MEA at 60 ºC

5.3.6 The Kinetic of CSC

An assumption was proposed in this study that the Nafion resin spreads uniformly on the cathode catalyst. The water diffuses through the Nafion layer and reaches the carbon surface for reactions. The thickness of this Nafion layer was calculated around 0.4 nm (ignore the volume of Pt, 20% Nafion loading on 20% Pt/C, carbon black with 50 nm dia.), which is quite small compared to the diameter of carbon black. Thus the interface of the carbon black with the Nafion layer is reasonably treated as flat for CSC study. This allows use the conclusions drawn from an electrochemical reaction happening on a flat interface.

Modeling the accelerated degradation requires an understanding of the kinetic characteristics of CSC, such as reversible or irreversible, kinetic controlled or diffusion controlled, Tafel parameters, and temperature dependence.

Potential cycling rate variation and potential step method were conducted to determine if an electrochemical reaction is reversible/irreversible and kinetic controlled/diffusion controlled. Figure 5-11 shows that peak II, III and V in DEMS spectra of CO_2 shift with potential scanning rates. This means that the CSC reactions at these potentials are irreversible or sluggish.

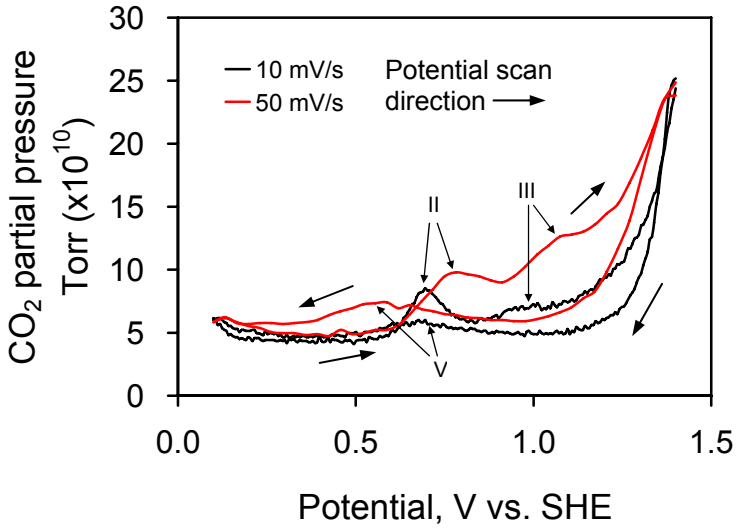

Figure 5-11 DEMS spectra of CO_2 of PtC-MEA at 10 and 50 mV/s at 40 ºC

However, this method is not feasible for peak I and IV in Figure 3-1c because they are located at the potential scanning limits and not real peaks. Peak I actually results from the chemical oxidation of carbon by H_2O_2, which is the product of the $2e^-$ ORR. Because the PEMFC hardly runs around this potential, it was not investigated in detail in this study.

Potential step method is the alternative method to determine if an electrochemical reaction is reversible and diffusion controlled. Figure 5-12a shows the chronoamperogram of CSC at 1400 mV. According to the Cottrell equation [32], the current is inversely proportional to the square root of time for reversible electrochemical reactions with diffusion limits. Thus the ln(CO_2 partial pressure) was plotted against ln(t) in the first 20 s range in Figure 5-12b. A slope of -0.51 means that the CSC is facile and diffusion controlled at 1400 mV.

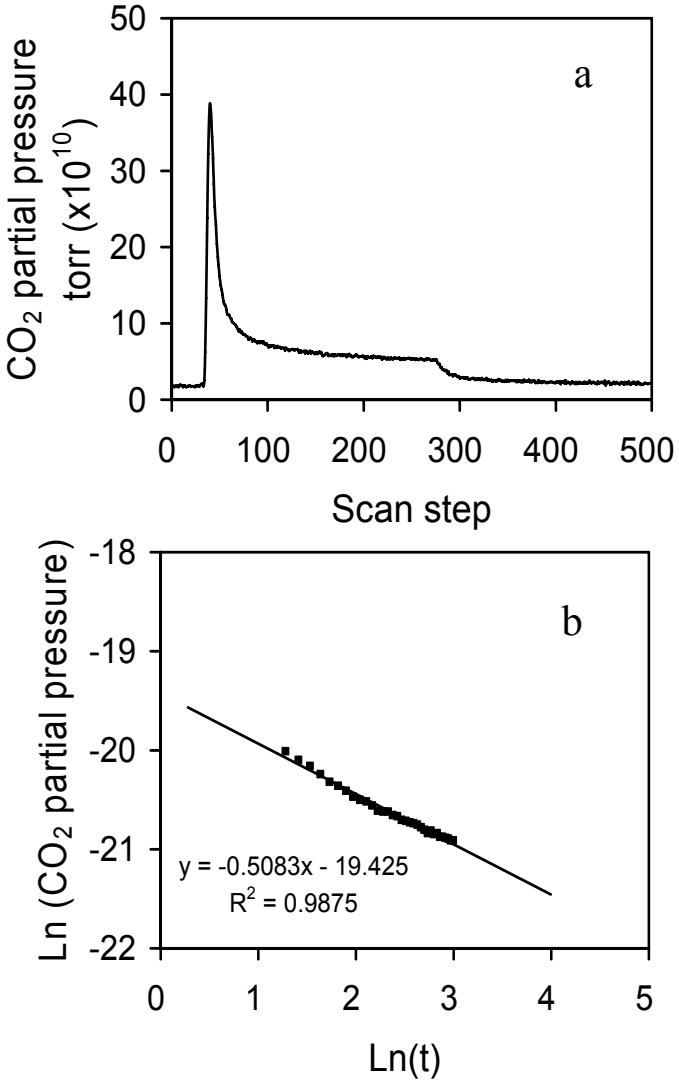

Figure 5-12 Chronoamperogram (a) and plot (b) of ln(CO_2 partial pressure) against ln(t) of CSC at the potential of 1400 mV

The five peaks except for the first peak in DEMS spectrum of CO_2 suggest the CSC has at least four electrochemical reactions. These reactions are not yet understood and neither are their standard potentials. However, it is still feasible to estimate the transfer coefficients of these reactions by Tafel plots using the slow potential scanning method. The oxidation Tafel plots of peaks II, III, and IV are shown in Figure 5-13. They are linear and the slopes are expressed in (1-α)F/2.3RT. The parameters of those Tafel plots are shown in Table 5-1.

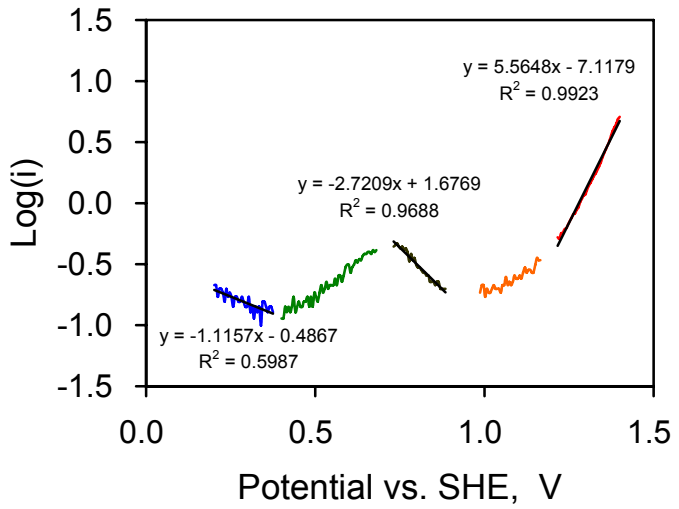

Figure 5-13 Anodic Tafel plot of CSC at the Pt/C cathode at 60 ºC

Table 5-1 Tafel parameters of peak II, III and IV in anodic direction

peak	slope	alpha
II	12	0.21
III	1.3	0.91
IV	3.8	0.75

Figure 5-14 shows the Tafel plots of the reverse anodic peak IV, and peak V in cathodic direction. Their parameters are shown in Table 5-2. Those parameters can be used in the CSC modeling and estimation of the standard potentials of these reactions.

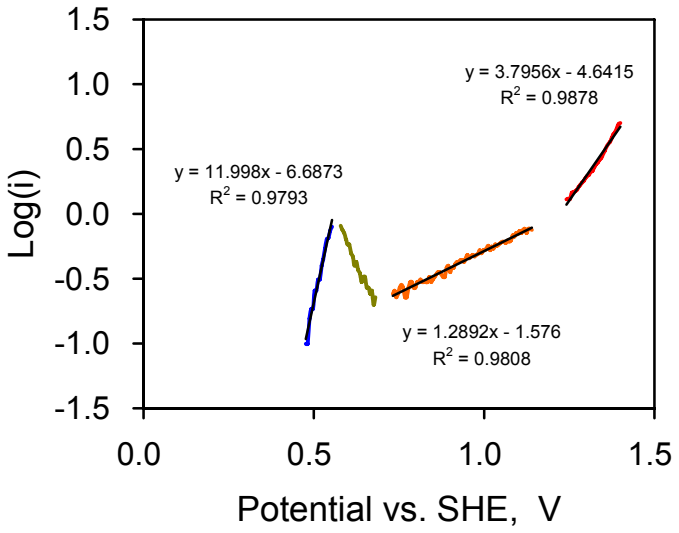

Figure 5-14 Cathode Tafel plot of CSC at the Pt/C cathode at 60 ºC

Table 5-2 Tafel parameters of peak IV and V in cathodic direction

Peak	Slope	alpha
IV	5.6	0.66
V	-2.7	0.16

Figure 5-15 shows that the plots for the logarithm of CSC rates of the peaks at 100, 600 and 1400 mV in anodic direction as well as at 750 mV in cathodic direction against inverse temperature (1/K) are linear, consistent with literature [5, 6]. However, there are no plots of logarithm of rate constants of CSC against 1/K, i.e. Arrhenius plot, in the literature, which is

commonly used to determine the activation energy of a chemical reaction or diffusion process. Carbon black, carbon surface oxides, and water are three reactants involved in the CSC in PEMFC. We assume that $r_{obs} = k_{obs}[H_2O]^a[C]^b[C_{oxi}]^c$, based on the conclusion that the carbon surface oxides and carbon do not affect each other in CSC [21]. Carbon and surface oxides are in the solid phase so that their activities can be set to unity. The rate equation then becomes $r_{obs} = k_{obs}[H_2O]^a$, where the $[H_2O]$ means the water activity in the Nafion resin wrapping the catalyst.

The linear plots in Figure 5-15 imply that $r_{obs} = k_{obs}$. It was reported [13] that the activity of water in the Nafion membrane depends on the temperature and partial pressure of water. Thus $a = 0$ has to be met to get $r_{obs} = k_{obs}$. However, the rate dependence on water molar concentration was shown to be linear by varying the total pressure but keeping the water partial pressure constant [5], which means the rate order of water for CSC is unity. According to this result, the r_{obs} is equal to $k_{obs}[H_2O]$, then the $k_{obs} = r_{obs}/[H_2O]$. Unfortunately, the logarithm of $r_{obs}/[H_2O]$ for CSC against 1/K is not linear.

The results conflict when treating the Arrhenius plot using kinetic equation as above. A straight Arrhenius plot could also imply the reaction is located in the diffusion controlled region. This matches the conclusions above that the peak II, III and IV are sluggish and peak IV is diffusion limited. The activation energies calculated from the plots in Figure 5-15 are 46, 25, 29, and 37 kJ/mol for peak I, II, IV, and V respectively.

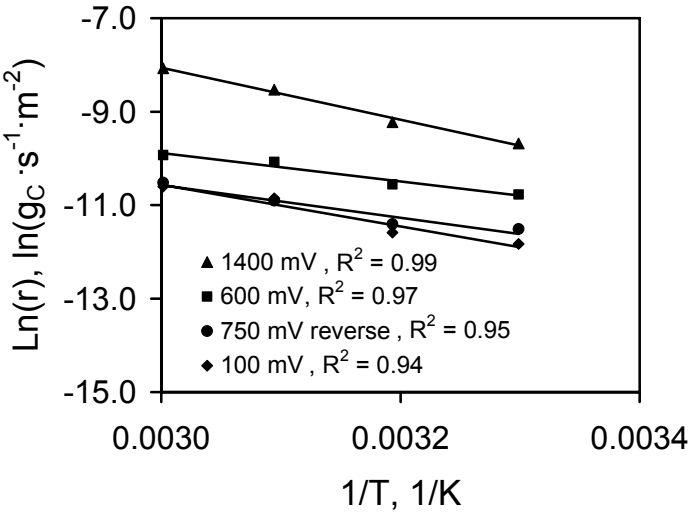

Figure 5-15 Logarithm of the CSC rates of the peaks at 100, 600 and 1400 mV in anodic direction as well as at 750 mV in cathodic direction against inverse temperature (1/K)

5.3.7 Accelerated Degradation Characterized by DEMS

Potential cycling and potential holding are two common methods to accelerate degradation of electrocatalyst. In this study, both methods were adopted to control the cathode potential of PEMFC with the cathode exhaust gases detected by a mass spectrometer, i.e. DEMS experiments with different potential control strategies. The more effective one was then conducted to accelerate the cathode catalyst. The changes of MS signals of exhaust gases CO_2, H_2 and O_2 were used to characterize the accelerated degradation of cathode catalyst in PEMFC.

Figure 5-16 shows the ECSA degradation of Etek Pt/C catalyst on a GC electrode in 0.5 M H_2SO_4 against time under conditions of constant potential at 1200 mV and potential cycling from 50–1200 mV at the rate of 50 mV/s. It was found that potential cycling causes faster degradation than constant potential. Pt dissolution and CSC are both electrochemical oxidation

reactions and their overpotentials increase with potential in the range of 50–1200 mV. Thus they are at the largest overpotential through the whole experiment under constant potential at 1200 mV, and at lower overpotential for most time under potential scanning from 50–1200 mV. However, the degradation is slower at constant potential than potential scanning. This implies that there are other factors with severe impact on the reactions.

Generally, the reaction rate is determined by the diffusion and kinetics in serial. When the potential is fixed, the gradient will continuously decrease. After certain time, the reaction becomes diffusion limited and the rate is very low. When the potential is scanning, the concentration gradient at the interface between the electrolyte and electrode are variable. These were verified in that the amount of CO_2 at 1400 mV in Figure 5-12a becomes very small and continuously decreases, whereas the amount of CO_2 by potential cycling is still significant as shown in Figure 5-7a. Thus the overall charge, current multiplied by time, at potential scanning is larger than that of the constant potential.

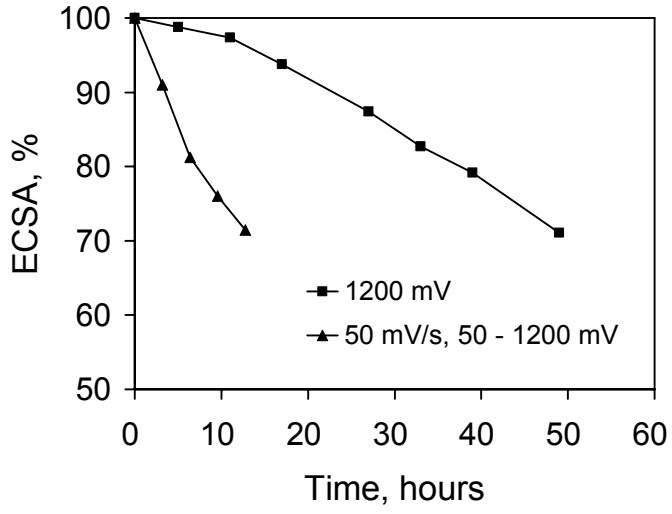

Figure 5-16 ECSA degradation against time of Etek Pt/C catalyst in 0.5 M H_2SO_4 using potential cycling and holding at 30 ºC

Figure 5-17 shows that the ECSA of MEA decreases with potential scanning from 100–1400 mV at the rate of 400 mV/s with the similar trend of catalyst coated on GC electrode in 0.5 M H_2SO_4. Though the ECSA decreases significantly, the H_2 MS peaks from the HER on Pt did not change significantly with cycles, shown in Figure 5-18. The reason is that the HER here is controlled by the H_2 diffusion through the PEM from the anode to the cathode. The hardly changed peaks also imply that the membrane did not degrade significantly during this accelerated testing using potential scanning. As is known, membrane degradation in PEMFC is mainly caused by the attack from the H_2O_2 produced by $2e^-$ ORR. In the DEMS experiments, the O_2 is leaking from the environment and the concentration is very low, which makes the degradation of PEM can be ignored.

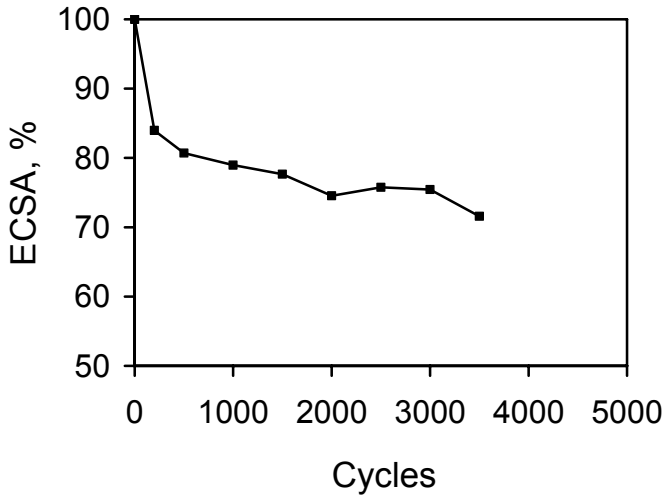

Figure 5-17 ECSA degradation against time of PtC-MEA using potential cycling at the scan rate of 400 mV/s in the range of 100–1400 mV at 30 ºC

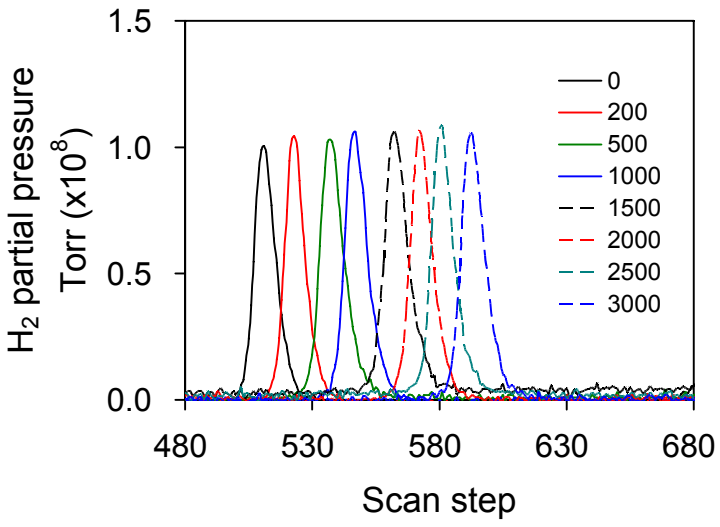

Figure 5-18 H_2 MS peak of PtC-MEA change with potential cycle number at 30 ºC

Figure 5-19 shows the H_2 plateaus decrease significantly with potential cycles. At the working electrode of the PEMFC in the DEMS experiments, hydrogen oxidation and Pt oxidation were occurred when the potential was scanned in the anodic direction. Because the permeation of H_2 from the anode did not change, the H_2 plateau in DEMS spectra is caused by the surface of Pt oxidation, leading to a loss in catalytic capability for hydrogen oxidation. The significant H_2 plateau decrease with cycles is attributed to the Pt oxidation decrease. This is consistent with the result [27] that the standard potential of Pt NPs increases with particle size. Besides, the catalyst is still over an amount required to catalyze the HOR because the concentration of H_2 is very low in the DEMS experiments.

This is one way to characterize the Pt degradation at the cathode of a PEMFC. The baseline of the plateau variation might be attributed to the changes of baseline of MS signal and water amount from the humidifier over time.

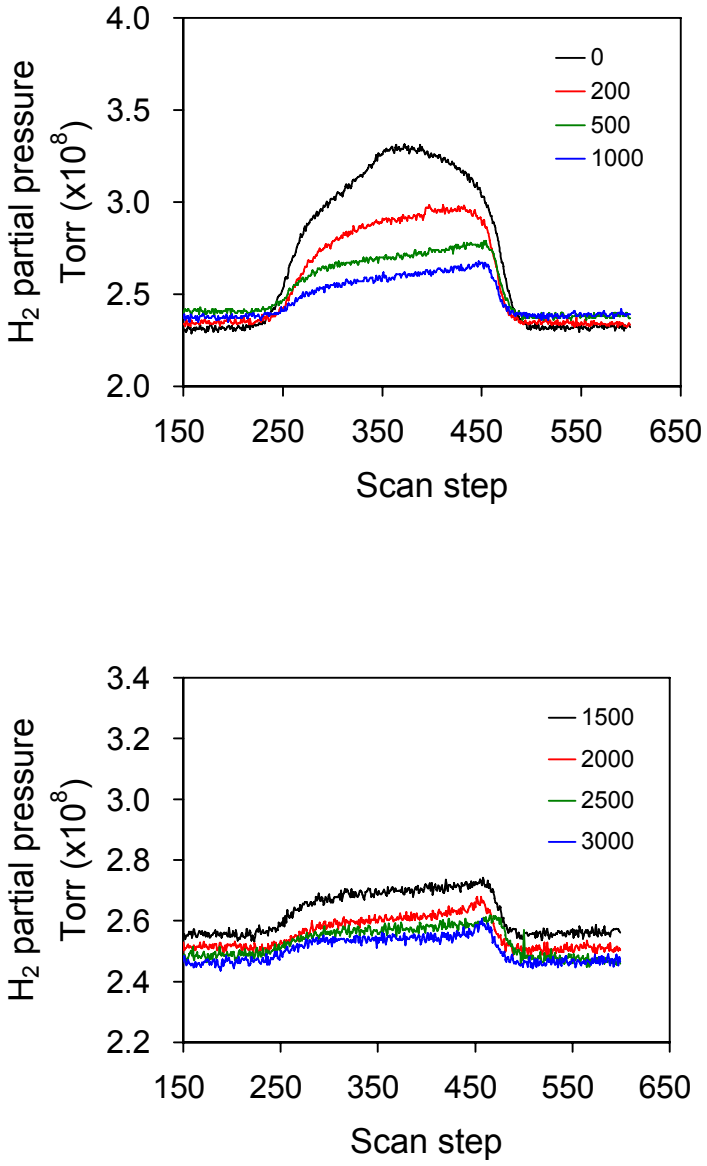

Figure 5-19 H_2 MS plateau of PtC-MEA change with potential cycle number at 30 ºC

Figure 5-20 shows that the height and width of the O_2 plateaus did not change significantly, which means the Pt change did not affect ORR significantly. This might be attributed to the lower concentration of O_2 than H_2. Thus the O_2 plateau is not suggested to characterize Pt degradation. The variation of the baselines might be ascribed to the shift of MS

detector sensitivity and the leakage of O_2 from the environment over time.

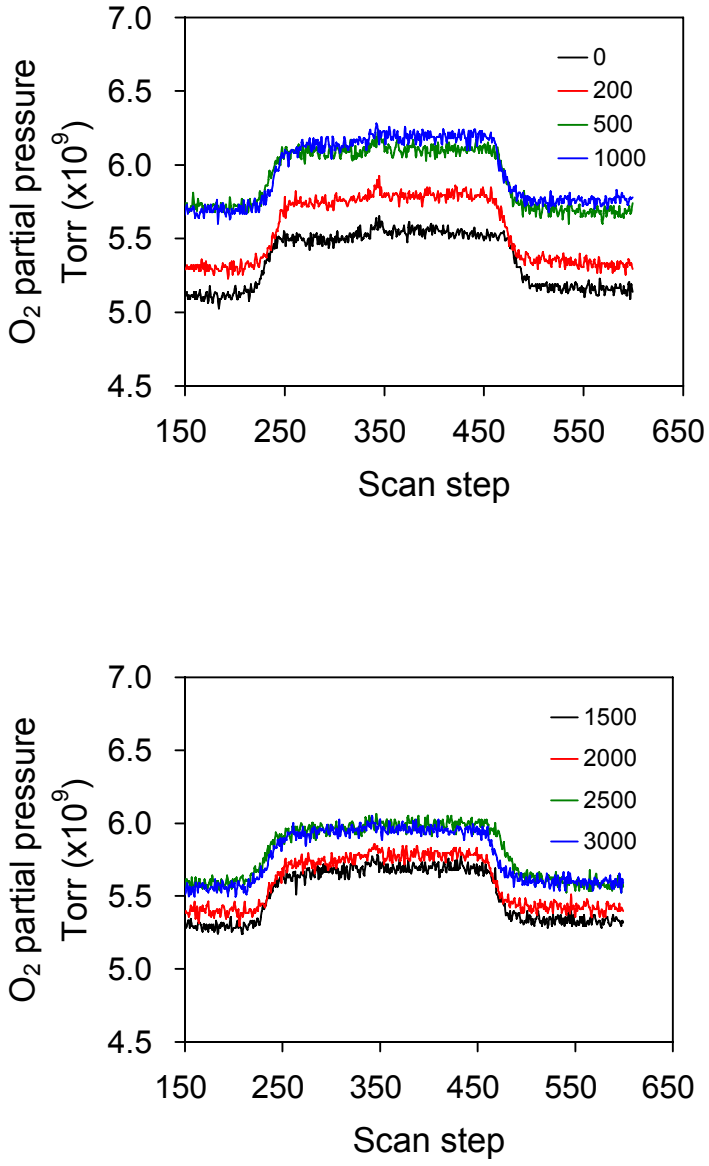

Figure 5-20 O_2 MS signal of PtC-MEA change with potential cycle number at 30 ºC

Figure 5-21 shows the CO_2 MS signal decrease with potential cycles. Though the intensity decreases, the profile still keeps similar, i.e. the two anodic peaks located around 600 mV and 1000 mV, as well as the reverse anodic peak around 750 mV are still apparent. This

means that the catalytic effects of Pt on CSC still exist but get weaker. In other words, it implies that the Pt is still active and in good contact with the carbon black well. The CO_2 signal at 1400 mV decreases fast before 2000 cycles and then become slow, which is similar with but decreases faster than the trend of ECSA in Figure 5-16. Because the CSC is diffusion controlled at this potential, the rate decrease might be ascribed to the decrease of geometric area of Pt/C caused by CSC.

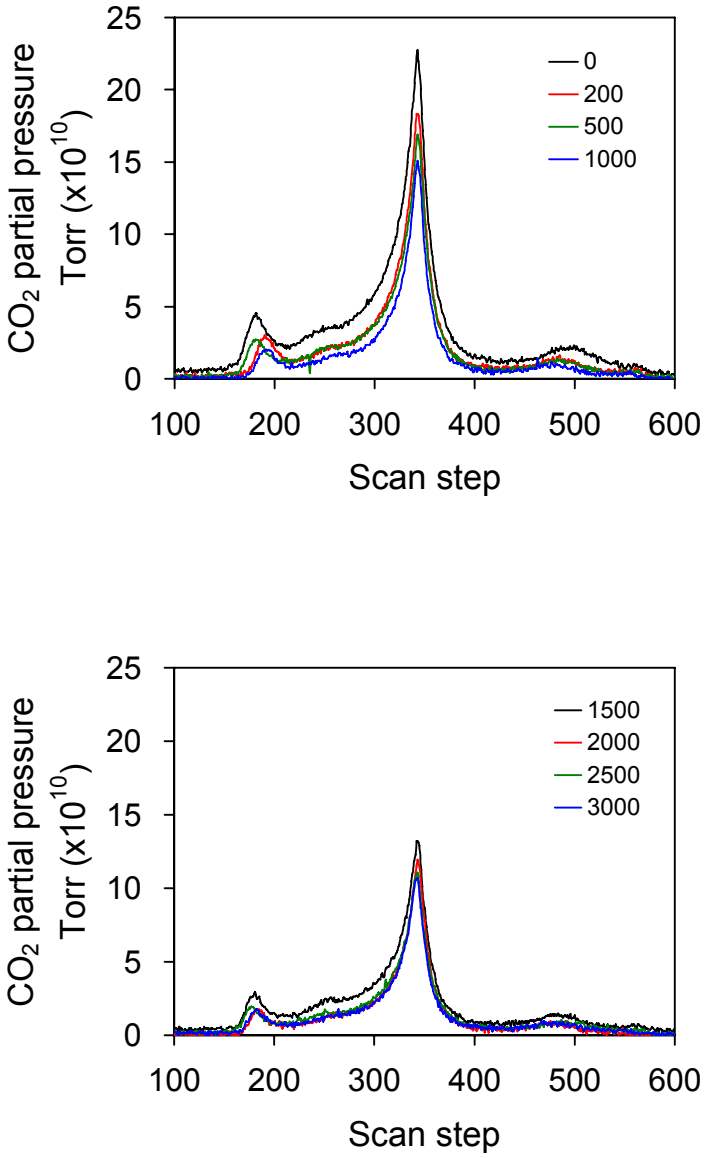

Figure 5-21 CO_2 MS signal of PtC-MEA change with potential cycle number at 30 ºC

5.4 Conclusions

Differential electrochemical mass spectrometry (DEMS) was utilized to characterize CSC and Pt redox reactions at the cathode in PEMFC by detecting the cathode exhaust gases, i.e. CO_2 (m/z = 44), H_2 (m/z = 2), and O_2 (m/z = 32). It was identified that the CO_2 signal change (five peaks in one potential cycle) comes from CSC, whereas the O_2 (a plateau in one potential cycle) and H_2 MS signal changes (a peak and a plateau in one cycle) are ascribed to the oxygen reduction reaction (ORR) and hydrogen electrochemical reactions coupled with Pt redox reactions.

DEMS experiment with H_2 replaced by deuterium gas at the anode and He replaced by Ar at the cathode confirmed that the changes of MS signal with m/z = 2 is caused by the changes of H_2 rather than H_2O. It was then deduced that the hydrogen evolution reaction (HER) contributes to the H_2 peak and the hydrogen oxidation reaction (HOR) to the H_2 plateau, with the H from H_2 not water. The H_2 peaks increased with temperature and decreased with potential scanning rate imply that they are limited by the diffusion through the membrane. However, the H_2 plateaus did not show any significant changes with temperature and potential scanning rate. It implies that they are not limited by the diffusion through the membrane. No evidences proved they are limited by the HOR. O_2 plateaus also did not show significant change because it is limited by the leakage of O_2 from the environment into the PEMFC.

The CO_2 MS signal was quantified and resolved from the Pt redox reactions in the CV. The current from CSC increased dramatically after 1.2 V at 60 ºC, which makes it non-negligible to model the total CV. It also suggests that if the potential is lower than 1.2 V at 60 ºC, it is not necessary to consider the CSC current in the modeling. It could be significant at higher temperature but need verification with experiments. CSC reactions at peak II, III, and V are

irreversible or sluggish because their potentials shift with potential scanning rate. Chronoamperometry at 1400 mV shows that CSC peak IV is facile and diffusion controlled.

Potential cycling between 100–1400 mV at the rate of 400 mV/s was used to accelerate the cathode catalyst degradation in PEMFC. The ECSA decreased fast at the beginning and then slowly with cycles. The HER H_2 peaks did not change after potential cycling of 4000 cycles, which means the membrane did not degradation with diffusion coefficient change. Thus the membrane degradation can be excluded from the consideration when using the potential cycling to accelerate the degradation of the cathode catalyst. On the other hand, these peaks can be used to check if the membrane degraded or not.

The H_2 plateau upper bases decreased with cycles means that HOR increased with cycles though the ECSA decreased also. It could be that the Pt particles size and surface properties changed, probably the oxide film coverage on Pt decrease, so as to activate the HOR on it.

The O_2 plateau did not change with cycles significantly because the O_2 concentration is very low in the DEMS experiments, leading to the ORR limited by the leakage of O_2 from the environment.

CO_2 MS signal decreased with cycles but its profile did not change significantly. This means that the CSC is still catalyzed by Pt and PtO_x and decreases with the ECSA of Pt decrease. CO_2 MS peak at 1400 mV decrease is ascribed to the decrease of the overall carbon black geometric surface caused by CSC.

Reference:

1. Borup, R., J. Meyers, B. Pivovar, Y.S. Kim, R. Mukundan, N. Garland, D. Myers, M. Wilson, F. Garzon, D. Wood, P. Zelenay, K. More, K. Stroh, T. Zawodzinski, J. Boncella, J.E. McGrath, M. Inaba, K. Miyatake, M. Hori, K. Ota, Z. Ogumi, S. Miyata, A. Nishikata, Z. Siroma, Y. Uchimoto, K. Yasuda, K.i. Kimijima, and N. Iwashita, *Scientific Aspects of Polymer Electrolyte Fuel Cell Durability and Degradation.* Chem. Rev., 2007. **107**(10): p. 3904-3951.

2. Yasuda, K., A. Taniguchi, T. Akita, T. Ioroi, and Z. Siroma, *Characteristics of a Platinum Black Catalyst Layer with Regard to Platinum Dissolution Phenomena in a Membrane Electrode Assembly.* J. Electrochem. Soc., 2006. **153**(8): p. A1599-A1603.

3. Yasuda, K., A. Taniguchi, T. Akita, T. Ioroi, and Z. Siroma, *Platinum dissolution and deposition in the polymer electrolyte membrane of a PEM fuel cell as studied by potential cycling.* Phys. Chem. Chem. Phys., 2006. **8**(6): p. 746-752.

4. Li, W. and A.M. Lane, *Investigation of Pt catalytic effects on carbon support corrosion of the cathode catalyst in PEM fuel cells using DEMS spectra.* Electrochem. Comm., 2009. **11**(6): p. 1187-1190.

5. Maass, S., F. Finsterwalder, G. Frank, R. Hartmann, and C. Merten, *Carbon support oxidation in PEM fuel cell cathodes.* J. Power Sources, 2008. **176**(2): p. 444-451.

6. Roen, L.M., C.H. Paik, and T.D. Jarvi, *Electrocatalytic Corrosion of Carbon Support in PEMFC Cathodes.* Electrochem. Solid-State Lett., 2004. **7**(1): p. A19-A22.

7. Willsau, J. and J. Heitbaum, *The influence of Pt-activation on the corrosion of carbon in gas diffusion electrodes--A dems study.* J. Electroanal. Chem., 1984. **161**(1): p. 93-101.

8. Matsumoto, M., T. Manako, and H. Imai, *Degradation of carbon supports in PEFC cathode investigated by electrochemical STM: effects of platinum and oxygen on enhanced carbon corrosion.* ECS Trans., 2008. **16**(2): p. 751-760.

9. Franco, A.A., M. Gerard, M. Guinard, B. Barthe, and O. Lemaire, *Carbon catalyst-support corrosion in polymer electrolyte fuel cells: mechanistic insights.* ECS Trans., 2008. **13**(15): p. 35-55.

10. Siroma, Z., M. Tanaka, K. Yasuda, K. Tanimoto, M. Inaba, and A. Tasaka, *Electrochemical corrosion of carbon materials in an aqueous acid solution.* Electrochem. (Tokyo, Jpn.), 2007. **75**(2): p. 258-260.

11. Chizawa, H., Y. Ogami, H. Naka, A. Matsunaga, N. Aoki, T. Aoki, and K. Tanaka, *Impacts of carbon corrosion on cell performance decay.* ECS Trans., 2007. **11**(1, Part 2, Proton Exchange Membrane Fuel Cells 7, Part 2): p. 981-992.

12. Srinivasan, S., E.A. Ticianelli, C.R. Derouin, and A. Redondo, *Advances in solid polymer electrolyte fuel cell technology with low platinum loading electrodes.* J. Power Sources, 1988. **22**(3-4): p. 359-375.

13. Zawodzinski, J.T.A., T.E. Springer, J. Davey, R. Jestel, C. Lopez, J. Valerio, and S. Gottesfeld, *A Comparative Study of Water Uptake By and Transport Through Ionomeric Fuel Cell Membranes.* J. Electrochem. Soc., 1993. **140**(7): p. 1981-1985.

14. Li, W. and C. He. *A Vapor-PEM sorption model based on Flory-Huggins theory*. in 2003 anniversary conference of China Solar Energy Society & the 7th national representative meeting. 2003.

15. Futerko, P. and I.M. Hsing, *Thermodynamics of Water Vapor Uptake in Perfluorosulfonic Acid Membranes.* J. Electrochem. Soc., 1999. **146**(6): p. 2049-2053.

16. U.S. DOE, *Multi-Year Research, Development and Demonstration Plan: Planned Program Activities for 2005-2015.* http://www1.eere.energy.gov/hydrogenandfuelcells/mypp/, 2007.

17. Wilkinson, D.P. and J. St.-Pierre, *Durability*, in *Handbook of Fuel Cells: Fundamentals, Technology, and Applications*, W. Vielstich, A. Lamm, and H.A. Gasteiger, Editors. 2003, Wiley.

18. Rand, D.A.J. and R. Woods, *A study of the dissolution of platinum, palladium, rhodium and gold electrodes in 1 m sulphuric acid by cyclic voltammetry.* J. Electroanal. Chem., 1972. **35**(1): p. 209-218.

19. Benke, G. and W. Gnot, *The electrochemical dissolution of platinum.* Hydrometallurgy, 2002. **64**(3): p. 205-218.

20. Johnson, D.C., D.T. Napp, and S. Bruckenstein, *A ring-disk electrode study of the current/potential behaviour of platinum in 1.0 M sulphuric and 0.1 M perchloric acids.* Electrochim. Acta, 1970. **15**(9): p. 1493-1509.

21. Kim, K., *Carbon electrochemical and physicochemical properties*. 1988: John Wiley & Sons, Inc.

22. Arvia, A.J., J.C. Canullo, E. Custidiano, C.L. Perdriel, and W.E. Triaca, *Electrochemical faceting of metal electrodes.* Electrochim. Acta, 1986. **31**(11): p. 1359-1368.

23. Canullo, J.C., W.E. Triaca, and A.J. Arvia, *Electrochemical faceting of single crystal platinum electrodes.* J. Electroanal. Chem., 1986. **200**(1-2): p. 397-400.

24. Egli, W.A., A. Visintin, W.E. Triaca, and A.J. Arvia, *The development of facetting and roughening at platinum polyfacetted single-crystal electrodes in a chloroplatinic acid solution.* Appl. Surf. Sci., 1993. **68**(4): p. 583-593.

25. Liu, D. and S. Case, *Durability study of proton exchange membrane fuel cells under dynamic testing conditions with cyclic current profile.* J. Power Sources, 2006. **162**(1): p. 521-531.

26. Freeman, R.G., K.C. Grabar, K.J. Allison, R.M. Bright, J.A. Davis, A.P. Guthrie, M.B. Hommer, M.A. Jackson, P.C. Smith, D.G. Walter, and M.J. Natan, *Self-Assembled Metal Colloid Monolayers: An Approach to SERS Substrates.* Science, 1995. **267**(5204): p. 1629-1632.

27. Darling, R.M. and J.P. Meyers, *Kinetic Model of Platinum Dissolution in PEMFCs.* J. Electrochem. Soc., 2003. **150**(11): p. A1523-A1527.

28. Takeuchi, N. and T.F. Fuller, *Modeling and Investigation of Design Factors and Their Impact on Carbon Corrosion of PEMFC Electrodes.* J. Electrochemical Society, 2008. **155**(7): p. B770-B775.

29. Koei, K., I. Minoru, H. Kanya, and K. Koichiro, *Kinetic study of isotopic exchange reaction between hydrogen and water vapor over a pt/sdbc hydrophobic catalyst sheet.* Can. J. Chem. Eng., 1988. **66**(2): p. 338-342.

30. Conway, B.E. and L. Bai, *Determination of adsorption of OPD H species in the cathodic hydrogen evolution reaction at Pt in relation to electrocatalysis.* J. Electroanal. Chem., 1986. **198**(1): p. 149-175.

31. Woods, R., *Chemisorption at Electrodes, Hydrogen and Oxygen on Nobel Metals and Their Alloys,* in *Electroanalytical Chemistry: A Series of Advances*, A. Bard, Editor. 1976, Dekker.

32. Bard, A.J. and L.R. Faulkner, *Electrochemical Methods: Fundamentals and Applications*. 2 ed. 2001, New York: Wiley.

CHAPTER 6

IN-SITU MITIGATION OF CARBON SUPPORT CORROSION BY ADDING GOLD NANOPARTICLES TO THE PLATINUM ON CARBON CATALYSTS

6.1 Introduction

Carbon support corrosion (CSC) is attributed to carbon black oxidation with water at high potential and low pH in a polymer electrolyte membrane fuel cell (PEMFC) [1-4]. It has been proposed to mitigate CSC at the cathode by replacing the carbon black with carbon nanotubes [5, 6], conductive metal oxides [7, 8], or by doping the carbon black with other elements [9]. CSC becomes more severe in the cases of fuel starvation [10, 11], high potential for a long time after shut down [11], and the catalytic effect of Pt [12-15]. The former two can be alleviated by optimizing the operating conditions [16]. As for the latter, because Pt is still the best catalyst for ORR in PEMFC, modifications of Pt with other metals or metal oxides were attempted to mitigate the CSC [7, 8]. The intention of this study is to determine if CSC can be mitigated by adding Au nanoparticles to the Pt/C.

CSC is catalyzed by accepting [O] from Pt redox reactions and/or the oxygen reduction reaction (ORR) on Pt [12]. No significant difference of CO_2 was detected from CSC when humidified air or He fed into the cathode, shown in Chapter 4. This implies that the Pt redox reactions affect the CSC dominantly. Apparently, CSC might be mitigated if the [O] transfer process is interrupted or suppressed. Ru has strong interaction with OH, and a MEA with PtRu/C

(atomic Pt/Ru ratio = 1:1) at the cathode exhibits the differential electrochemical mass spectrometry (DEMS) spectra of CO_2 without peaks at 600 and 1000 mV [14], indicating fewer CSC pathways and less CO_2 production. However, Ru has a low oxidation potential which makes it impossible to be used as a cathode catalyst component.

Au is the noblest metal in the nature, and more difficult to be oxidized than Pt [17]. It was reported that Au clusters deposited on Pt nanoparticles (NPs) can suppress or mitigate the underlying Pt oxidation [18]. It was also found that the OH prefers to adsorb on Au sites on a AuPt/C catalyst during the methanol oxidation reaction [19]. A hypothesis was thus proposed here that the Au clusters on Pt might mitigate the CSC by suppressing the underlying Pt oxidation, i.e. the Pt catalytic effects on CSC of the cathode catalyst. The DEMS spectrum of CO_2 from the cathode with AuPt/C would then have fewer and/or weaker peaks than that from the cathode with Pt/C.

Au was usually considered a relatively inert metal and not a promising candidate for catalysis until supported Au NPs were found in the 1980s to have high activity for CO oxidation at low temperature [20]. Recently, AuPt/C has evoked interest as a cathode catalyst for ORR in PEMFC after it was shown to exhibit better performance and durability than Pt/C [18]. Au is known to be more active for the $2e^-$ ORR to H_2O_2 than for the $4e^-$ ORR to H_2O at most crystal faces. This counterintuitive observation was explained by the efficient spillover of H_2O_2 from Au clusters to the surrounding Pt atoms, where it is further reduced to H_2O, leading to a $4e^-$ ORR activity increase [18]. The reported underpotential deposition (UPD) method used to synthesize the AuPt/C on the glassy carbon (GC) electrode is difficult to be used to prepare a large amount (50–100 mg) of catalyst required for the 5 cm^2 MEA used in DEMS measurements. The larger substrate surface area for large amount of catalyst would exhibit unacceptable iR drop for a

method requiring rigorous control of potential. A suitable catalyst preparation method needs to be developed to study these catalysts by DEMS.

According to the hypothesis, the Au NPs need to remain their own distinct structure. Emphasis was thus placed on synthesizing a bimetallic AuPt/C catalyst and the strategy was as follows. Common catalyst preparation methods, such as deposition precipitation (DP), two phase liquid-liquid colloidal, polyol (specifically ethylene glycol, EG), microwave-assisted polyol (MW-EG), and surface redox (SR), were employed to synthesize Pt/C (20 wt% Pt) with electrochemically active surface area (ECSA) and/or ORR performance compatible to a commercial Pt/C catalyst (20 wt% Pt, Etek). The successful methods were then utilized to prepare Au NPs, Au/C and AuPt/C. The appropriate catalyst preparation methods and conditions were thus developed and determined to make AuPt/C (20 wt% Pt, 5 wt% Au) catalysts (50–100 mg) with high dispersion (3–5 nm) and narrow particle size distribution, with the metal NPs located uniformly on carbon surface.

Transmission electron microscopy (TEM) was used to determine the catalyst particle size distribution and to check if metal NPs were uniformly located on the carbon support. The ECSA and ORR performance were measured by cyclic voltammetry and rotating ring-disk electrode (RRDE) method, respectively. Energy dispersive X-ray spectroscopy (EDX) and the ring current of the RRDE were used to verify Au existence on Pt/C.

Finally, MEAs with Etek Pt/C and promising AuPt/C catalysts used at the cathode were fabricated and the CSC was measured and compared by the DEMS spectra of CO_2 to check if the CO_2 peaks change, decrease or even disappear.

6.2 Experimental

6.2.1 Catalyst Preparation

6.2.1.1 Materials

Dihydrogen hexachloroplatinate (IV) hexahydrate ($H_2PtCl_6 \cdot 6H_2O$, 99.9% on metal basis) and hydrogen tetrachloroaurate (III) trihydrate, ($HAuCl_4 \cdot 3H_2O$, 99.99% on metal basis), 1-dodecanethiol ($CH_3(CH_2)_{11}SH$, DT, 98%), sodium borohydride ($NaBH_4$, 98%), isopropanol (GC grade) and formaldehyde (HCHO, 37%) were purchased from Alfa Aesar. Tetraoctylammonium bromide ($[CH_3(CH_2)_7]_4N(Br)$, TOABr, 98%) and oleylamine ($CH_3(CH_2)_7CH=CH(CH_2)_7CH_2NH_2$, OAM, 70%) were obtained from Sigma-Aldrich. Ethylene glycol (EG), hexane (HPLC grade) and sulfuric acid (95.9%) were from Fisher Scientific. All the chemicals were used as received. Carbon black (Vulcan XC-72R) was a gift from Cabot Inc. Pt/C (20% Pt on Vulcan XC-72R) was ordered from Etek.

6.2.1.2 DP Method

The DP method [21] was employed to synthesize Pt/C (20% Pt) catalysts. A Vulcan XC-72R carbon black dispersion (10 mg/mL) was made by dispersing carbon black in a 10:1 (v/v) DI water/isopropanol mixture for 4 h. Precursor solution (0.10 M, water as solvent) of H_2PtCl_6 and $HAuCl_4$ were added dropwise to the carbon black dispersion in the desired molar ratio of AuPt/C and stirred for 4 h. NaOH solution (1.0 M) was then added dropwise to the solution by a pipette or a syringe pump (kdScientific Model 100 Series). The volume of base solution was determined by a specific ratio or pH measured by a pH electrode (accumet® accuTupH®). After stirring for 30 min, formaldehyde solution (37%) was added dropwise in the molar ratio of 10:1 and stirred for 30 min. The solution was then heated to 80 ºC at a water bath and held for 1 h for reduction. The solution was then filtered using an acetate cellulose membrane (pore size 0.22 μm) and

washed with a 15:1 (v/v) DI water/ethanol mixture (150 mL) to remove the chloride ion, which was checked by a 1 M $AgNO_3$ solution. The Pt/C and the filter membrane were dried in the oven at 50 ºC first for 1 h and then at 80 ºC for 2 h.

6.2.1.3 Colloidal Method

The two-phase liquid-liquid colloidal method [22, 23] was modified to synthesize the Pt NPs and Au NPs. Pt/C and AuPt/C were then made by depositing Pt NPs and a mixture of Pt NPs and Au NPs on carbon black, respectively. To synthesize Au NPs (20.0 mg) for example, tetraoctylammonium bromide (120 mg) was dissolved with toluene (20 mL) in a round bottom flask and stirred for 15 min. $HAuCl_4$ (1015.2 μL, 0.10 M, water as solvent) was diluted with DI water (5 mL) and then added to the TOABr solution with vigorous stirring for ca. 30 min until the precursor transferred completely into the organic layer. This could be observed by the aqueous layer turning colorless and the organic layer turning dark orange for $HAuCl_4$ and orange for H_2PtCl_6. DT (35.0 μL) was then added dropwise to the reaction solution with vigorous stirring for ca. 30 min. The solution turned to light orange for $HAuCl_4$ with DT or OAM, and for H_2PtCl_6 with OAM, or milk color for H_2PtCl_6 with DT.

A freshly prepared aqueous solution of $NaBH_4$ (3.3 mL, 0.4 mol/L) was slowly added to the reaction solution with vigorous stirring. The solution turned to dark brown in seconds for $HAuCl_4$ with DT or OAM, and for H_2PtCl_6 with OAM, or orange color for H_2PtCl_6 with DT. After further stirring for 4 h (or overnight) the organic layer was separated from the aqueous layer using a separation funnel.

The organic solution with the Au NPs was evaporated to 1-2 mL and then allowed to cool down to room temperature. Ethanol (50 mL) was introduced while stirring to the left solution to wash and precipitate the NPs. After 5 min sonication, it was filtered using an acetate cellulose

membrane (pore size 0.22 μm). The NPs were then washed off the membrane with 2-3 mL toluene. The precipitation and filtration were repeated once. The membrane and the NPs on it were dried at room temperature for 30 min, and then in oven at 50 ºC for 30 min. The NPs were collected by washing the membrane with 2-3 mL hexane. Sonication was used to assist in washing and dispersing them in hexane.

The carbon black was dispersed in the hexane (10 mg/mL) by stirring and ultrasonicating for 30 min, respectively. The NPs were then loaded onto carbon black by adding dropwise the hexane dispersion of NPs to the hexane dispersion of carbon black with stirring, followed with ultrasonication for 1 h. The catalyst solution was then diluted by ethanol (50 mL) and then filtered.

6.2.1.4 EG Method and MW-EG Method

EG was used as solvent, stabilizer and reductant to prepare Pt/C and AuPt/C. The only difference between EG method and MW-EG method is the reduction procedure. The former heated the solution using an oil bath while the latter using a microwave oven.

Carbon black (129.2 mg) was dispersed in EG (8 mL) in a 25 mL round flask, stirred for 1 h, and then ultrasonicated for 15 min. Pt precursor (1656.4 μL, 0.10 M) was then added dropwise to this carbon black dispersion with stirring for 2 h, followed by ultrasonication of 30 min. NaOH solution (1325.1 μL, 1.0 M) was then added to adjust the pH. The Pt precursor was reduced by the EG heated in an oil bath from room temperature to 135±5 ºC and kept at this temperature for 2.5 h, or heated in a microwave oven (Emerson, 700 W) for 60 s. To absorb excess microwave energy, 45 mL of water in four vials surrounded the sample. The solution was then cooled down to room temperature, and DI water (22 mL) was introduced with stirring for 15

min to precipitate the catalyst. The catalyst was collected after filtration, washing with a 15:1 (v/v) DI water/ethanol mixture (160 mL), and drying in an oven at 50 ºC for 1 h and then at 80 ºC for 1 h.

6.2.1.5 Surface Redox Method

Pt NPs or Pt/C were prepared using the EG method described above. The Pt surface was protected from air oxidation by bubbling the solution with Ar (100 mL/min, UHP, Airgas) during the preparation. The reaction solution was then allowed to cool to 50 ºC and adjusted to pH = 1 by HCl (1.0 M, water as solvent). Au precursor (0.10 M, EG as solvent) was introduced in the desired ratio of AuPt/C and stirred at 50 ºC for 30 min. As for deposition on Pt NPs, the product, AuPt NPs, was then mixed with carbon black EG dispersion and ultrasonicated for 1 h. The AuPt/C was precipitated, filtered, washed and dried as those in EG method.

6.2.2 Catalyst Characterization

The electrochemical and physical properties of Pt NPs, Au NPs, Pt/C and AuPt/C were characterized by cyclic voltammetry, rotating ring-disk electrode (RRDE) technique, transmission electron microscopy (TEM), high angle annular dark field (HAADF) scanning transmission electron microscopy (STEM) and energy dispersive x-ray spectroscopy (EDX).

6.2.2.1 Cyclic Voltammetry and RRDE Methods

The ECSA of the electrocatalyst and the ORR kinetic current were evaluated by cyclic voltammetry and the RRDE method respectively in a 0.50 M H_2SO_4 electrolyte using a bipotentiostat (AFCBP1, Pine Instrument) and a 150 ml three-electrode electrochemical cell

(Pine Instrument). Before each usage, the working electrode, a glassy carbon (GC) electrode (RRDE with 4.57 mm OD of the disk and 4.93 mm ID and 5.38 mm OD of the ring, Pine instrument), was polished for 2 min using a 0.05 μm γ-alumina micropolish (Buehler LTD, No. 40-6365-006) on a microcloth PSA (Buehler LTD, 40-7212), followed in sequence by rinse and ultrasonication for 2 minutes in DI water. Catalyst ink (2.0 mg_{cat}/mL) was prepared by dispersing the catalyst in a 3:1 (v/v) DI water/isopropanol mixture. It was stirred overnight and ultrasonicated for 10 min and then cast on the electrode with a loading of 14 $\mu g_{Pt}/cm^2$ using a syringe (10 μL, Hamilton). The catalyst coating on the electrode was dried at room temperature under a plastic cap with ventilation holes. A Pt wire and a mercurous sulfate electrode (MSE, Pine Instrument) were used as the counter and reference electrode, respectively. Argon (Ar, 100 mL/min, UHP, Airgas) was bubbled into the electrolyte for 15–20 min to remove dissolved oxygen and then kept flowing above the electrolyte surface to form a gas curtain during the analysis. The working electrode potential was cycled 30 times between 0.05–1.2 V (all the potentials in this chapter vs. SHE) at a scan rate of 100 mV/s to remove slight contamination to get a clean catalyst surface. The working electrode potential was held at 0.5 V during idle time. PineChem 2.8.0 software (Pine Instrument) was used to integrate the H_{UPD} charge in the cyclic voltammogram (CV).

The ORR kinetic current was measured by the RRDE method. The electrolyte (0.50 M H_2SO_4) was bubbled with O_2 (100 mL/min, research grade, Airgas) for 15–20 min, and the O_2 was kept flowing above the electrolyte surface to form a gas curtain during the analysis. The rotation rates for the RRDE were 400, 900, 1600 and 2500 rpm. K-L plots were used to determine the kinetic current.

6.2.2.2 Transmission Electron Microscopy

A FEI Tecnai F-20 TEM equipped with EDX was employed as the primary tool to characterize the nanoparticle size distribution and composition.

Samples for TEM and EDX were prepared by spreading a dilute particle dispersion on a copper TEM grid with a carbon film on the backside (400-mesh, Electron Microscopy Sciences), followed by solvent evaporation in air at room temperature. The bright field (BF) images were acquired at an accelerating voltage of 200 kV to illustrate the catalyst particle dispersion and distribution. At high magnifications, the images are commonly referred to as high resolution TEM (HRTEM) images, which show lattice fringes in TEM mode. The compositional analysis of Pt NPs, Au NPs, Pt/C and AuPt/C was performed with EDX in the high angle annular dark field (HAADF) scanning transmission electron microscopy (STEM) mode. The determination and distinction of Au and Pt was based on the $E_{Pt\text{-}L\alpha}$ = 9.44 keV and $E_{Au\text{-}L\alpha}$ = 9.71 keV emission lines.

6.2.2.3 DEMS

The MEA preparation, DEMS setup and testing were detailed described in chapter 3.

6.2.3 Temperature Programmed Techniques

Temperature programmed techniques were used to study the surfactants removal of the catalysts made by the colloidal method. Catalyst (30 mg) made by the colloidal method was loaded in a small vial, and then placed in the big chamber of a "U" type reactor for temperature programmed experiments. The temperature rose from room temperature to 250 or 300 ºC at 10 ºC/min and held there for 30 min. Temperature programmed oxidation (TPO) and temperature

programmed desorption (TPD) were conducted when feeding with air and He, respectively. The outlet gases were analyzed by a quadrupole mass spectrometer (Inficon).

6.3 Results and Discussion

A commercial Pt/C catalyst (20 wt% Pt, Etek) was used as the reference for the home-made Pt/C and AuPt/C catalysts. The Etek Pt/C catalyst has Pt NPs with mean particle size 3.8 nm and standard deviation 1.28 nm, shown in Figure 6-1 and Figure 6-2 respectively. It has ECSA of 61 m^2/g_{Pt} (65 m^2/g_{Pt} in ref. [24]) by the calculation using the Eq. 2-8 with the H_{UPD} charge of 297 μC from the H_{UPD} waves in the CV in 0.50 M H_2SO_4 shown in Figure 6-3a. Its ORR kinetic current of 350 mA/mg_{Pt} at 0.75 V at 23±1ºC in 0.5 M H_2SO_4 saturated with O_2 was obtained from the K-L plot in Figure 6-3c, based on the disk current of the RRDE in Figure 6-3b.

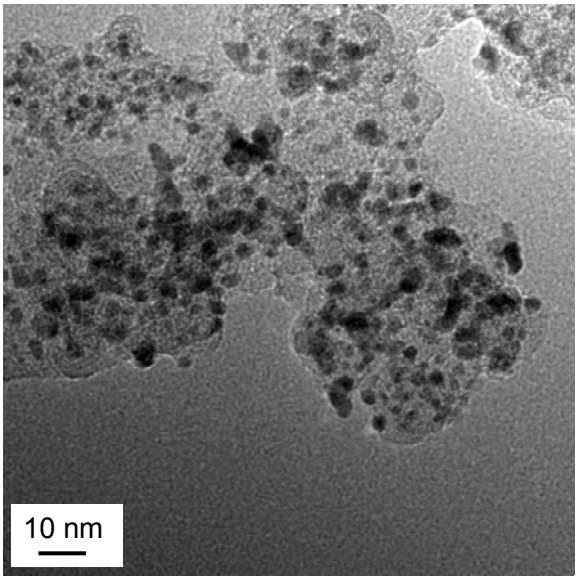

Figure 6-1. TEM of Etek 20 wt% Pt/C

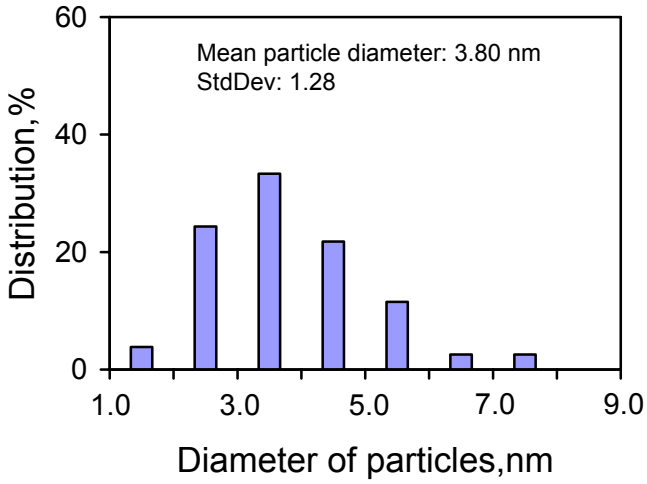

Figure 6-2. Particle size distribution of Etek 20 wt% Pt/C from TEM picture

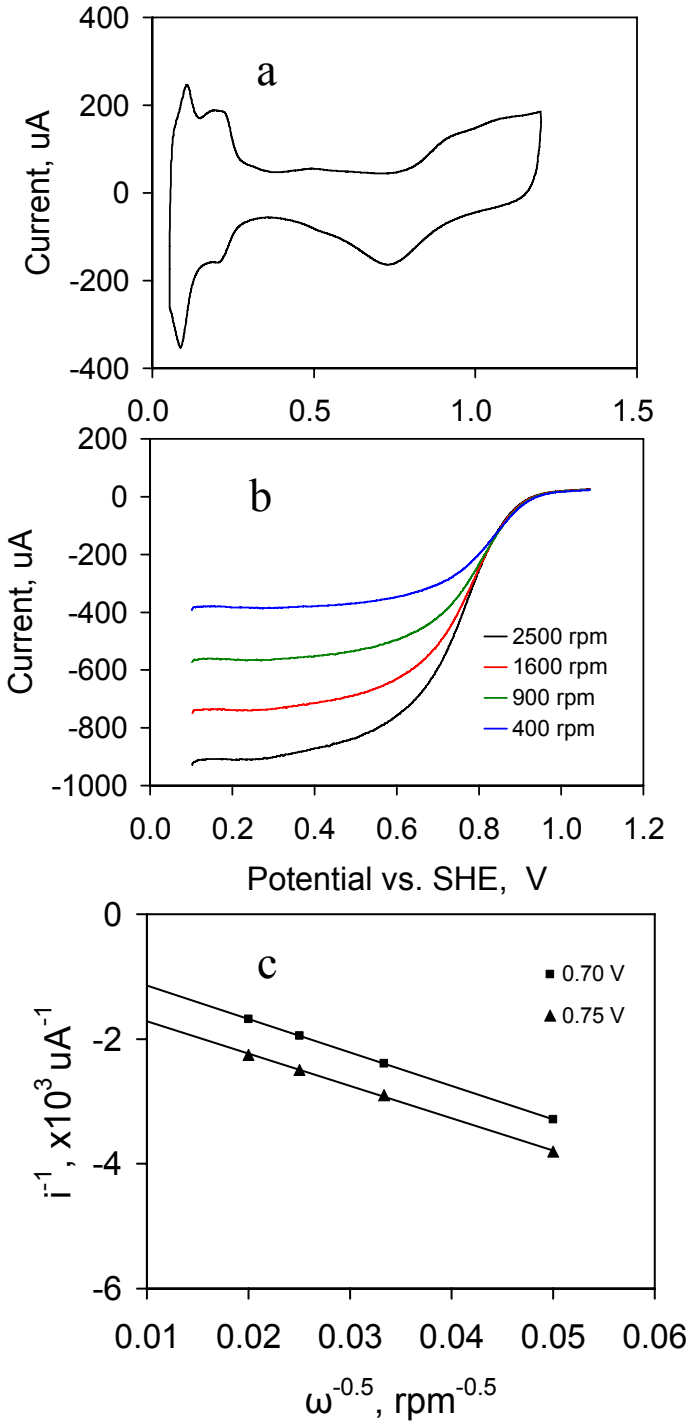

Figure 6-3. CV (a), Rotating disk hydrodynamic voltammogram (b) and Koutecky-Levich plot (c) of Etek 20 wt% Pt/C

6.3.1 Pt/C Made by DP Method

The DP method, a relatively simple and widely used method, was first employed to synthesize Pt/C with high dispersion and uniform distribution, with the details of the synthesis in the experimental section. The TEM picture in Figure 6-4a shows that the Pt NPs are agglomerated and do not distribute on carbon black uniformly, though most particles have size ca. 5 nm.

To impede aggregation, the Pt/C was then prepared in the ultrasonic bath at its high temperature limit of 60 ºC. Unfortunately, the Pt NPs still aggregated on carbon black shown in Figure 6-4b. It reveals that the sonication does not hinder the Pt NPs aggregation and improve their distribution significantly, which is consistent with the literature [25]. It was reported [25] that a higher temperature in the range of 75 to 90 ºC is favorable for higher Pt dispersion on the carbon black support in water. Our lower synthesis temperature of 60 ºC might compensate the positive effect of sonication on particle size to some extent.

pH plays a vital role on the dispersion and distribution of Pt NPs on carbon black. It influences the precipitation of Pt precursor, which turns into a Pt complex and deposits on carbon black. High dispersion and uniform distribution of Pt NPs on carbon black could be achieved by increasing the pH of reaction system gradually and uniformly using a syringe pump to add 1 M NaOH. Unfortunately, the particles size and distribution were still not improved significantly shown in Figure 6-4c.

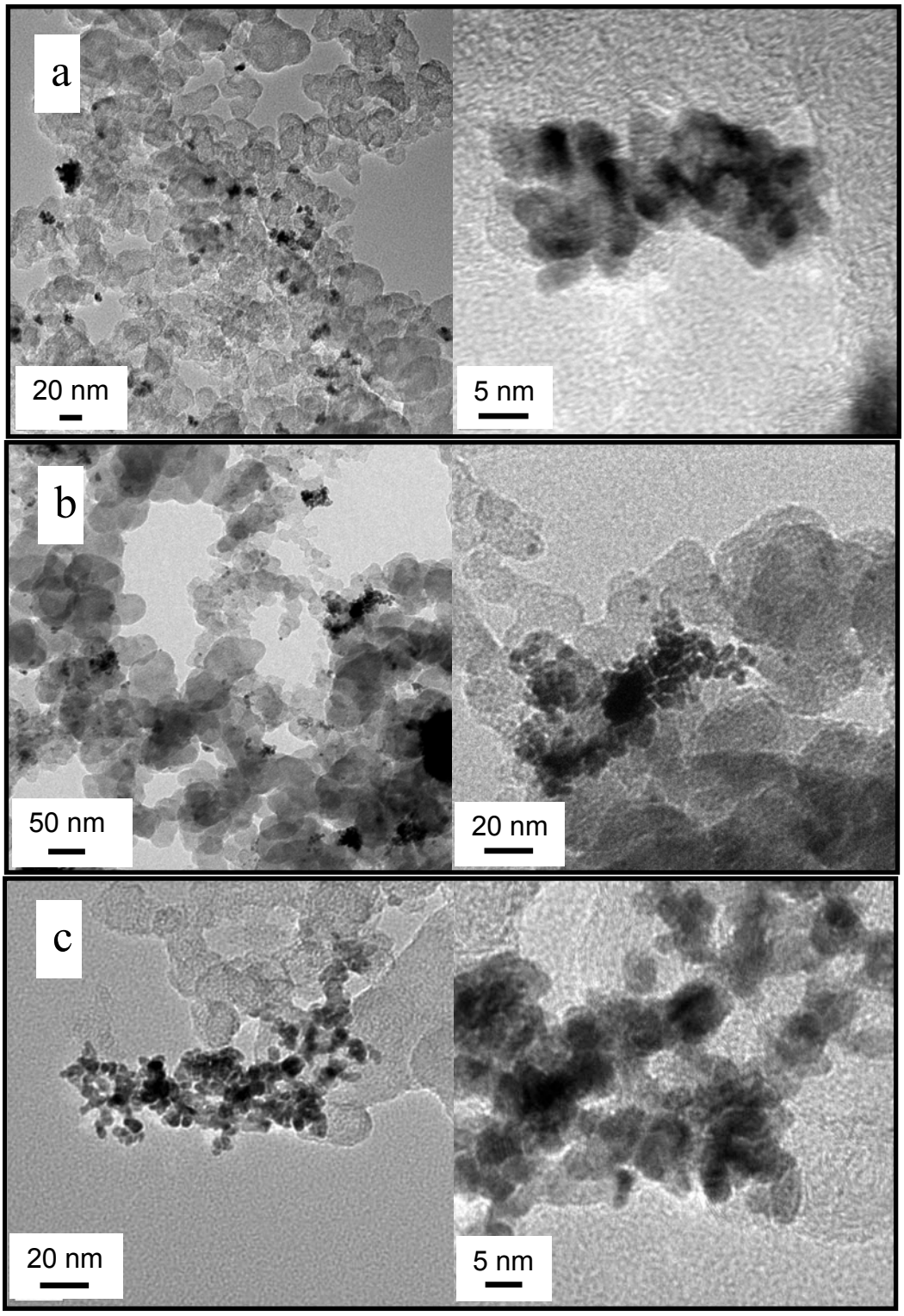

Figure 6-4. TEM pictures of Pt/C made by DP method (a), DP method with ultrasonication (b) and NaOH added using a syringe pump (c)

It can be concluded that a consistent problem is that the Pt NPs are agglomerated on carbon black support. It is possible that the particles already agglomerate before the deposition on the support, or that the particles can only deposit on the regions of carbon back support that are wet well by the solvent (water plus a small portion ethanol) or have strong affinity with Pt NPs. It is still controversial in the literature whether DP method is a suitable method to prepare catalysts with metal NPs on carbon black support.

It was not necessary to run a cyclic voltammetry or RRDE experiment until we get acceptable particle size and distribution of Pt NPs on carbon black. Using a solvent with better wetting of the carbon black could improve the dispersion and distribution. This is why the polyol method was employed in next step.

6.3.2 Pt/C and AuPt/C Made by EG Method and MW-EG Method

A EG method is a polyol method using EG as solvent, stabilizer, and reductant. EG is the most popularly used polyol, and wet thus disperse carbon black very well. Figure 6-5 shows a TEM picture and particle size distribution of Pt/C made by the EG method, with the details in the experimental section. The mean particle size is 2.39 nm with standard deviation 0.425 nm, which is better than the commercial Etek catalysts shown in Figure 6-2.

However, the EG method does not work well for Au/C. The prepared Au NPs on carbon black have a size around 20 nm as shown in the TEM picture in Figure 6-6. It was speculated that the reducing capability of the carbon black causes the Au precursor to be adsorbed, reduced and grown up on the carbon black in an uncontrolled fashion before the EG starts to reduce the Au precursor.

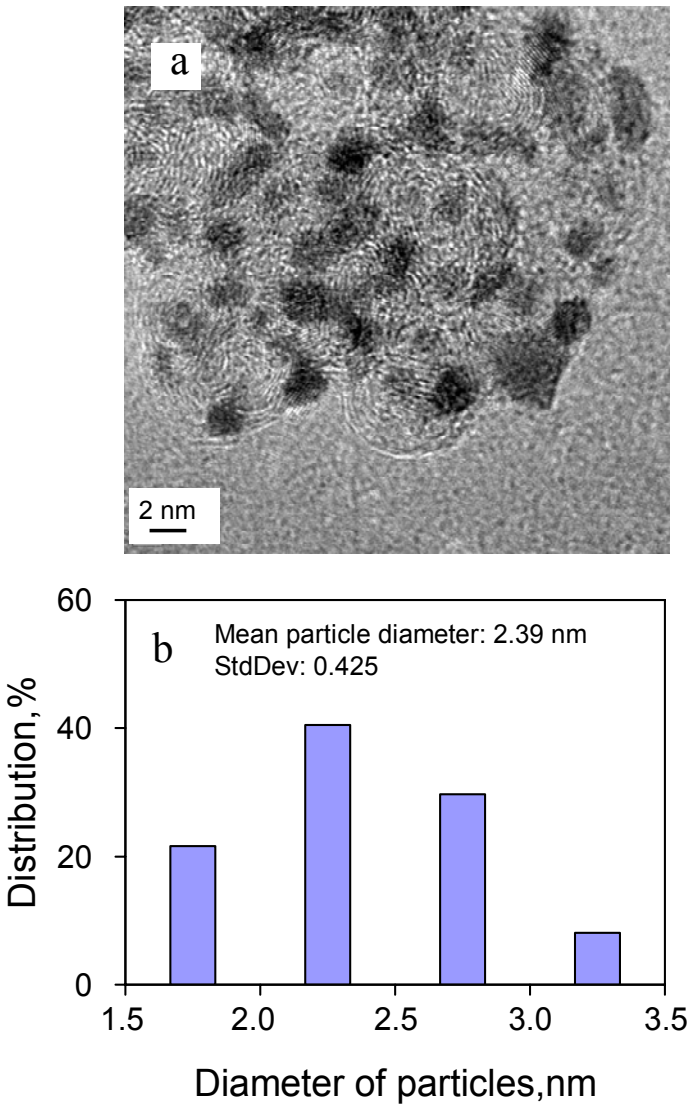

Figure 6-5. TEM picture (a) and particle size distribution (b) of Pt/C made by EG method

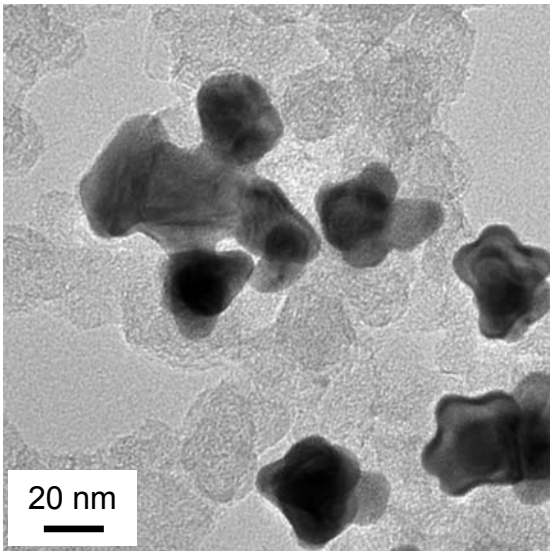

Figure 6-6. TEM picture of Au/C made by EG

The microwave-assisted EG (MW-EG) method can reduce the reduction time from hours to 1 min. We hypothesized that the slow and weak reduction caused by the carbon black could be ignored compared with this fast microwave assisted EG reduction. It might improve the Au NPs dispersion and distribution on carbon black.

First, a Pt/C catalyst was prepared by the MW-EG method as described in the experimental section. It was found that this Pt/C has a rather good dispersion and uniform distribution as shown in the TEM picture in Figure 6-7. Its ECSA is 65 m^2/g_{Pt} based on the total H_{UPD} desorption charge (316 μC) in the CV in Figure 6-8. The ring current is shown in Figure 6-9 for comparison with that of AuPtC to determine the Au existence later.

Unfortunately, the Au NPs on carbon black made by MW-EG method are still pretty large, with particle size from 10 to 20 nm as shown in Figure 6-10. It could be that the carbon black reduction on the Au precursor was also increased by microwave radiation. A control experiment was conducted by reducing the Pt precursor in EG using microwave radiation heating

without carbon black. The solution did not show any color change (no reaction) after the same reduction conditions. This result confirms that the microwave radiation interacts with the carbon black, which enhances the reduction and actually decreases the Pt and Au precursors reduction time.

AuPt/C preparation was also conducted using a mixture of Pt and Au precursors with the MW-EG method. There were also some large NPs shown in the TEM picture in Figure 6-11. The particle size could be acceptable for testing the CSC hypothesis. But the colloidal method with a reputation for particle size control to get well dispersed particles was tried instead.

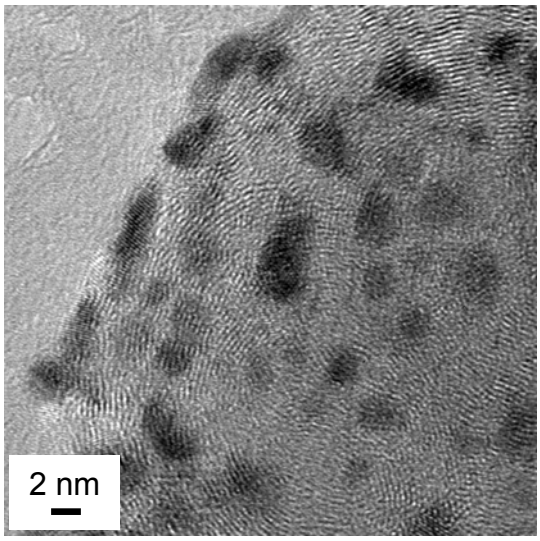

Figure 6-7. TEM picture of Pt/C made by MW-EG

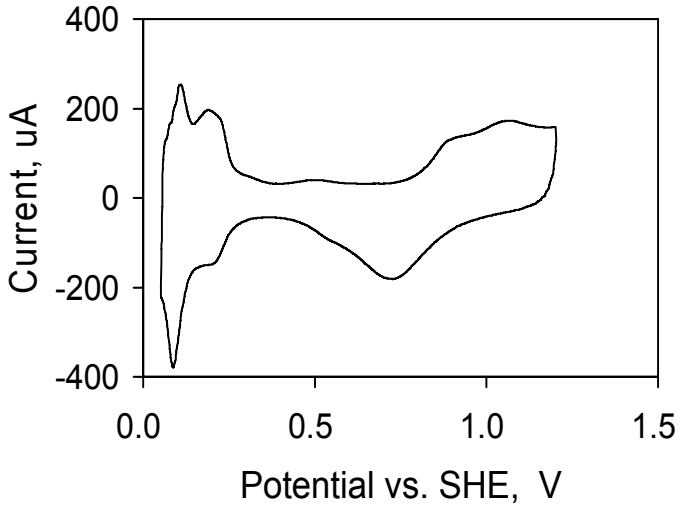

Figure 6-8. CV of Pt/C made by MW-EG

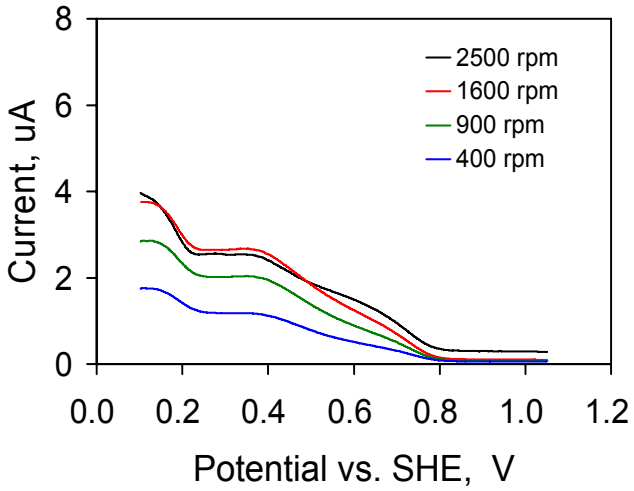

Figure 6-9. Ring current of Pt/C made by MW-EG

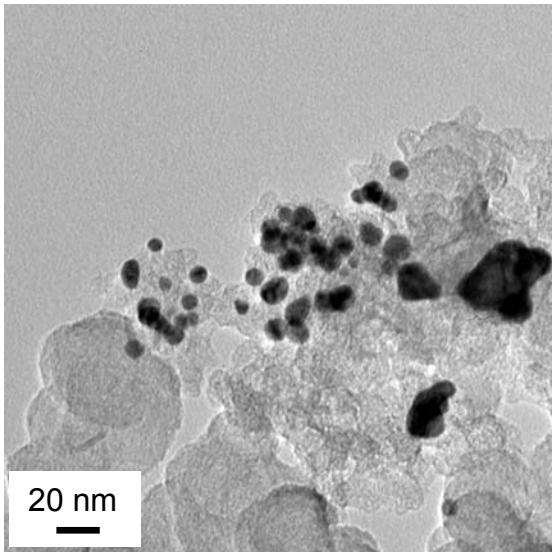

Figure 6-10. TEM picture of Au/C made by MW-EG

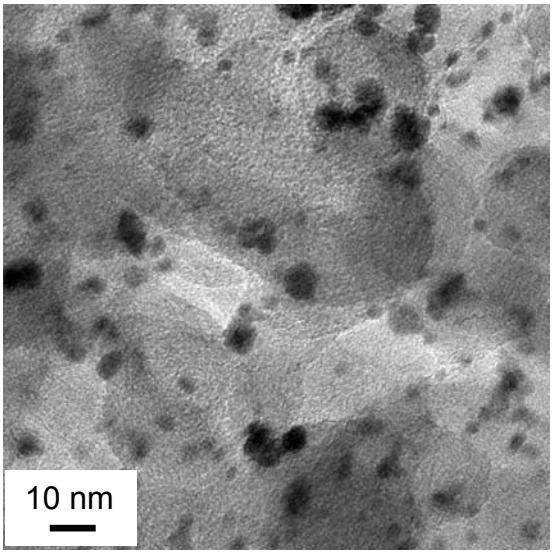

Figure 6-11. TEM picture of AuPt/C made by MW-EG

6.3.3 Pt/C and AuPt/C Made by Colloidal Method

Au NPs and Pt NPs were made by colloidal methods respectively. They were then mixed in the mass ratio of 1:4 and loaded on carbon black to get AuPt/C (5 wt% Au and 20 wt% Pt). Generally, the capping agent employed in preparation helps to make high dispersion, uniform distribution, and stable NPs. But it increases the complexity of the synthesis and requires removing the capping agent to expose the catalytically active surface of the NPs to reactants.

6.3.3.1 Capping Agent Effects on Precursor Reduction and Particle Size

The Pt or Au precursor is in the organic phase in this two phase liquid-liquid colloidal method. The organic phase changes to a dark color when the precursor is reduced significantly. It was found that the organic solution color did not change fast or significantly when DT was used as the capping agent to synthesize Pt NPs, which means the precursor was not reduced significantly as Eq. 2-6. This implies that this two phase charge transfer reaction [26, 27] was sluggish because the charges transfer through the two phase interface slowly when DT is involved in the organic phase, or that too strong an interaction between DT and Pt ions makes the reduction difficult.

This is the reason why the prepared AuPt/C catalyst did not show any significant H_{UPD} waves in CV, when Au and Pt NPs are made together using DT as the capping agent. It was noticed that the organic solution turned dark, meaning metal NPs were produced. This was caused by the occurrence of Au NPs. Actually, there were very few Pt NPs produced.

When using OAM as a capping agent, the organic phase color darkens in seconds after adding the fresh $NaBH_4$ solution. The prepared Pt NPs have mean particle diameter of 2.23 nm and standard deviation of 0.39 nm shown in Figure 6-12 and Figure 6-13 respectively, which are

better than those of commercial catalysts.

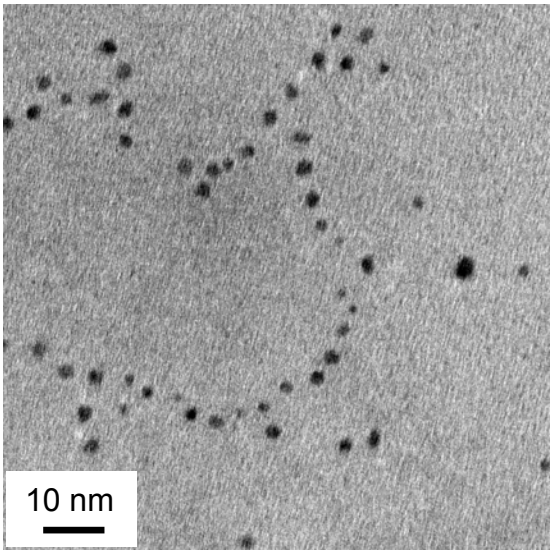

Figure 6-12. TEM picture of Pt NPs made with Oleylamine

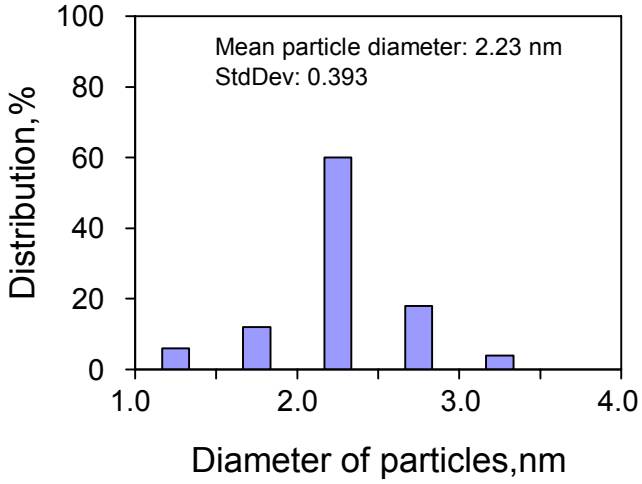

Figure 6-13. Particle size distribution of Pt NPs made with Oleylamine

As for Au NPs, the Au precursor in the organic phase was reduced rapidly and completely either using DT or OAM as the capping agent. However, the resulting Au particle dispersion is quite different. When using OAM as the capping agent, the Au NPs are around 10 nm dia. as shown in the TEM picture in Figure 6-14. On the contrary, when using DT as the capping agent, the TEM picture in Figure 6-15 shows the Au NPs have a very small particle size and uniform distribution on carbon black, with mean particle size of 2.11 nm and standard deviation of 0.485 nm shown in Figure 6-16.

The molar ratio of each capping agent to Pt precursor is 1:1 in this study. It can be concluded that OAM and DT are appropriate to make high dispersion and uniform distribution Pt NPs and Au NPs, respectively. The difference could come from the different interaction between metal NPs/complex ion and capping agents, as well as the charge transfer between the two phase interface [27].

Au NPs and Pt NPs were then prepared using DT and OAM respectively, mixed with the atomic ratio of 1:4, and loaded on carbon black to get AuPt/C (5% Au and 20% Pt) at last. The next step was to remove the capping agent and phase transfer reagent from the Pt/C and AuPt/C.

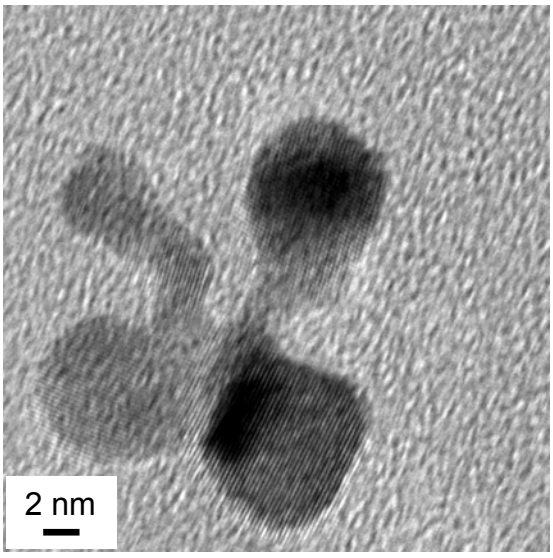

Figure 6-14. TEM picture of Au NPs made with Oleylamine

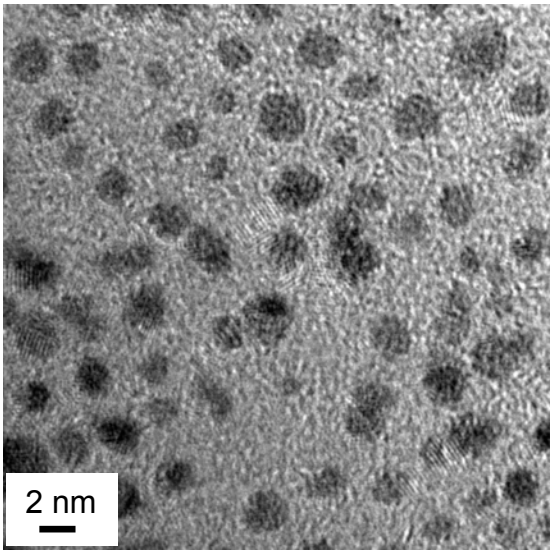

Figure 6-15. TEM picture of Au NPs made with dodecanethiol

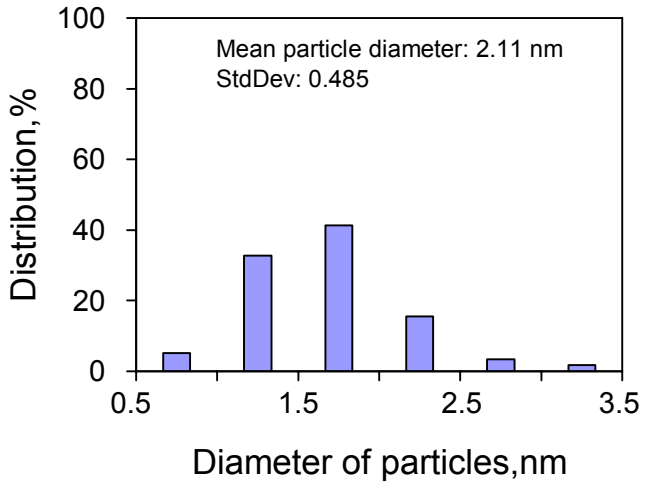

Figure 6-16. Particle size distribution of Au NPs made with dodecanethiol

6.3.3.2 Capping Agent and Phase Transfer Agent Removal

The group $–NH_2$ of OAM and group $–SH_2$ of DT have strong interaction with the metal (Pt or Au) NPs or ions, which make it hard to remove the capping agents by washing with solvents only. The phase transfer agent (TOABr used in this study) could also reside and cover the catalyst surface with certain interaction. Oxidation with oxygen gas is a common way to remove those organic chemicals residues. However, the temperature and time should be minimized to avoid severe thermal sintering of the metal NPs and carbon support oxidation with O_2 to produce CO and CO_2, leading to catalyst degradation. Pt/C made with OAM showed a slight increase in H_{UPD} waves after 1 h oxidation in air at 300 ºC followed by reduction with hydrogen gas.

Temperature programmed techniques were applied to investigate the removal mechanism and to propose suitable procedures to remove them from metal NPs. Temperature programmed oxidation (TPO) spectra of Pt/C (30 mg) made by colloidal method using OAM in Figure 6-17 showed one broad NO_2 MS peak (m/z = 46) starting from ca. 120 ºC to ca. 210 ºC and one sharp NO_2 peak at ca. 250 ºC. These two NO_2 peaks mean there are two thermal oxidation reactions of $–NH_2$ with O_2.

It was not known if OAM still partially remained on the catalyst after oxidizing the $–NH_2$ with O_2 and released as NO_2. When only 50 μL (0.813 g/mL) OAM was placed in the reactor, no such NO_2 peaks were observed in the TPO spectra in Figure 6-18. This means that the Pt NPs actually catalyze the oxidation reaction of $–NH_2$ (of OAM) with O_2 to produce NO_2. After the TPO experiment, a black solid material (ca. 77%) was observed left in the reactor and some brown material was also found around the outlet of the reactor. It implies that there could be two reactions with heavy and light products, respectively, and not all the capping agent can be

removed by thermal oxidation with O_2. That no significant fragment molecules were detected by the mass spectrometer could be attributed to gradual vaporization and decomposition of OAM at a very low rate. The black solid residue can be dissolved in acetone and ethanol. Washing the catalyst after TPO could remove the residual surfactant.

One interesting result was obtained that only about 7% dark brown material was left after OAM was heated in He by temperature programmed desorption (TPD) with the same temperature program. No significant NO_2 MS signal was observed during this procedure. This implies that OAM was removed by vaporization and/or thermal decomposition much more than by thermal oxidation in air.

It could be also similar for the phase transfer agent. TOABr (10 mg) was thus heated in air from room temperature to 250 ºC and held for 1 h. It was found about 12% dark solid materials remained in the vial with some brown material at the reactor outlet. However, if the TOABr was heated in He with the same temperature program, there was only a tiny amount of dark residue (much less than 1%).

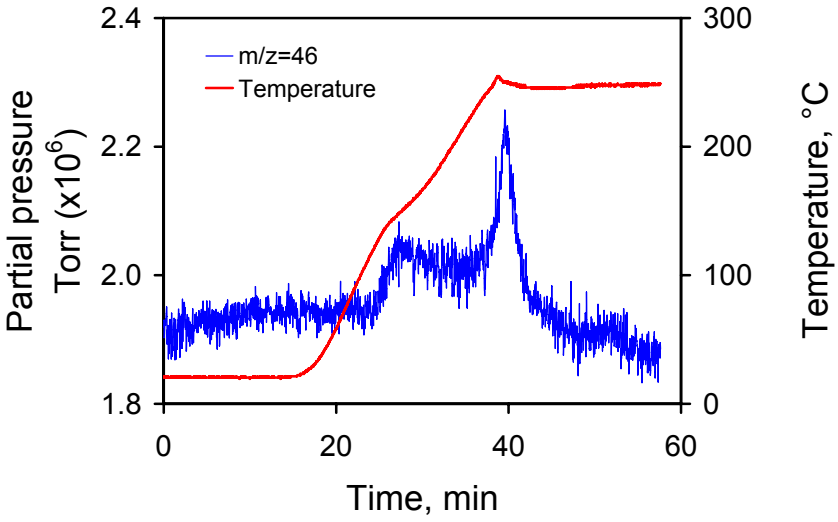

Figure 6-17. TPO spectrum of Pt/C made with OAM

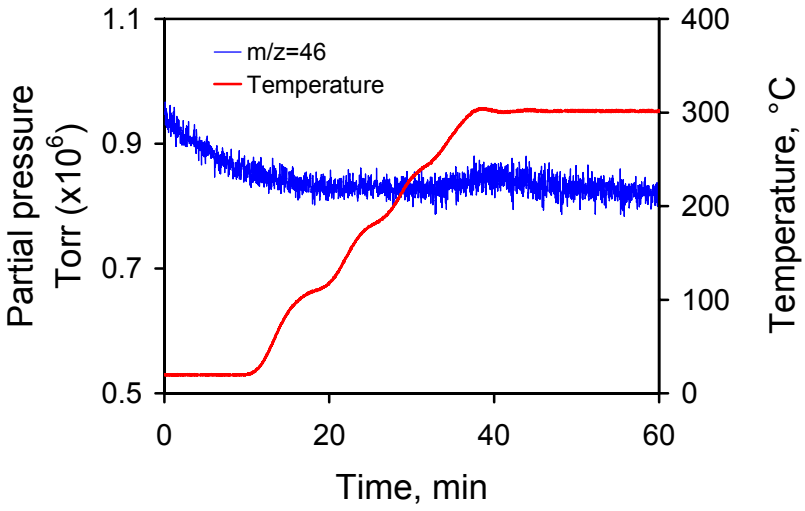

Figure 6-18. TPO spectrum of OAM

Two strategies were compared to remove the organic chemicals on the catalysts. One was to heat the Pt/C in He from room temperature to 250 ºC at 10 ºC/min and hold for 1 h. Still at 250 ºC, air was then fed to replace He and held for 15 min to oxidize the group $–NH_2$ or $–SH_2$. After that, He was fed to exclude air, followed by feeding H_2 to reduce the NPs at 250 ºC for 15 min and then cooling to room temperature. The other strategy was to heat the Pt/C in air from room temperature to 250 ºC at 10 ºC/min and hold for 1 h. He was fed then to exclude air, followed by feeding H_2 to reduce the NPs for 30 min at 250 ºC and then cooling to room temperature.

Pt/C treated with the first strategy had an ECSA (38.7 m^2/g), calculated from the desorption H_{UPD} charge in the CV in Figure 6-19. It is larger than the ECSA (29.1 m^2/g) of Pt/C treated using the second strategy, calculated from the CV shown in Figure 6-20. However, the ECSA is still less than that (65 m^2/g) of Pt/C made by the EG method and that (61 m^2/g) of Etek Pt/C.

The products left after TPO in air and TPD in He, and how to remove them completely need further investigation. A decent removal procedure for a capping agent and phase transfer agent is proposed as three steps: (1) heat the catalyst in inert gas atmosphere, (2) oxidize the bonding group on metals with O_2, and (3) reduce the partially oxidized metals back to metallic state if necessary. The time and temperature for each step might depend on the type of capping agents and metals. If necessary, washing the catalyst again could further remove the oxidation products of capping agent or phase transfer agent on catalyst surface. The solvent could be determined by trying to dissolve the TPO products of capping agents without catalysts.

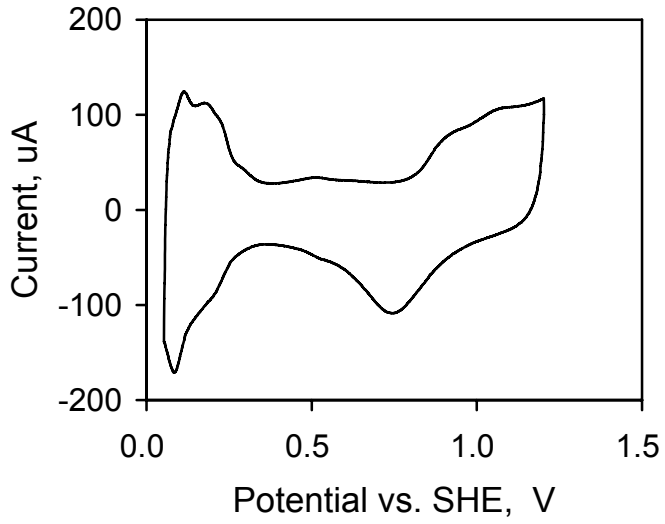

Figure 6-19. CV of Pt/C NPs made by colloidal method after heated in He

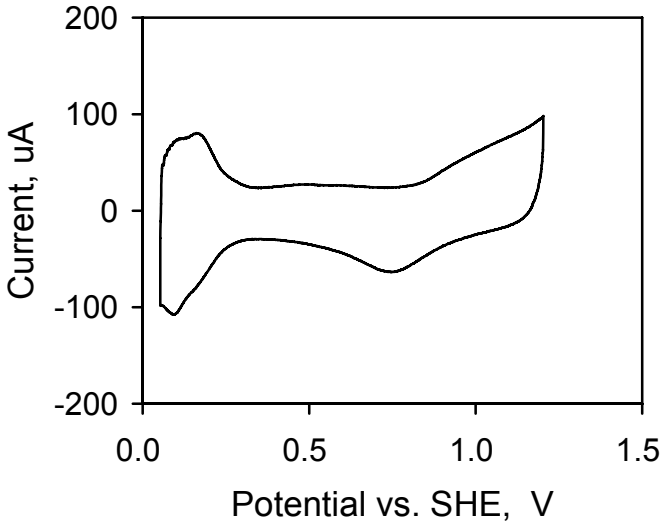

Figure 6-20. CV of Pt/C NPs made by colloidal method without heated in He

6.3.4 AuPt/C Made by Combination of EG and Colloidal Method

Pt/C made by EG and colloidal methods respectively have a similar dispersion and distribution, shown in Figure 6-5, Figure 6-12 and Figure 6-13. However, the ECSA of Pt/C made by colloidal method is lower than that of Pt/C made by EG method. The reason is that the active sites on Pt, that is the reactive component of the ORR catalyst made by colloidal method, are partially blocked by the residual capping agent and phase transfer agent.

Furthermore, Au/C made by the EG and the MW-EG have a large particle size (>10 nm) and poor distribution on the carbon support, shown by the TEM picture in Figure 6-6 and Figure 6-10 respectively. These are much worse than that made by the colloidal method, which has a mean particle size of 2.1 nm with standard deviation of 0.49 nm shown in Figure 6-15 and Figure 6-16.

Thus, a combination method (EG-Colloidal method) is proposed to prepare AuPt/C by loading the Au NPs made by colloidal method on Pt/C made by EG method. The advantage is that the main reactive component, Pt NPs, does not have capping agent or phase transfer agent on it to block the active sites, and the Au NPs has quite good dispersion and distribution. Figure 6-21 and Figure 6-22 show the AuPt/C catalyst has mean particle size of 2.46 nm with standard deviation of 0.50 nm.

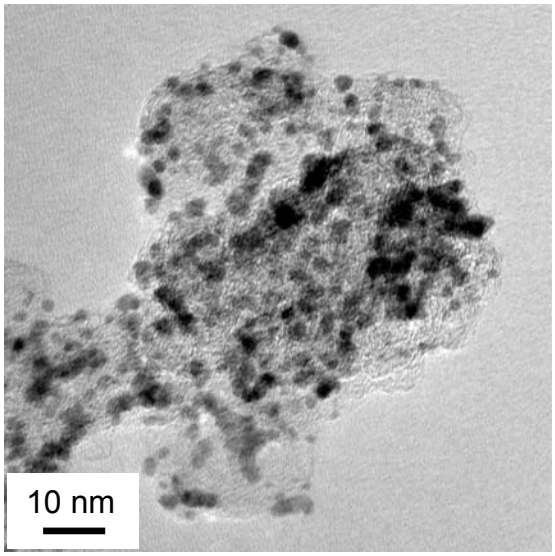

Figure 6-21. TEM picture of AuPt/C made by EG-Colloid

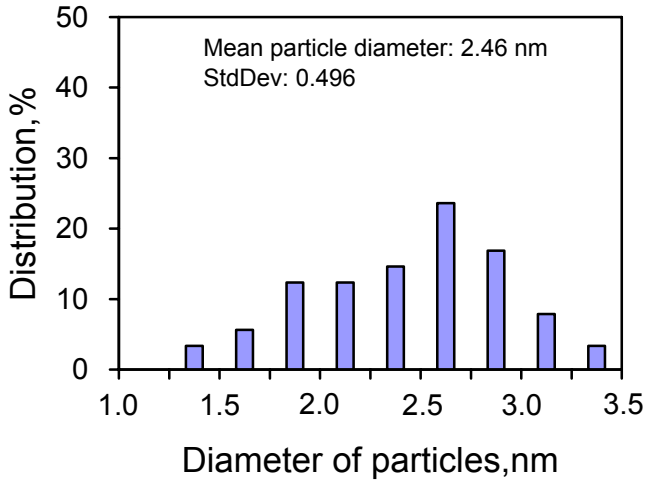

Figure 6-22. Metal NPs particle size distribution of AuPt/C made by EG-Colloid

Figure 6-23 shows the CV of the AuPt/C catalyst made by combination method. The ECSA is 54.5 m^2/g_{Pt}, less than that (65 m^2/g_{Pt}) of PtC catalyst made by MW-EG method. This decrease could be attributed to the residual organic chemicals transferring from Au NPs to the active sites of Pt NPs, as well as the coverage of Au NPs on Pt surface. The larger ring current in Figure 6-24 compared to that of Pt/C in Figure 6-9 verifies the Au existence. To confirm the Au existence, EDX was measured on a specific metal particle, shown in a STEM image in Figure 6-25. The EDX spectra in Figure 6-26 shows a weak $E_{Au\text{-}L\alpha}$ = 9.71 keV emission line, confirming Au existence on Pt/C.

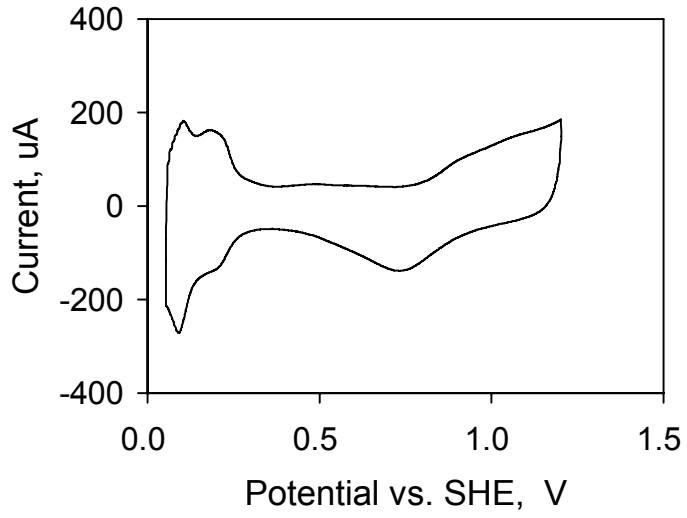

Figure 6-23. CV of AuPt/C made by EG-Colloidal method

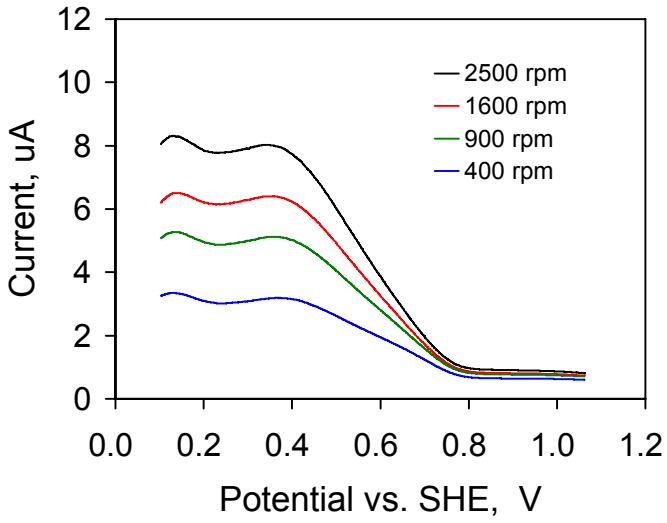

Figure 6-24. Ring current of AuPt/C made by EG-Colloidal method

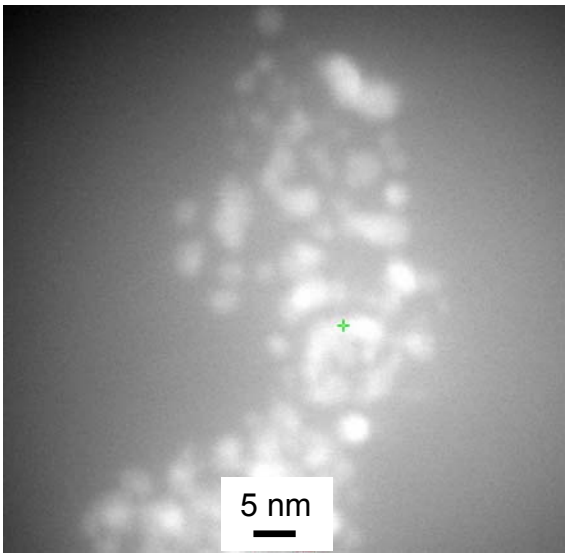

Figure 6-25. STEM picture of AuPt/C made by EG-Colloid

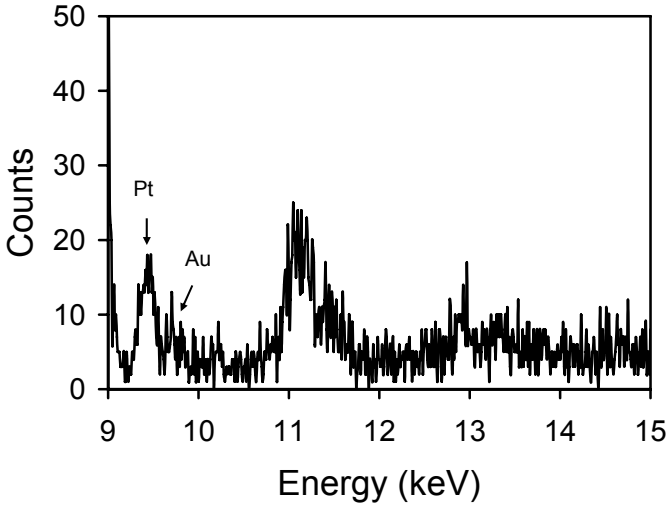

Figure 6-26. EDX spectrum of AuPt/C made by EG-Colloidal

6.3.5 AuPt/C Made by Surface Redox Method

Au/C made by EG method and MW-EG method has large particles size shown in Figure 6-6 and Figure 6-10, respectively. We thought that the carbon black has certain effects on Au NPs growth. This might be avoided if no carbon black exists in the reaction system when Au is reduced.

The MW-EG and EG methods were also employed to make Pt NPs. It was found that the Pt precursor was not reduced when using microwave radiation to assist reduction without carbon black. In other words, it implies that carbon black helps to reduce the Pt precursor with microwave radiation. Pt NPs made by EG method without carbon black have a mean particle size of 2.8 nm with standard deviation of 0.58 nm shown in Figure 6-27 and Figure 6-28, which are comparable with Pt NPs made by colloidal method and smaller than those of commercial Etek Pt/C. The Pt NPs was then loaded on C to make Pt/C. Its ECSA from CV in Figure 6-29 is 62

m^2/g_{Pt}, which is similar with that of Etek Pt/C.

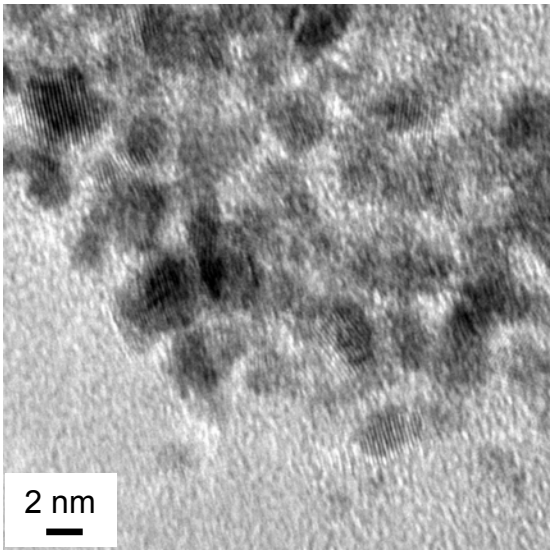

Figure 6-27. TEM picture of Pt NPs made by EG method

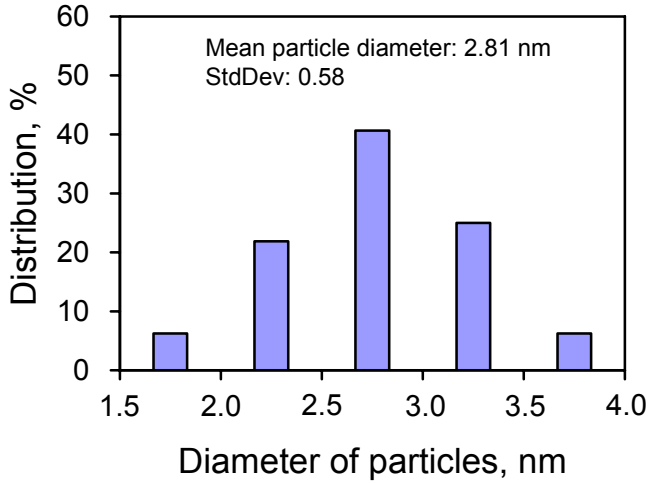

Figure 6-28. Particle size distribution of Pt NPs made by EG method

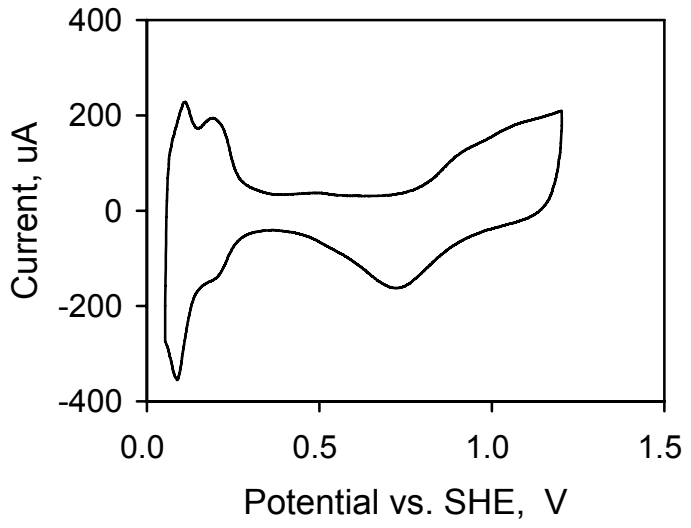

Figure 6-29. CV of Pt/C made by loading Pt NPs (made by EG method) on carbon black

Surface redox reactions require clean surfaces of Pt NPs to reduce the Au precursor. Thus, Au precursor was added to the freshly prepared Pt NPs in the original solution to deposit on Pt NPs. Those metal particles, Au on Pt NPs, were then loaded on carbon black to make AuPt/C catalyst.

Figure 6-30 shows quite good dispersion and uniform distribution of AuPt on carbon black. The ECSA from CV in Figure 6-32 is 64 m^2/g_{Pt}, which is quite close to 65 m^2/g_{Pt} and 61 m^2/g_{Pt} of PtC made by MW-EG method and Etek Pt/C respectively, especially considering the 5% Au covering on the Pt. The larger ring current in Figure 6-33 than that from Pt/C in Figure 6-9 verifies the Au existence. The STEM image in Figure 6-34 shows the location for the EDX in Figure 6-35, which shows there is a $E_{Au\text{-}L\alpha}$ = 9.71 keV emission lines, double confirming Au existence on Pt/C.

This AuPt/C was then used as the cathode catalyst in a MEA to test the hypothesis that

Au NPs can mitigate CSC.

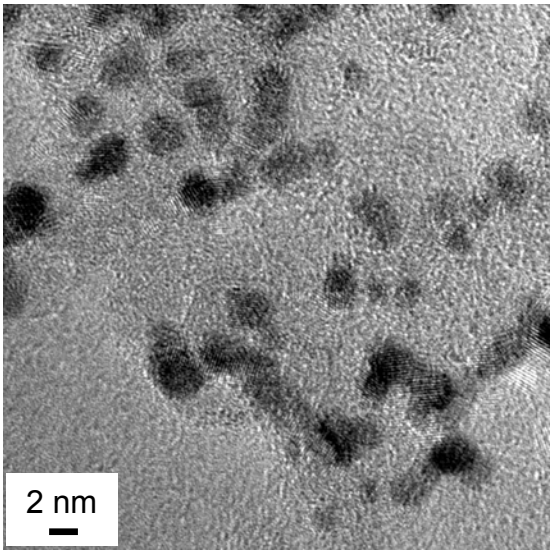

Figure 6-30. TEM picture of AuPt/C made by EG-SR method

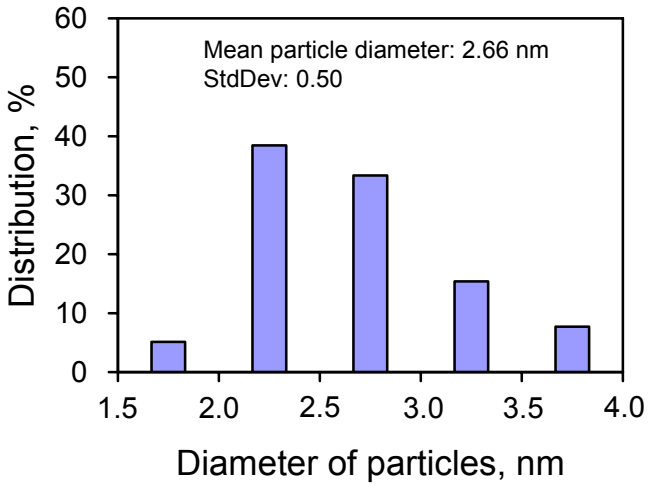

Figure 6-31. Particle size distribution of AuPt/C made by EG-SR method

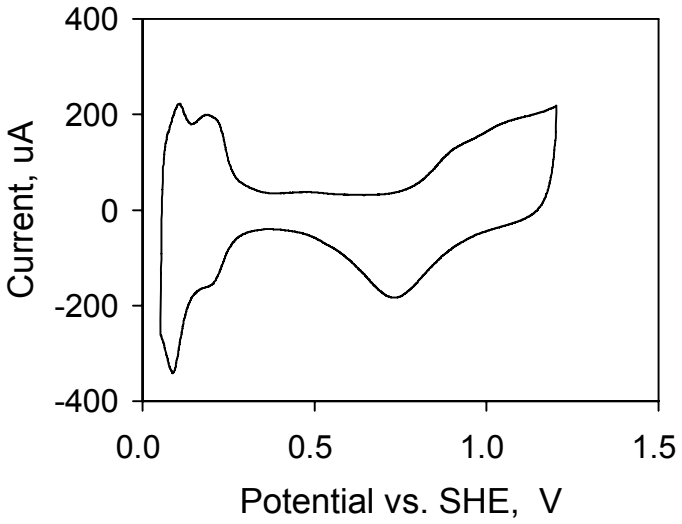

Figure 6-32. CV of AuPt/C made by EG-SR method

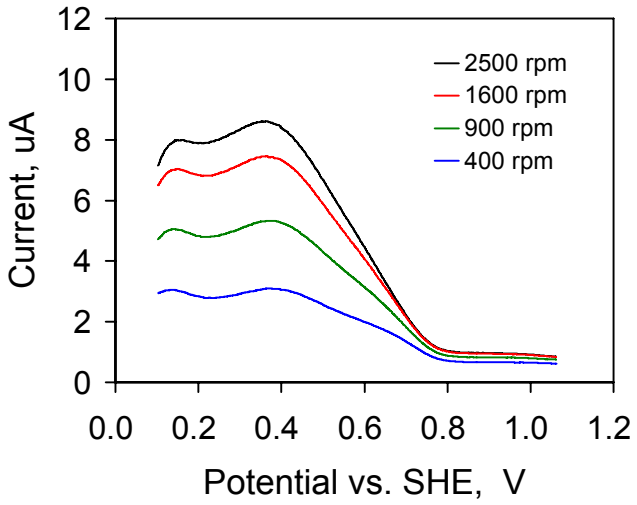

Figure 6-33. Ring current of AuPt/C made by EG-SR method

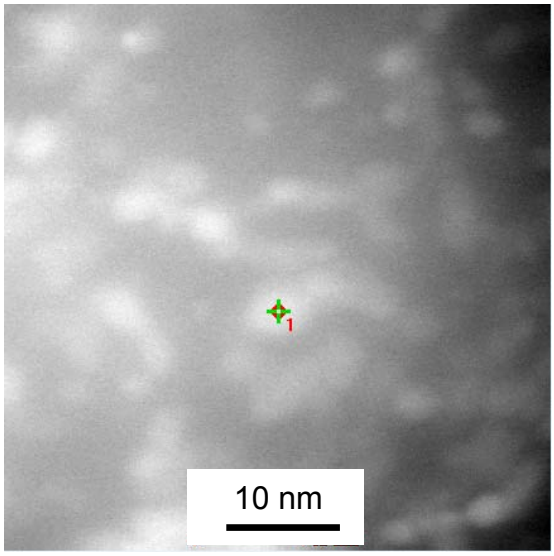

Figure 6-34. STEM picture of AuPt/C made by EG-SR

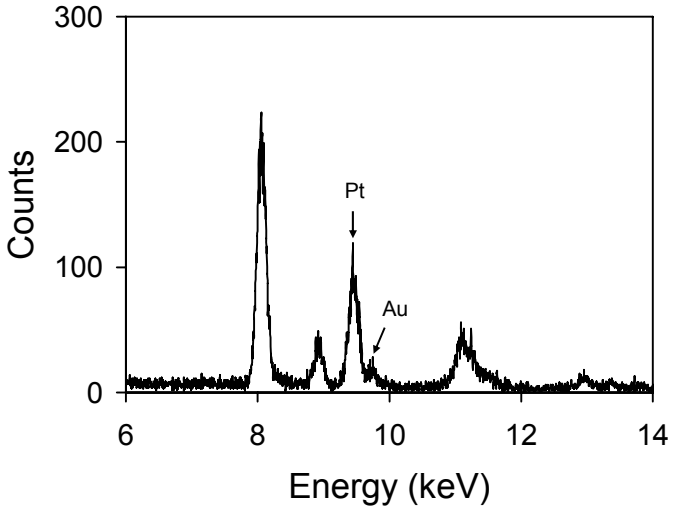

Figure 6-35. EDX spectrum of AuPt/C made by EG-SR

6.3.6 CSC comparison

Three 5 cm^2 square MEAs, with Etek Pt/C, AuPt/C (AuPtC-EG-SR) made by EG-SR method and AuPt/C (AuPtC-EG-SR) made by EG-colloidal method as cathode catalyst respectively, were prepared for CSC measurement and comparison to test the hypothesis. The anode of each MEA has the same catalyst of Etek Pt/C.

Figure 6-36 shows the CVs and DEMS spectra of CO_2 for Etek Pt/C, AuPtC-EG-SR, and AuPtC-EG-Col. Their H_{UPD} charges from CVs are 160, 295, and 156 mC, respectively. Generally, because the Pt catalyzes the CSC, cathode with larger H_{UPD} charge has more Pt actives sites so as to produce more CO_2 from CSC. The H_{UPD} charge of cathode with AuPtC-EG-Col is almost same with that of the cathode with Etek Pt/C. However, its CO_2 peak at 1400 mV is significantly higher than that of Etek Pt/C cathode. The results showed negative effect of Au on CSC mitigation at the cathode of PEMFC. This could be that the Au NPs are not located on the Pt NPs but on the carbon black. As for the cathode with AuPtC-EG-SR, the H_{UPD} charge is significantly larger than that of the cathode with Etek Pt/C. However, its CO_2 signal between 1.1–1.4 V is less intensity than that of Etek Pt/C cathode.

Figure 6-37 shows the CVs and DEMS spectra of CO_2 for Pt/C and AuPtC-EG-SR. Their H_{UPD} charges from CVs are 285 and 295 mC, respectively. Although their H_{UPD} charges are similar, the cathode with AuPtC-EG-SR also has less CO_2 produced above 1.1 V.

Less CO_2 produced at the cathode with AuPtC-EG-SR suggests there was a mitigation effect of Au on CSC. Pt oxidation has catalytic effect on CSC above 1.0 V, verified in Chapter 3. The CSC is thus mitigated because the Pt oxidation is suppressed by Au clusters. It verifies the hypothesis that Au existence on Pt can mitigate the CSC at the cathode of PEMFC. Further mechanisms investigation needs other in-situ spectroscopes under electrode potential control.

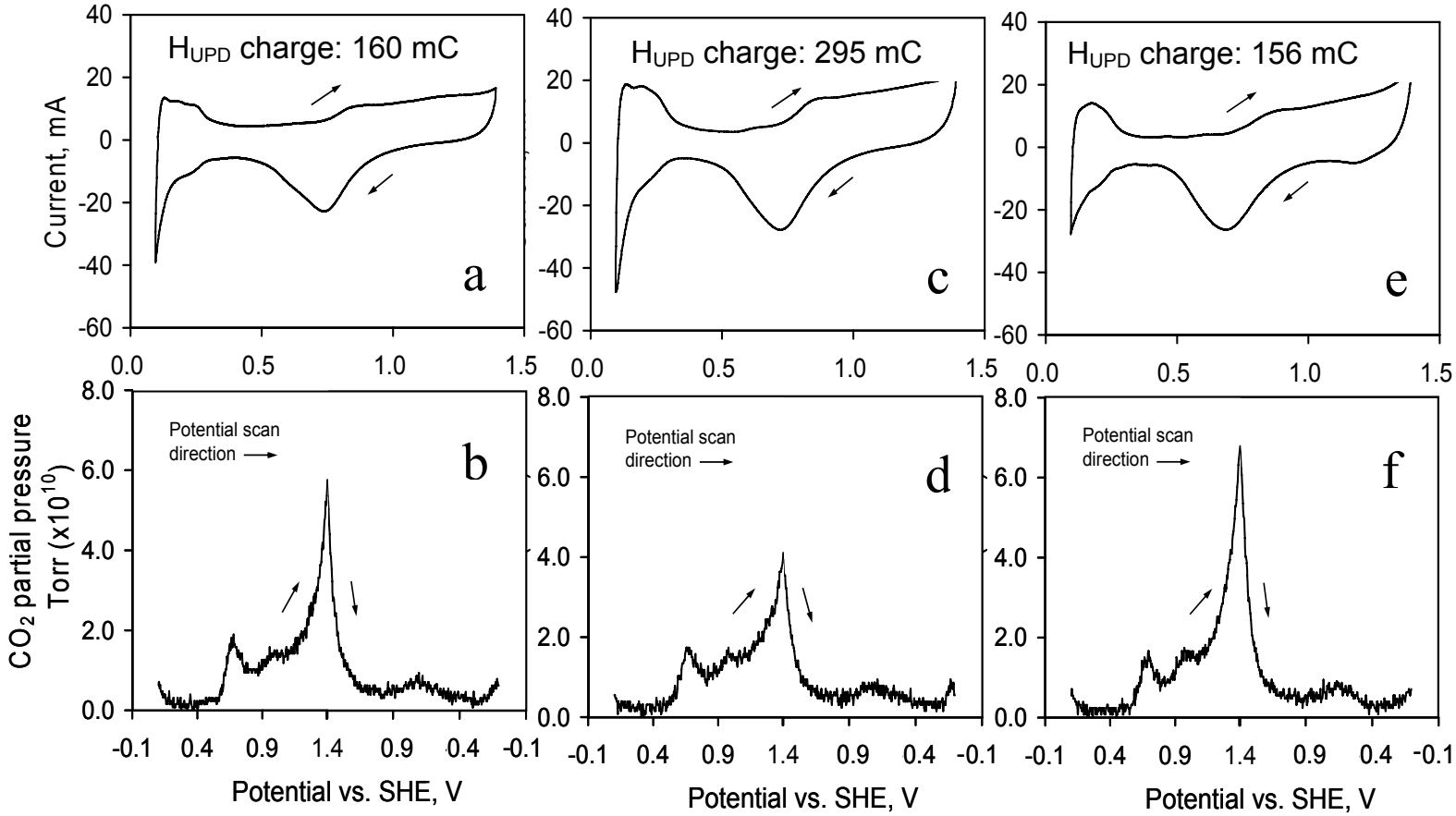

Figure 6-36 CV (a, c, e) and DEMS spectrum of CO2 (b, d, f) from the CSC of Etek Pt/C, AuPt/C-EG-SR, and AuPt/C-EG-Col, respectively

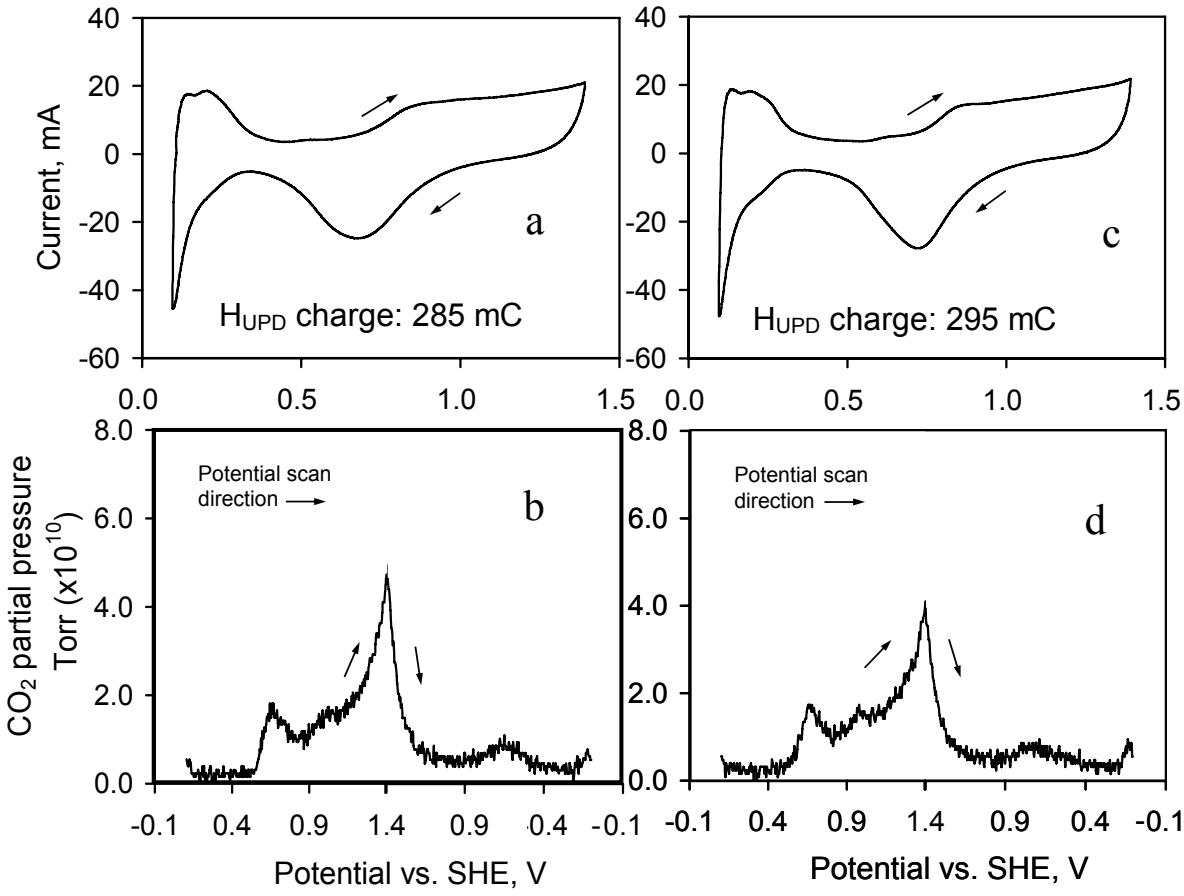

Figure 6-37 CV (a, c) and DEMS spectrum of CO_2 (b, d) from the CSC of Pt/C and AuPt/C-EG-SR, respectively (Pt/C is prepared by loading Pt NPs on carbon black.)

6.4 Conclusions

Pt/C was prepared using deposition precipitation (DP) method. It was found that Pt NPs are agglomerated and do not distribute on carbon black uniformly. Reaction assisted by ultrasonication or increasing the pH of reaction system gradually did not significantly impede aggregation of Pt NPs on carbon black support. It is possible that the Pt NPs already agglomerate before the deposition on the support, or that they can only deposit on the regions of carbon back support that are wet well by the solvent (water plus small portion ethanol) or have strong affinity

with Pt NPs.

Ethylene glycol (EG) can wet and disperse carbon black very well. It also works as solvent, stabilizer, and reductant in the EG method. Pt/C made by the EG method has mean particle size of 2.39 nm with standard deviation 0.425 nm, which is better than the commercial Etek Pt/C. However, the EG method does not work well for Au/C. It was then assisted with microwave to reduce the reduction time from hours to 1 min. Pt/C made by the Microwave-assisted (MW) EG method has a rather good dispersion and uniform distribution. However, Au/C made by MW-EG method still has large particle size of Au NPs from 10 to 20 nm.

Pt precursor in EG using microwave radiation heating without carbon black did not show any color change (no reaction) after the same reduction conditions. This result confirms that the microwave radiation interacts with the carbon black, which enhances the reduction and actually reduces the reduction time for Pt and Au precursors.

Au NPs and Pt NPs were synthesized using colloidal method, mixed with the atomic ratio of 1:4, and then loaded on carbon black to get AuPt/C (5% Au and 20% Pt). The results showed that that OAM and DT are appropriate capping agents to make high dispersion and uniform distribution Pt NPs and Au NPs, respectively. As for the capping agent removal from the metal NPs, it was found heating the metal NPS in He is more effective than in Air.

AuPt NPs made by EG-SR method have high dispersion and narrow particle size distribution. AuPt/C catalyst was then prepared by loading the AuPt NPs on the carbon black uniformly. The Au existence of AuPt/C was confirmed by its larger ring current than Pt/C made by EG method and the $E_{Au\text{-}L\alpha}$ = 9.71 keV emission line in EDX spectrum. DEMS results showed less CO_2 produced of the cathode with AuPt/C in the range of 1.1–1.4 V than the cathodes with commercial Etek Pt/C and Pt/C made using EG method.

References:

1. Matsumoto, M., T. Manako, and H. Imai, *Degradation of carbon supports in PEFC cathode investigated by electrochemical STM: effects of platinum and oxygen on enhanced carbon corrosion.* ECS Trans., 2008. **16**(2): p. 751-760.

2. Franco, A.A., M. Gerard, M. Guinard, B. Barthe, and O. Lemaire, *Carbon catalyst-support corrosion in polymer electrolyte fuel cells: mechanistic insights.* ECS Trans., 2008. **13**(15): p. 35-55.

3. Siroma, Z., M. Tanaka, K. Yasuda, K. Tanimoto, M. Inaba, and A. Tasaka, *Electrochemical corrosion of carbon materials in an aqueous acid solution.* Electrochem. (Tokyo, Jpn.), 2007. **75**(2): p. 258-260.

4. Chizawa, H., Y. Ogami, H. Naka, A. Matsunaga, N. Aoki, T. Aoki, and K. Tanaka, *Impacts of carbon corrosion on cell performance decay.* ECS Trans., 2007. **11**(1, Part 2, Proton Exchange Membrane Fuel Cells 7, Part 2): p. 981-992.

5. Wang, X., W. Li, Z. Chen, M. Waje, and Y. Yan, *Durability investigation of carbon nanotube as catalyst support for proton exchange membrane fuel cell.* J. Power Sources, 2006. **158**(1): p. 154-159.

6. Wang, J., G. Yin, Y. Shao, Z. Wang, and Y. Gao, *Electrochemical durability investigation of single-walled and multi-walled carbon nanotubes under potentiostatic conditions.* J. Power Sources, 2008. **176**(1): p. 128-131.

7. von Kraemer, S., K. Wikander, G. Lindbergh, A. Lundblad, and A.E.C. Palmqvist, *Evaluation of TiO2 as catalyst support in Pt-TiO2/C composite cathodes for the proton exchange membrane fuel cell.* J. Power Sources, 2008. **180**(1): p. 185-190.

8. Huang, S.-Y., P. Ganesan, S. Park, and B.N. Popov, *Development of a Titanium Dioxide-Supported Platinum Catalyst with Ultrahigh Stability for Polymer Electrolyte Membrane Fuel Cell Applications.* J. Am. Chem. Soc., 2009. **131**(39): p. 13898-13899.

9. Acharya, C.K., W. Li, Z. Liu, G. Kwon, C. Heath Turner, A.M. Lane, D. Nikles, T. Klein, and M. Weaver, *Effect of boron doping in the carbon support on platinum nanoparticles and carbon corrosion.* J. Power Sources, 2009. **192**(2): p. 324-329.

10. Patterson, T.W. and R.M. Darling, *Damage to the Cathode Catalyst of a PEM Fuel Cell Caused by Localized Fuel Starvation.* Electrochem. Solid-State Lett., 2006. **9**(4): p. A183-A185.

11. Reiser, C.A., L. Bregoli, T.W. Patterson, J.S. Yi, J.D. Yang, M.L. Perry, and T.D. Jarvi, *A Reverse-Current Decay Mechanism for Fuel Cells.* Electrochem. Solid-State Lett., 2005. **8**(6): p. A273-A276.

12. Li, W. and A.M. Lane, *Investigation of Pt catalytic effects on carbon support corrosion of the cathode catalyst in PEM fuel cells using DEMS spectra.* Electrochem. Comm., 2009. **11**(6): p. 1187-1190.

13. Maass, S., F. Finsterwalder, G. Frank, R. Hartmann, and C. Merten, *Carbon support oxidation in PEM fuel cell cathodes.* J. Power Sources, 2008. **176**(2): p. 444-451.

14. Roen, L.M., C.H. Paik, and T.D. Jarvi, *Electrocatalytic Corrosion of Carbon Support in PEMFC Cathodes.* Electrochem. Solid-State Lett., 2004. **7**(1): p. A19-A22.

15. Willsau, J. and J. Heitbaum, *The influence of Pt-activation on the corrosion of carbon in gas diffusion electrodes--A dems study.* J. Electroanal. Chem., 1984. **161**(1): p. 93-101.

16. Perry, M.L., T.W. Patterson, and C. Reiser, *Systems strategies to mitigate carbon corrosion in fuel cells.* 210th ECS Meeting, 2006. **Abstract #597**.

17. Charlot, G., J. Badoz-Lambing, and B. Trémillon, *Les réactions électrochimiques*. 1959, Mason et Cie, Paris.

18. Zhang, J., K. Sasaki, E. Sutter, and R.R. Adzic, *Stabilization of Platinum Oxygen-Reduction Electrocatalysts Using Gold Clusters.* Science, 2007. **315**(5809): p. 220-222.

19. Mott, D., J. Luo, P.N. Njoki, Y. Lin, L. Wang, and C.-J. Zhong, *Synergistic activity of gold-platinum alloy nanoparticle catalysts.* Catal. Today, 2007. **122**(3-4): p. 378-385.

20. Haruta, M., T. Kobayashi, H. Sano, and a.N. Yamada, *Novel Gold Catalysts for the Oxidation of Carbon Monoxide at a Temperature far Below 0 °C.* Chem. Lett., 1987. **2**: p. 405-408.

21. Bianchi, C., F. Porta, L. Prati, and M. Rossi, *Selective liquid phase oxidation using gold catalysts.* Top. Catal., 2000. **13**(3): p. 231-236.

22. Brust, M., M. Walker, D. Bethell, D.J. Schiffrin, and R. Whyman, *Synthesis of thiol-derivatised gold nanoparticles in a two-phase Liquid-liquid system.* J. Chem. Soc., Chem. Comm. 1994: p. 801-802.

23. Luo, J., M.M. Maye, V. Petkov, N.N. Kariuki, L. Wang, P. Njoki, D. Mott, Y. Lin, and C.-J. Zhong, *Phase Properties of Carbon-Supported Gold&-Platinum Nanoparticles with Different Bimetallic Compositions.* Chem. Mater., 2005. **17**(12): p. 3086-3091.

24. Paulus, U.A., T.J. Schmidt, H.A. Gasteiger, and R.J. Behm, *Oxygen reduction on a high-surface area Pt/Vulcan carbon catalyst: a thin-film rotating ring-disk electrode study.* J. Electroanal. Chem., 2001. **495**(2): p. 134-145.

25. Kim, H., J.-N. Park, and W.-H. Lee, *Preparation of platinum-based electrode catalysts for low temperature fuel cell.* Catal. Today, 2003. **87**(1-4): p. 237-245.

26. Samec, Z., V. Marecek, J. Weber, and D. Homolka, *Charge transfer between two immiscible electrolyte solutions: Part VII. Convolution potential sweep voltammetry of Cs+ ion transfer and of electron transfer between ferrocene and hexacyanoferrate(III) ion across the water/nitrobenzene interface.* J. Electroanal. Chem., 1981. **126**(1-3): p. 105-119.

27. Cunnane, V.J., D.J. Schiffrin, C. Beltran, G. Geblewicz, and T. Solomon, *The role of phase transfer catalysts in two phase redox reactions.* J. Electroanal. Chem., 1988. **247**(1-2): p. 203-214.

CHAPTER 7

CONCLUSIONS AND FUTURE WORK

7.1 Conclusions

In-situ investigation on carbon support corrosion (CSC) mechanism was conducted using differential electrochemical mass spectrometry (DEMS) and isotope labeling ^{18}O-DEMS. The hypothesis that CSC might be mitigated by adding Au clusters on Pt/C was verified.

7.1.1 CSC Mechanism at the Cathode in PEMFC

DEMS spectra of cathode exhaust gases CO_2, H_2, and O_2 from a small 5 cm^2 PEMFC were utilized to characterize the CSC, and correlate it with the Pt redox reactions and Pt-catalyzed oxygen reduction reaction (ORR). It indicated that CSC was catalyzed by Pt with different oxidation states.

O_2 does not affect the CSC significantly during potential cycling from 100–1400 mV at 10 mV/s. ^{18}O-DEMS spectra of carbon dioxides from the cathode confirmed that water and original surface oxides on carbon are oxygen sources of CSC; but water is the main source. Moreover, water reacts with carbon to produce at least three types of carbon surface oxides in the potential range of 100–500 mV, 700–1400 mV, and 1000–1400 mV, respectively, which are further oxidized with water to produce CO_2. These surface oxides are also originated from the preparation of the carbon black and catalysts. The total reactions of CSC producing CO_2 follow

the pathways below:

$$C + H_2O \xrightarrow{Pt, PtO_x} CO_{surf} + 2e^-$$

$$CO_{surf} + H_2O \xrightarrow{Pt, PtO_x} CO_2 + 2e^-$$

Potential cycling between 100–1200 mV at the rate of 400 mV/s was used to accelerate the cathode catalyst degradation in PEMFC, shown by the electrochemically active surface area (ECSA) of Pt/C decreases. The CO_2 mass spectrum (MS) peaks decreased without significant change of profile, which means that Pt catalytic effects still existed but decreased.

It was deduced that the hydrogen evolution reaction (HER) contributes to the H_2 peak and the hydrogen oxidation reaction (HOR) to the H_2 plateau. The H_2 peaks are limited by the diffusion through the membrane and do not change after potential cycling of 4000 cycles, which means the membrane did not degrade significantly in permeability. Therefore, the membrane degradation can be excluded from the consideration when using the potential cycling to accelerate the degradation of the cathode catalyst.

O_2 MS plateaus is ascribed to oxygen reduction reactions (ORR) on Pt. it did not change significantly with potential cycles because the ORR is limited by the leakage of O_2 from the environment.

7.1.2 Mitigate the CSC by Adding Au Clusters on Pt/C

Pt/C prepared using deposition precipitation (DP) method has the issue that Pt NPs are agglomerated and do not distribute on carbon black uniformly. It has not been solved with assisted by ultrasonication or increasing the pH of reaction system gradually. Ethylene glycol (EG) method and Microwave-assisted (MW) EG method can prepare Pt/C with high dispersion and narrow particle size distribution Pt NPs loaded uniformly on the carbon black, which is

better than the commercial Etek Pt/C. Unfortunately, Au/C synthesized by EG and MW-EG methods has large Au NPs.

Au NPs and Pt NPs with high dispersion and narrow particle size distribution were synthesized using colloidal method with DT and OAM respectively. They were mixed with the mass ratio of 1:4, and then loaded on carbon black to get AuPt/C (5% Au and 20% Pt). It was found that the capping agent was removed more effectively by heating the metal NPs in He than in Air. However, the AuPt/C has smaller ECSA but stronger CO_2 produced than E-tek Pt/C.

AuPt/C prepared by EG-surface redox (EG-SR) method has AuPt NPs with high dispersion, narrow particle size distribution, and loaded uniformly on carbon black support. It has larger ECSA and less CO_2 produced than E-tek Pt/C in the range of 1.1–1.4 V. This verified the hypothesis.

7.2 Future Work

The ^{18}O-DEMS experiments give information about how many types of surface oxide involved in CSC at certain potentials. However, it cannot tell the detail information about those surface oxides on molecular level. This inspires further in-situ investigation of CSC mechanism on molecular level as well as on structure sensitivity.

7.2.1 Understand CSC on Molecular Level with In-situ DRIFTS and on Structure with In-situ Raman

A special PEMFC hardware with an IR and Raman transparent window and a special MEA with no carbon paper covering on the cathode catalyst will be made for in-situ diffuse reflectance infrared Fourier transform spectroscopy (DRIFTS) and Raman study. The IR bands

of surface oxides related to potentials will be recorded for interpretation of CSC mechanisms on molecular level. The Raman bands of different structure carbon could be changed over time to elucidate structure sensitivity for CSC.

DRIFTS is a version of FTIR to analyze a powder or rough surface sample by collecting the diffuse scattered radiation. The applications of DRIFTS for the characterization of carbon-supported metal catalysts [1-4] and different kind of carbon surfaces [5-12] are plentiful in literature. However, to my knowledge, there is still no in-situ DRIFTS study on CSC of Pt/C catalysts in real PEMFC or even in simulated PEMFC conditions.

DRIFTS could be applied in-situ to explore what surface groups and adsorbates are on Pt/C at the cathode and how they vary during potential cycling. It helps to further identify the reactions contributing the peaks in DEMS spectra of CO_2. The carbon black has main types of surface oxides, such as carboxylic, phenolic or hydroquinone, quinones and nonacidic groups containing one O, and lactones and nonacidic groups containing two O. Their IR bands are in the range of 1000 – 5000 cm^{-1}.

A special PEMFC hardware with a Ge IR window at the cathode will be made for testing. The properties of insolubility in water and acid as well as good and stable transmittance (ca. 50 %) in the appropriate wavenumber range (1000 – 5000 cm^{-1}) make Ge suitable material for IR window for in-situ PEMFC study. The part of cathode illuminated by IR does not have carbon paper, and the catalyst is coated directly on the membrane. The distance between the catalyst and the Ge IR window is around 100 μm, less than the focal length of the lens (larger than 1 cm). When running at 30 ºC, the water vapor pressure should not larger than 0.042 atm (the saturated vapor pressure at 30 ºC). This small amount of water in the IR path should not cause severe adsorption. DRIFTS spectra will be recorded during potential cycling. The position shift and/or

intensity change of bands at different potentials will be utilized to identify surface oxides and their variation.

IR and Raman complement each other, and Raman could also detect the surface groups in theory. However, because of relative low sensitivity compared with IR, Raman can just give the bands of graphite and disordered graphite in carbon black. The band at ca. 1360 cm^{-1} is attributed to the disordered carbon, termed as D-band, and the band at ca. 1610 cm^{-1} consists of the band at ca. 1580 cm^{-1} for sp^2 carbon, termed as G-band and D-band at ca. 1640 cm^{-1}. Analyzing the changes of those bands over time can elucidate the preferential place that CSC happens.

7.2.2 Model the CSC of C-MEA and Pt/C-MEA

Models based on Butler-Volmer equation [13, 14] were proposed recently to fit the CVs at different age of MEA to describe cathode catalyst degradation. Both models only considered the Pt redox reaction and neglected CSC. Actually, CSC contributes a quite large to degradation and cannot be ignored. The CSC was modeled in several papers [15-17] to investigate the effects on cathode catalyst degradation, with only consideration on the current wave above 1.0 V. The reason is a shortage of knowledge on the mechanisms of CSC in PEMFC.

DEMS has the capacity to resolve the CSC from Pt redox in CV and helps to understand their mechanisms and modeling. Based on an understanding of the mechanisms and kinetics of CSC, it is feasible to propose a mechanistic model for CSC based on the Butler-Volmer equation. The cyclic voltammograms of the cathode catalysts with different ages can be fitted by a combination of this CSC model and a Pt redox or dissolution model. The ultimate object is to predict the normal degradation based on the accelerated catalyst degradation.

References:

1. Venter, J.J. and M.A. Vannice, *Modifications of a diffuse reflectance cell to allow the characterization of carbon-supported metals by DRIFTS.* Appl. Spectrosc., 1988. **42**(6): p. 1096-1103.

2. Venter, J.J. and M.A. Vannice, *Applicability of "drifts" for the characterization of carbon-supported metal catalysts and carbon surfaces.* Carbon, 1988. **26**(6): p. 889-902.
3. Venter, J.J., *A DRIFTS (Diffuse Reflectance Infrared Fourier Transform Spectroscopy) characterization of carbon-supported osmium, ruthenium, iron, and iron-manganese catalysts*. 1988. p. 685 pp.

4. Venter, J.J. and M.A. Vannice, *A diffuse reflectance FTIR spectroscopic (DRIFTS) investigation of carbon-supported metal carbonyl clusters.* J. Am. Chem. Soc., 1987. **109**(20): p. 6204-5.

5. Fanning, P.E. and M.A. Vannice, *A DRIFTS study of the formation of surface groups on carbon by oxidation.* Carbon, 1993. **31**(5): p. 721-730.

6. Figueiredo, J.L., M.F.R. Pereira, M.M.A. Freitas, and J.J.M. Órfão, *Modification of the surface chemistry of activated carbons.* Carbon, 1999. **37**(9): p. 1379-1389.

7. Meldrum, B.J. and C.H. Rochester, *Infrared spectra of carbonaceous chars under carbonization and oxidation conditions.* Fuel, 1991. **70**(1): p. 57-63.

8. Meldrum, B.J. and C.H. Rochester, *Fourier-transform infrared study of surface species on carbon mixed with potassium bromide and reacted with carbon dioxide, oxygen, and carbon monoxide.* J. Chem. Soc., Faraday Trans., 1990. **86**(21): p. 3647-52.

9. Meldrum, B.J. and C.H. Rochester, *In situ infrared study of the surface oxidation of activated carbon dispersed in potassium bromide.* J. Chem. Soc., Faraday Trans., 1990. **86**(17): p. 2997-3002.

10. Meldrum, B.J. and C.H. Rochester, *In situ infrared study of the modification of the surface of activated carbon by ammonia, water and hydrogen.* J. Chem. Soc., Faraday Trans., 1990. **86**(10): p. 1881-4.

11. Meldrum, B.J., J.C. Orr, and C.H. Rochester, *Diffuse reflectance Fourier-transform infrared spectroscopy: in situ surface oxidation of carbon.* J. Chem. Soc., Chem. Commun., 1985(17): p. 1176-7.

12. Wood, D.J., *Characterization of charcoals by DRIFT.* Mikrochim. Acta, 1988. **2**(1-6): p. 167-9.

13. Darling, R.M. and J.P. Meyers, *Kinetic Model of Platinum Dissolution in PEMFCs.* J. Electrochem. Soc., 2003. **150**(11): p. A1523-A1527.

14. Bi, W. and T.F. Fuller, *Modeling of PEM fuel cell Pt/C catalyst degradation.* J. Power Sources, 2008. **178**(1): p. 188-196.

15. Franco, A.A., M. Gerard, M. Guinard, B. Barthe, and O. Lemaire, *Carbon catalyst-support corrosion in polymer electrolyte fuel cells: mechanistic insights.* ECS Trans., 2008. **13**(15): p. 35-55.

16. Meyers, J.P. and R.M. Darling, *Model of Carbon Corrosion in PEM Fuel Cells.* J. Electrochem. Soc., 2006. **153**(8): p. A1432-A1442.

17. Takeuchi, N. and T.F. Fuller, *Modeling and Investigation of Design Factors and Their Impact on Carbon Corrosion of PEMFC Electrodes.* J. Electrochem. Soc., 2008. **155**(7): p. B770-B775.